Aalto University
School of Engineering
Degree Programme in Structural Engineering and Building Technology

Numerical simulation of fire performance and test conditions for façade insulation materials

Master's Thesis

1.9.2015

Gleb Bytskov

Thesis submitted in partial fulfillment of the requirements for the degree of
Master of Science in Technology
Espoo, September 1, 2015

Supervisor: Professor Simo Hostikka

Author: Gleb Bytskov

Title:
Numerical simulations of fire performance and test conditions for façade insulation materials

Date:	September 1, 2015	**Pages:**	113
Major:	Structural Engineering	**Code:**	R3001
Supervisor:	Professor Simo Hostikka		
Advisors:			

Development and harmonization of test standards for fire classification of building products is actively investigated at current moment. Investigation of such standard test characteristics and sensitivities is a part of each standard development process. While the full-scale tests with alternative details cannot be avoided, many of the phenomena can be studied using Computational Fluid Dynamics simulations.

The main task of this thesis was to investigate the sensitivity of the building façade fire test standard ISO 13785-2 on the details of the test setup. The practical tasks were to prepare a validated model for the ISO 13785-2, to characterize insulation materials for simulation purposes, and to demonstrate the use of CFD in façade fire test simulation.

The validation of the simulation model was performed by the simulation of specific fire test of non-combustible façade conducted in TUS (Tokyo University of Science) laboratory which results was published in Journal of Fire Science and Technology in 2012. In the test series, a range of different heat release rates was used. After the validation, the model was used for investigating heat fluxes at different heights above the opening and temperatures at different depths.

Excluding the fires with small fire load as they were not representative to the standard test conditions, the model provides results with bias of 0.84 for heat flux and 1.05 for temperature on façade wall. The test series with only one additional opening in rear side of combustion chamber gave the most accurate results. The largest deviation between numerical and experimental results was observed in the tests with fuel flow rate smaller than ½ of ISO (60 g/s). In addition, significant differences between the measured and simulated temperatures inside the combustion chamber were found.

A series of small flammability test, such as TGA, MCC, DSC and Cone Calorimeter test, were conducted for common combustible insulation materials. All achieved results were used for determining fire protection of combustible insulation materials in large-scale test conditions. As a result, 70 mm of fire protection is needed for defending EPS against burning and 60 mm against melting in the most critical region from 0 mm to 400 mm above window. For PIR this layer thickness should be not less than 90 mm.

Keywords:	FDS, fire, insulation, external wall, façade, simulation, test
Language:	English

Tekijä:	Gleb Bytskov		
Työn nimi:	Julkisivueristeiden palokäyttäytymisen ennustaminen koeolosuhteissa numeerisen simuloinnin avulla		
Päiväys:	1. syyskuuta 2015	**Sivumäärä:**	113
Pääaine:	Rakennetekniikka	**Koodi:**	R3001
Valvoja:	Professori Simo Hostikka		
Ohjaajat:			

Rakennustuotteiden palokäyttäytymistä säätelevien standardien kehittäminen ja harmonisointi on aktiivisen tutkimuksen kohteena. Näiden standardikokeiden piirteiden ja herkkyyden tutkiminen on osa standardien kehittämisprosessia. Vaikka täyden mittakaavan kokeita ei voidakaan täysin välttää, useita yksityiskohtia voidaan tutkia CFD-pohjaista palosimulointia käyttäen.

Tämän diplomityön tavoitteena on tutkia ISO 13785-2 kokeen paloaltistuksen herkkyyttä koeasentelun yksityiskohdille. Päämääränä oli valmistaa toimiva simulointimalli ISO 13785-2-kokeelle, kuvata eristysmateriaaleja simulointia varten sekä soveltaa CFD simulointia julkisivun palotestin tutkimiseen.

Mallin validoinnissa hyödynnettiin Tokion yliopistossa tehtyjä kokeita. Testien tulokset oli julkaistu Journal of Fire Science-lehdessä vuonna 2012. Kokeissa käytetyt julkisivut olivat palamattomia ja kokeet oli toteutettu erilaisilla palotehoilla. Validoitua mallia käytettiin lämpövirtojen ja lämpötilojen arviointiin eri kohdissa julkisivua.

Validointitulosten perusteella FDS-malli aliarvioi julkisivuun kohdistuvia lämpövirtoja 16 % ja yliarvioi lämpötiloja 5 %. Tarkimmat tulokset saatiin koesarjassa, jossa oli vain yksi tuuletusikkuna palokomeron takaseinällä. Suurin poikkeama simulaation ja kokeen välillä havaittiin testeissä, joissa polttoaineen massavirta oli alle puolet ISO standardin mukaisesta maksimimassavirrasta. Palotilan lämpötiloissa erot olivat merkittäviä niissäkin kokeissa, joissa lämpövirran ja lämpötilojen arvot julkisivulla olivat lähellä toisiaan.

Julkisivueristeiden palo-ominaisuuksia tutkittiin TGA-, MCC-, DSC- ja kartiokalorimetrikokeiden avulla. Materiaalien paloteknisiä ominaisuuksia käytettiin palosuojakerroksen paksuuden arvioinnissa ison mittakaavan testin olosuhteissa. Tulosten perusteella voitiin päätellä, että EPS-eristeen suojaamiseksi syttymiseltä tarvitaan 70 mm suojan 0 - 400 mm alueella ikkunan yläpuolella. PIR-eristeelle tämän suojakerroksen paksuuden tulee olla vähintään 90 mm.

Asiasanat:	FDS, tulipalo, eriste, ulkoseinä, julkisivu, simulointi, testi
Kieli:	Englanti

Contents

Acknowledgements

This Master's thesis was done in Aalto University School of Technology at Department of Civil Engineering during January 2015 – September 2015.

I would like to thank all those, who helped me to accomplish this study. I would like specially to thank Simo Hostikka for suggesting this burning topic for my thesis and for the guidance given, without which this work would not have been possible.

I am also grateful to Dr. Hideki Yoshioka from the National Institute for Land Infrastructure Management (NILIM), Japan, for invaluable support in FDS model validation completed in this work. Without this, the result would not be even close to the quality it is now.

I am grateful for the help of employees of VTT fire testing laboratory, especially Tuula Hakkarainen and Anna Matala, who provided me advanced comments and material for my thesis. Also I would like to thank the Foundation for Aalto University Science and Technology for funding this research.

Last but not least, I would like to thank my family and dear friend Olga Goncharko for their moral support.

Espoo, September 1,
Gleb Bytskov

List of symbols

Abbreviations used in equations

A	area of the window (m^2)
F_v	ventilation factor ($m^{3/2}$)
B	width of the window (m)
c_p	specific heat of air at constant pressure ($J\ kg^{-1}\ K^{-1}$)
D	side wall separation distance (m)
D_e	effective domain extension (m)
D_h	hydraulic diameter of opening (m)
D^*	characteristic fire diameter
g	gravitational acceleration (m/s^2)
H	height of the window (m)
h	window neutral plane height above the ground (m)
l_1	characteristic length (m)
m_{air}	air mass flux (kg/s)
m_{fuel}	fuel mass flux (kg/s)
P	ambient air pressure (kPa)
P_o	perimeter of the window (m)
Q	total heat release rate of the fire (kW)
Q_D	non-dimensional heat flow rate of window jet
Q_{ex}	heat release rate outside compartment (kW)
Q_{inside}	heat released inside the compartment (kW)
q''	heat flux upon facade (kW/m^2)
T_∞	ambient temperature (K)
T_0	initial compartment temperature (K)
T	temperature (K)
t	time (s)
t_0	time of incubation period (s)
Z	vertical position on the façade (m)
Z_f	mean flame height (m)
$Z_{f,D}$	mean flame height with side wall distance of D (m)
α_f	fire growth coefficient (kW/s^2)
λ	thermal conductivity (W/mK)

ρ_∞	ambient air density (kg/m^3)
η_e	effective domain extension factor
Δ	difference between variables
ΔH_c	lower heat of combustion (kJ/kg)
χ	combustion efficiency
Θ	non-dimensional temperature
δx	nominal size of the grid cell

Insulating materials

EPS	expanded polystyrene
PIR	polyisocyanurate
PIR-Al	polyisocyanurate with aluminum covering
PIR-COV	polyisocyanurate with fire retardant covering

Tests

DSC	differential scanning calorimetry
TGA	thermogravimetric analysis
MCC	micro-scale combustion calorimetry
STA	simultaneous thermal analysis

1 Introduction

1.1 Background to the research

The main theme of this Master's thesis is fire safety of insulated façade. The façade fire safety is relevant theme because façades have a large potential to contribute to the spread of fire between floors and apartments of residential buildings.

Fire is a complex phenomenon that consists of chemical reactions between combustible species and oxygen from the air. Many combustible and non-combustible materials are used today to improve the energy performance of the building required by the regulations. The combustibility of the assembly materials directly affects the fire hazard. (White 2014, p. 3).

There are many reports on fire accidents proving that the fire spread over the facade can be a very dangerous fire scenario. Proceeding upward, this specific scenario is under scrutiny at this moment. Investigating the 'façade in fire'- scenario helps to develop current test methods and potential mitigating strategies. (White 2014, pp. 3-5).

Korhonen and Hietaniemi carried out a survey on Finish National Accident Database (PRONTO) recorded in years 1996-2001 finding out that the most dangerous fire scenario in the buildings is an apartment fire that has developed through flashover to engulf the whole room-of-fire origin. Moreover, exterior ignitions (balcony fire excluded) are rare and hence, the most likely route the flames can come into contact with the façade is either vie windows broken in an apartment fire or from balconies. (Korhonen & Hietaniemi 2005, p. 12). Therefore, the highest interest with relation to the fire safety of insulated facades is their influence on the fire spread in the case of a flashed over apartment fire.

National regulations related to the fire safety are the different for each European country; however, the main streamlines are taken at European level. This means that almost every European country has own full-scale façade fire test method and equipment for examination the façade insulation products. A big amount of national tests make producing of façade systems more expensive for industry, not to mention trade problems with façade's materials between countries of European Union based on differences in testing and classification. A common European system for products reaction to fire testing, also known as Euroclass system, was created to solve this problem.

The present European method of fire testing is based on the scenario of a fire within a room which means that it is not relevant to materials mounted outside of the room. It is focused on investigation of materials causing flashover inside the small room with ignition source. At post-flashover stage, fire plume breaks out from the windows and other openings. These high-temperature plumes can cause the spread of fire to the upper floors and finally occupy the whole building that will lead to catastrophic consequences.

Consequently, the present testing method problem can be solved by one harmonized full-scale scale fire test in Europe. For this purpose, international organization of standardization developed and published method for determining the reaction to fire of façade materials in 2002. This ISO test method (ISO 13785-2 2002, p. 1) can be one of possible alternatives, but there are still no classification criteria for its use.

1.2 The research problems and aims

A large-scale test forms a 'reference scenario' for the building component which comprises a realistic end-use configuration. (Wade 2003, p. 2). Large-scale test (ISO 13785-2 2002, p. 1) studied in this work represents a reference scenario for façade systems respectively.

The fact that Europe needs a harmonized full-scale fire test for the façades, therefore ISO 13785-2 should be further investigated. The number of performed real tests is too small to establishment of an operational database. Numerical simulation of the real test conditions could be an auxiliary tool for this purpose. The most importantly, that numerical simulation has many advantages such as unlimited usage and repeating tests without the high cost required for real full-scale experiment.

Numerical model of 13785-2 fire test may be useful for prediction the heat release rates and temperatures on facade for this reference scenario. Model can be also used for investigation the sensitivity of the exposure at the exterior wall to the physical and numerical parameters. In addition, it helps in obtaining a complete picture of test characteristics and its suitability for testing façade building products.

Despite the almost complete absence of real tests results published, simulation needs to be validated for its reliability. Therefore, the test validation stands in first place among the tasks. Briefly, problem of this work and position of simulation in testing scheme can be presented as follows:

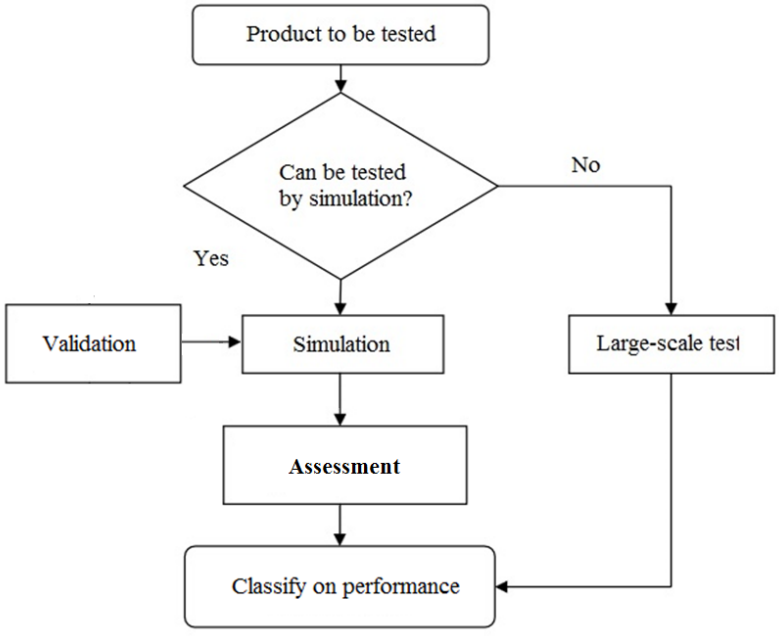

Figure 1. The principle of numerical simulation testing scheme.

Another topic of this work is to determine is the model can be used to estimation requirements for the fire protection of façade wall combustible insulation materials. Stone wool is non-organic material, that is neither burn nor ignites, and it can be used for a protection against fire exposure and spread of fire. It also can protect another insulation materials located behind it. Therefore, it is important to determine sufficient thickness of stone wool covering for different combustible façade insulation materials fabricated with polymer such as EPS, PIR, etc.

1.3 Research approach

While in the past, most fire safety design systems and specifications were based on empirical relationships, the use of CFD (Computational Fluid Dynamics) software has become an alternative mean to predict the effects of a fire (Klopovic & Turan 1998, p. 117).

In this study ISO full-scale test conditions were simulated with Fire Dynamics Simulator program, version 6 (FDS6). FDS is a CFD software developed by National Institute of Standards and Technology (NIST) and Technical Research Centre of Finland (VTT). It is a field model program related to the safety and fire engineering. It is intended for fire-driven fluid flow solving.

However, before numerical models can be used in conjunction with performance-based codes, their predictions need to be validated against full-scale experiments. (Kolbrecki 2015, p. 136). Numerical model is an imitation of the real fire. Validation checks the accuracy of results that are received from simulation. For these purposes, the experiments performed at Tokyo University by Yoshioka et al. (2012) were simulated.

According to the modelling results, this work tries to gain better understanding of the behavior of fire development of case of compartment fire with fire plume from window. In the case, when fire plumes directly determine damage to the thermal insulation materials, one of the most important parameters is the heat flux (Lu 2014, p. 14). For this purpose, this research will investigate relationships between test conditions and measurements on the façade wall such as heat fluxes and temperatures.

The absence of classification for this particular test (ISO13785-2) means the impossibility to do meaningful prediction of specimen fire performance between different scale tests. Therefore, the main objectives of the work is to access the possibility and reliability of using test ISO 13785-2 for classification of façade insulation materials, which requires identifying the sensitivity of model to test condition, surveying the expected behavior of typical insulation materials and determining the relationships between different scale test results.

This research does not explore some of the important issues related to fire on the facades such as fire spreading to the apartments above and to adjacent building or ‘leap frog effect’, because these incidents are not possible under the test conditions.

1.4 Layout of the thesis

This thesis is organized in the following way:

Chapter 2 is based on the technical literature found during writing process, which concerns to fire development in an enclosure and different ways for prediction and evaluation of the main characteristics of this fire type. Also, Chapter 2 includes a general overview on fire physics of ‘façade in fire’ specific scenario and on fire plume characteristics affecting on the façade. Materials commonly used as façade insulation and their properties are presented in Chapter 3, after which a description of used material fire tests and their simulation results are given in Chapters 4 and 5. Chapter 6 introduces the numerical solution of Large-scale façade fire test including model description, sensitivity and validation study of given problem. Results and conclusion based on the all collected information are presented in Chapters 7 and 8, respectively.

2 Thermal exposure from a compartment fire

2.1 Compartment fire development

For the better understanding of the scenario with fire coming out from the opening to façade wall, we first need to determine the fire development inside an apartment and the reasons for the flashover occurrence. This will be discussed in the current chapter.

Fire development in an enclosure can be divided into 4 stages. These phases are referred as incipient, growth, fully developed and decay phases. Rapid transition stage between growth and fully developed fire is called flashover. (Drysdale 2011, p. 350). Stages of compartment fire are shown on Figure 2.

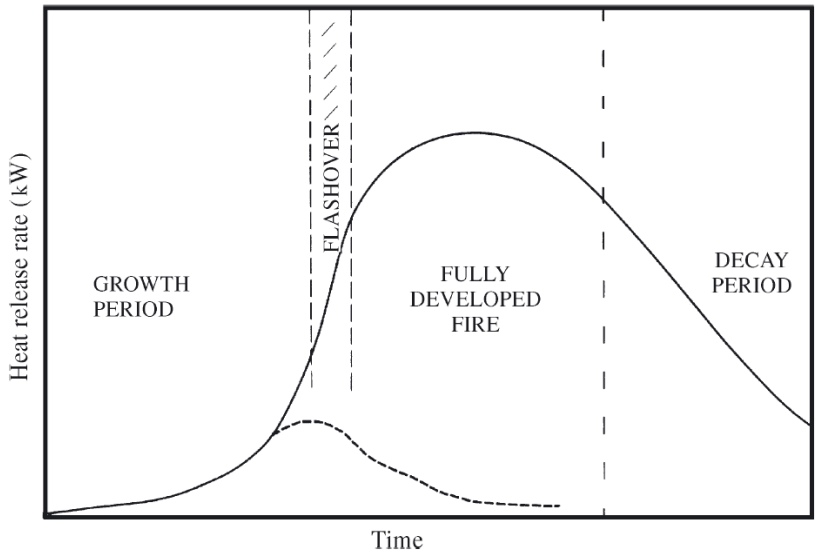

Figure 2. Compartment fire development. (Drysdale 2011, p. 350).

Figure 2 also shows the relative dependence of heat released during the whole enclosure fire process from ignition to complete attenuation. Compartment fires do not always follow the idealized fire development curve illustrated in Figure 2. Fire development depends on the ventilation profile conditions and fuel involved. Those parameters also affect to the peak of heat release rate, and duration of burning. (Chen & Lu 2012, pp. 258-265).

Incipient stage also called as 'ignition' occurs, when heat, oxygen and a fuel combine and have a chemical reaction. Combustion beginning is very delicate process. It is largely depended on the characteristics and configuration of fuel involved, so-called fuel controlled fire. (Drysdale 2011, pp. 157-349).

If there is adequate oxygen, within the compartment, additional fuel will become involved and fire continues to increase in size which contributes the heat release rate from the fire will increase. As the fire moves further into the growth stage, the dominant heat transfer mechanism within the fire compartment shifts from convection to radiation (Hartin 2008, p. 5).

Heat release rate (HRR) profile during growth stage can be presented by parabolic (t^2) or exponential fire growth model. Exponential and t^2 forms are commonly used for visualization of growth stage of fire development; neither characterization is unique and both are useful for

conveying the acceleratory nature of enclosure fire development (Mowrer 1990, pp. 367-387). The following equation presents the HRR profile based on a t^2 fire growth model:

$$Q = \alpha_f (t - t_0)^2 \quad , \tag{1}$$

where α_f is a fire growth coefficient (kW/s^2) specified by the nature of burning materials, t_0 is the length of the incubation period (s). (Drysdale 2011, p. 384).

Flashover is generally associated with enclosed spaces. It is the sudden transition from a growth stage to fully developed fire. When flashover occurs, there is a rapid transition to a state of total surface involvement of all combustible material within the compartment. Conditions for flashover are defined in a variety of different ways. In general, ceiling temperature in the compartment must reach 500-600 ºC or the heat flux to the floor of the compartment must reach 15-20 kW/m^2. When flashover occurs, temperatures throughout the enclosure reached the maximum. It is important to remember that flashover does not always occur. There must be sufficient fuel and oxygen for the fire to reach flashover. (Drysdale 2011, p. 385).

Energy release at greatest at fully-developed stage or post-flashover stage, but it is generally limited by ventilation (Figure 2). Therefore the maximum heat release rate can be presented as an expression depending on the ventilation factor. Ventilation factor was originally identified by Kawagoe (1958, p. 202) in his classic study of compartment fires. It looks as follows:

$$F_v = A \cdot H^{1/2} \tag{2}$$

where A and H are the area and height of the ventilation opening. The maximum heat release rate and mass flux in compartment at post-flashover stage are:

$$Q_{inside} = 1500 \cdot A \cdot H^{1/2} \ kW \tag{3}$$

$$\dot{m}_{air} = 0.52 \cdot A \cdot H^{1/2} \quad kg/s \tag{4}$$

The average gas temperature within a compartment during a fully developed fire ranges from 700ºC to 1200ºC. At fully developed stage all unburned gases accumulate and can frequently burn as they leave the room, resulting in flames showing from doors or windows.

A compartment fire may enter the decay stage as the available fuel is consumed or due to limited oxygen. In the decaying period, the temperature decreases gradually. Commonly the transition to the decay stage is considered to occur when the temperatures are below a nominated percentage of the maximum mean enclosure temperature (e.g. 80%). (Drysdale, 2011, p. 349). It is worth pointing out that this period is also important to the structural fire engineering because internal temperature of structure cross-section will still increase significantly even though it is the decaying period. (Ma 2000, p. 13).

2.2 Fire models based different temperature-time correlations

Experimental research can be good way for obtaining temperature-time correlations and fire resistance of a material, but these purposes can be also accomplished by analytical approach. According to the test ISO 13785-2 facade specimen is presented as vertical wall without any sloping or projections. (Side wall influence is desirable to show). The complexity of fire model greatly depends on chosen heating model and structural model. The more complicated

model used as a basis in analytical approach can do the imitation of fire more realistic. (Guo-qiang & Wang 2013, p. 7). Some alternative approaches for modelling a compartment fire are presented in Figure 3.

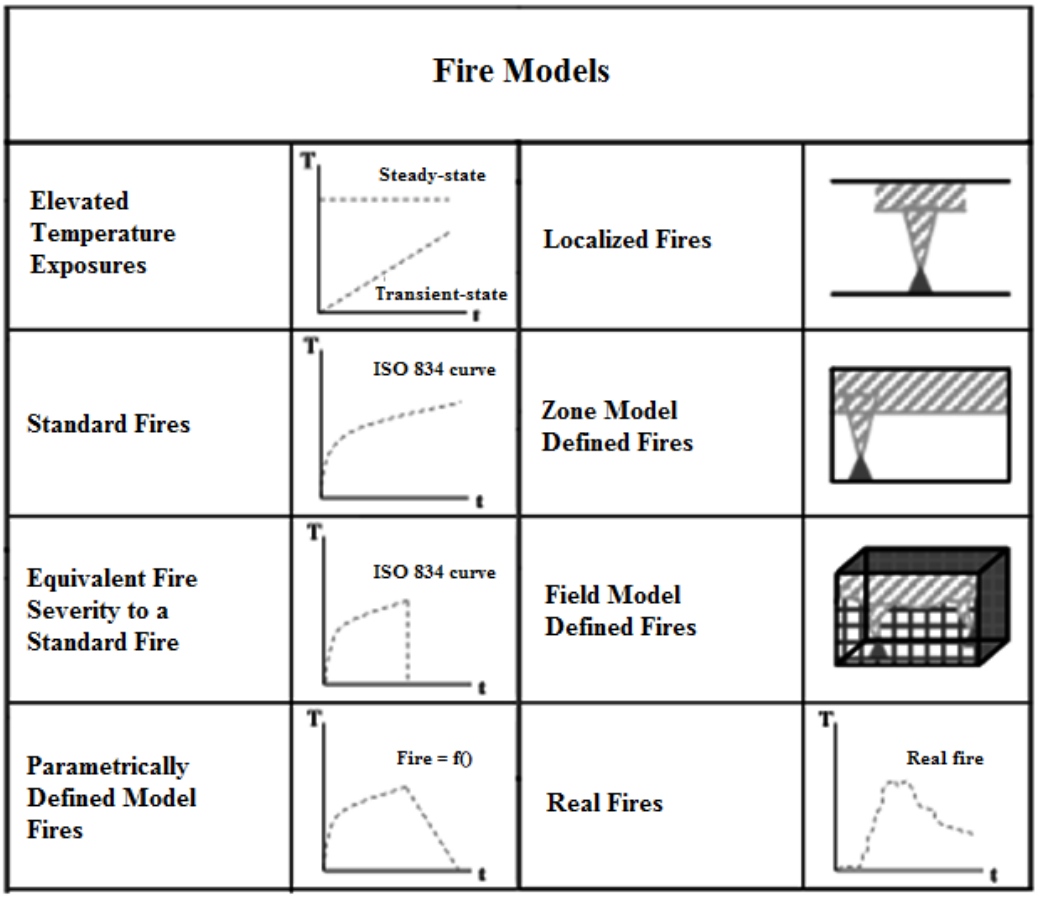

Figure 3. Fire models used in fire testing.

Elevated temperature exposures

Temperature rises linearly over time, so called transient state. At certain temperature it stops increasing and becomes to steady state.

Standard fires

Standard fire curves can be found from the European standard EN 1363-1:2012. Used in this standard fire curves are technically related to another standard ISO 834-1. So-called ISO curve, also known as cellulosic curve, is used to test the fire resistance of materials. ISO curve represents a fully developed fire in a compartment. Standard temperature-time relationship according to ISO 834 (for representing a fully developed compartment fire) is:

$$T = T_0 + 345\log(8t + 1) \qquad t > 10\,\text{min} \tag{5}$$

Another temperature-time curve to representing standard fire is BS 476 curve. This curve can be represented with following equation:

$$T = T_0 + 345\log(0.133 \cdot T + 1) \tag{6}$$

where T_0 is the temperature in the compartment at the start of the fire (usually 20ºC). The only difference from ISO curve, that time (t) is presented in seconds. (Blagojevich, 2011, p. 340).

Equivalent Fire

The equivalent fire model is based on the standard fire curve, but the duration of the fire exposure is determined by the equivalent fire duration time. The duration time depends on the characteristics of the compartment, most importantly on the fire load, internal surface and openings area. (Guoqiang & Wang 2013, p. 7).

Parametric fire curves

Parametric fire is described by a temperature-time curve, which however depends on a considerable number of environmental parameters and therefore provides a more realistic approach to how a fire hazard develops and evolves. A parametric fire curve takes into account the compartment's ventilation conditions and thermal properties of its bounding walls. Parametric fire curves furthermore, consider the fire's decay phase, thus allowing for a temperature decrease once the fire load has been exhausted. As temperatures are assumed to be uniformly distributed within the compartment, those fire models should in principle only be applied to compartments of a moderate size. Parametric fires are valid for the compartments up to 500 m^2 of floor area, with maximum height of 4 m and without openings in the roof. (Blagojevich 2011, p. 342). Some recent publications point out that the uniform temperature assumption is not quite correct (Stern-Gottfried 2010, pp. 249-261).

A typical parametric fire curve in accordance with BS EN 1991-1-2 is shown on Figure 4, on the left side. A complete fire curve comprises a heating phase represented by an exponential curve that lasts until it reaches a maximum temperature T_{max}., followed by a linearly decreasing cooling phase until a residual temperature (usually the ambient temperature). The maximal temperature T_{max} and fire duration t_{max} are two primary factors affecting the behavior of a structure in fire.

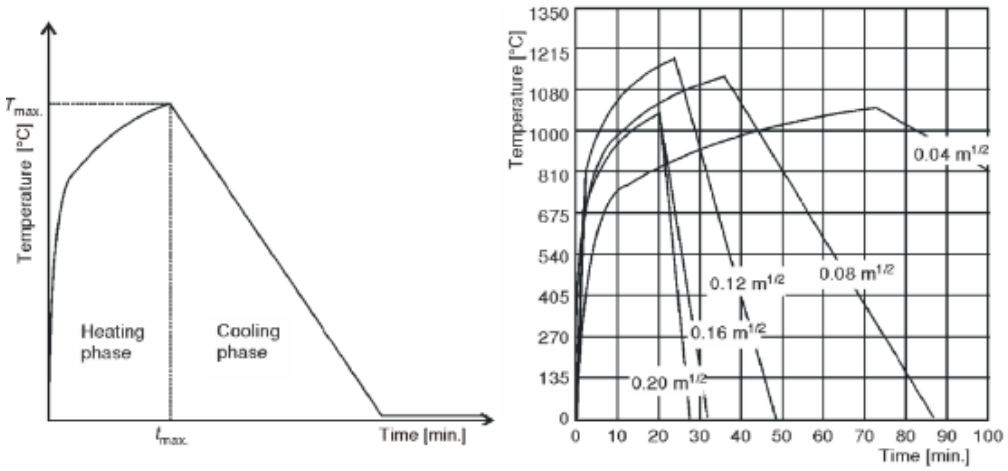

Figure 4. Parametric fire curves.
(Blagojevich 2011, 342).

The parametric curves for compartment with area of 300 m^2 and fire load of 800 MJ/m^2, are shown on the right side in Figure 4. Shape of those curves depends on the opening factor (0.04 $m^{1/2}$, 0.08 $m^{1/2}$, etc.). (Blagojevich 2011, p. 342).

Localized fires

Localized fire model consists of two region. They are the combustion (flame) region and the non-combustion (plume) region. Figure 5 shows schematically this fire model structure.

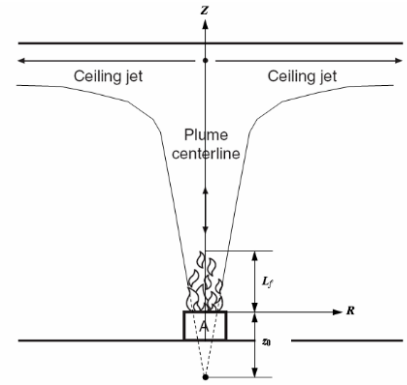

Figure 5. Illustration of the Localized Fire Model. (Zhang 2012, p. 125).

In Figure 5, hot gas rises through the plume region to the ceiling and generates a thin layer below the ceiling. Both temperature and speed can be solved by the classic plume theory. This model takes into account plume temperature and air velocities and for this reason widely used in smoke control calculation, but is not relevant in this study. (Zhang 2012, p. 125).

Zone model defined fires

Zone models divide an enclosure into one, two or more zones. Zone model assumes that each zone has homogeneous properties. The most frequently used zone models are the single and two-layer zone models. (Zhang & Hadjisophocleous 2012, p. 63). Two zones model includes upper and lower layers. The upper level consists from combustion products. Heated combustion products increase the temperature of this zone. The lower layer is composed of cool air and this zone is relatively free of combustion products. (Gorbett 2008, p. 25).

Two-zone model assumes a clear separation between the two zones and assume that they are well mixed. This means that the conditions within each layer are constant. (Gorbett 2008, p. 25).

Many of the models include prediction of room furnishings characteristics. Outputs typically include prediction of sprinkler or fire alarm activation time, time to flashover, upper and lower temperatures, the height of the interface between the upper and lower layers, and combustion gas concentrations. Zone room fire models are available from several sources including the NIST. (Gorbett 2008, p. 25).

Field model defined fires

Computational fluid dynamics model (CFD) is the second name of field models. In these models, the computational domain is divided into small three-dimensional cells. Cell size varies from millimeters to meters depending on the size of the domain, preferred accuracy of results, available computational resources and time. Field models are based on the basis laws of mass, momentum, and energy conservation. (Gorbett 2008, p. 26).

The properties within each cell are usually assumed to be constant in field models. The conditions in the enclosure can be predicted in much greater detail, because of larger number of

cells than in zone models. Field models are capable of predicting the conditions in both large and small spaces, in spaces with complex shapes, and in complex multiple room configurations that are not possible with zone models. (Putorti 1998, pp. 1-2). An advanced field model, specifically designed for the fire safety analysis is Fire Dynamics Simulator (FDS).

Real Fires

The real fire model directly simulates fire development with consideration for the actual characteristics of the compartment.

2.3 Heat flux profiles on façade

2.3.1 Overview on analytical model development history

Façade flame behavior is recently extensively investigated. Yokoi investigated the characteristics of a buoyant fire plume ejecting from window during enclosure fires. He established the spill fire plume dimensionless temperature distribution model. (Yokoi 1960, pp. 89-102). As a model room for experiments he used a rectangular made of steel-plate, having an opening on one vertical plane room with dimensions 40 x 40 cm in square ground plane area, and 20 cm in height. Openings had various dimensions. (Yokoi 1960, p. 83). The most common form of Yokoi's non-dimensional temperature is defined as:

$$\Theta = \left(\frac{\Delta T / T_\infty}{Q_D^{*2/3}} \right) / \left(\frac{T}{T_\infty} \right)^{2/3} \tag{7}$$

where T_∞ is ambient temperature, ΔT is the temperature rise and Q_D is the non-dimensional heat flow rate of window jet defined as:

$$Q_D^* = \frac{Q_D}{c_p \rho_\infty T_\infty \sqrt{g} r^{5/2}} \tag{8}$$

Here ρ_∞ is the ambient air density. (Yamaguchi 2005, p. 18).

After Yokoi's study, several works were carried out to investigate the façade fire behavior under different outside constraints and boundary conditions. Oleszkiewics conducted a series of full-scale experiments with different window dimensions and heat release rates (HRR). Research showed a significant drop in heat transfer to the façade when a horizontal projection was deployed immediately above the opening. It was also found that a narrow window causes a small heat flux upon the façade wall. (Oleszkiewics 1989, pp. 163-170). and (Oleszkiewics 1990, pp. 357-375).

Yamaguchi et al. conducted small scale cubic fire compartment experiments to study the effect of window eave on the spill plume behavior. Figure 6 shows examples of the non-dimensional temperature profiles of the window jet plumes from windows with eaves. (Yamaguchi 2005, pp. 28-29). Figure 6 shows that as the width of eaves becomes large, the window jet plume axis is kept more remote away from the surface of the wall.

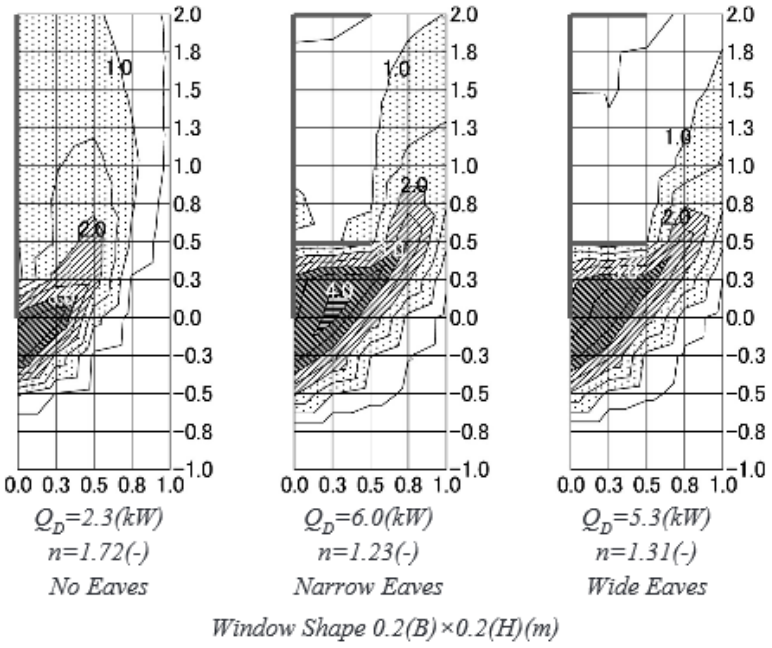

Figure 6. Non-dimensional isotherms.
(Yamaguchi 2005, p. 29).

Himoto et al. did a theoretical and experimental analysis to predict the trajectory of window ejected flame from a fire rooms. (Himoto et al. 2009, pp. 250-258).

Lee et al. have proposed non-dimensional flame height and heat flux formula considering the window dimension effect. The effect of an opposite building on the flame height and heat fluxes upon façade wall was also considered. (Lee et al. 2007, pp. 2521-2528).

Ohmiya et al. found that the heat flux profile upon the façade wall is determined by the façade flame height as well as the heat accumulation near the window. (Ohmiya 2003, pp. 121-129).

Cheng and Hadjisophocleous studied the impact of different window sizes, separation distances between the fire building and a target wall, and different fuels on the radiation heat fluxes on target wall. They also presented a modelling of radiation heat flux on target wall from post-flashover compartment fire. (Cheng & Hadjisophocleous 2012).

Huang et al. studied the effect of the external wind conditions on the compartment fire growth. They found that the external wind has two opposing effects. One is to promote combustion within the compartment, thus raising the temperature, the other is to blow away and dilute the combustible gases in the compartment and decrease the temperature, thus hastening its extinction. Which effect dominates depends on the approaching wind velocity, the position of the fuel, and the geometry of the opening and compartment. When the approaching wind velocity is high, the ejected plume is greatly inclined to the downwind side, and the flame becomes wider. Also was observed that the dimensionless temperature of the ejected flame was a little lower than the results from Yokoi's experiments without wind. (Huang et al. 2009, pp. 311-321).

The effect of side wall constraints has also been addressed, showing that the presence of side wall cannot influence the temperature inside the enclosure and the critical heat release rate $1500A\sqrt{H}$ kW. Recently, Sun et al. have mentioned experiments on the facade flame heights with side walls based on a small-scale model of 0.4 m cubic as well as scaling analysis on the

plume entrainment change due to the side walls. They found that the side walls can restrict the entrainment from side direction so that for "(half) axisymmetric fire" the facade flame height changed with side walls separation distance. The study on the effect of facing wall was also mentioned. It was found that when the distance from the facing wall to the facade decreased to a critical value, the entrainment from front direction was strongly restricted and the facade flame height was increased. (Sun et al. 2013).

2.3.2 The common model of the heat flux on facade

In this model the heat flux profile is divided into three regimes (continuous flame region, intermittent flame region, and convective region) based on the normalized height Z/Z_f, where Z_f is the flame height. For continuous flame region, where $Z/Z_f \leq 0.8$, the heat flux is dominated by the flame radiation and remains relatively constant. For the intermittent flame region, where $0.8 < Z/Z_f < 1.3$, the heat flux starts to decrease vertically due to the combined effect of flame radiation and convection. The region of $Z/Z_f \geq 1.3$ is defined as the buoyant plume regime above the flame tip where the heat flux is dominated by convection. (Lee 2006, pp. 2-30). Flame regions positions is demonstrated on the Figure 7. The neutral plane in this model is about *0.4H* above the bottom of the window, where H is the height of the window.

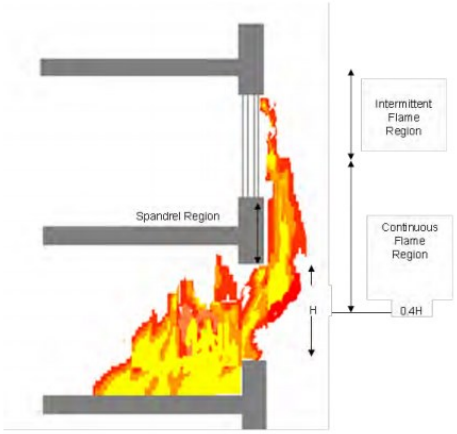

Figure 7. Flame model on façade wall. (Delichatsios 2013, p. 8).

2.3.3 Heat flux profile on a façade without side wall

The venting flames and the risk they pose to the external façade are greatest during the fully developed phase of the fire (Law, 1991, pp. 147-153). Lee et al (2009) and Tang et al. (2012) proposed the following basic non-dimensional formula for the heat flux profile upon the façade wall due to the window-ejected flame:

$$\frac{\dot{q}'' Z_f}{\dot{Q}_{ex}/l_1} e^{0.6(H/l_1)} \propto function\left(\frac{Z}{Z_f}\right) \tag{9}$$

where $\dot{q}''$ is the total heat flux to the façade wall, H is the height of the window, and Z and Z_f are the vertical position on the façade and the mean flame height from the neutral plane (about *0.4H* above the bottom of the window) of the window, respectively.

Outflow from the compartment determines two length scales (one parallel and the other normal to the opening) in characterizing the geometry of the origin of spill plume. Correlations of the flame height have shown that the one of them is sufficient for correlating the flame heights because their ratio is a weak function of the window aspect ratio. Characteristic length scale is determined as:

$$l_1 = (A\sqrt{H})^{2/5} \tag{10}$$

(Tang 2012, pp. 93-101).

Moreover, for an under-ventilated condition, the total combustion HRR ($\dot{Q}$) can be divided into two parts. The heat released inside the compartment ($\dot{Q}_{inside}$) contributed by the fuel reaction with inflow fresh air into the compartment through the window, and $\dot{Q}_{ex}$, the excess HRR due to the burning of excess fuel outside the compartment. Then, $\dot{Q}_{ex}$ defined as:

$$\dot{Q}_{ex} = \dot{Q} - \dot{Q}_{inside} \tag{11}$$

Total combustion heat release rate ($\dot{Q}$) is determined from equation of air mass inflow rate for under/ventilated conditions in the following way for normal atmospheric pressure:

Air mass inflow ($\dot{m}_{air}$):

$$0.133\rho_\infty A\sqrt{gH} = 0.5A\sqrt{H} \quad \textit{(kg/s)} \tag{12}$$

Heat release inside the enclosure ($\dot{Q}_{inside}$):

$$0.133\frac{\Delta H_{oxygen}}{c_p T_\infty} c_p T_\infty \rho_\infty A\sqrt{gH} = 3000 * 0.5A\sqrt{H} = 1500A\sqrt{H} \quad \textit{(kW)} \tag{13}$$

The calculation of heat flux for ISO 13785-2 standard conditions is presented in Appendix 14.

2.3.4 Heat flux profile on a façade with side wall

This chapter investigates the heat flux profile upon the building façade with side wall constraints. The radiation heat from surface of side walls heated may also influence the heat flux. This kind of effect is much less that of flames because of two factors: the flame temperature is much higher compared with the surface of side wall and almost all of thermal energy that impinges on the side wall is emitted. The change of heat flux upon the façade wall is mainly depended on the different façade flame height for various side wall separation distances and the influence of radiation heat from side walls can be neglected. (Lu 2014, p. 19).

Lu et al. (2014) were concluded that there are two different behavioural regimes for the effect of presence of side wall on the heat flux upon the façade. Heat flux increases for relatively small windows where non-dimensional excess heat release rate $Q_D^* \geq 1.3$ with decreasing in side walls separation distance (‘half’ axisymmetric fire regime). At the same time heat flux remains almost unchanged from the side walls separation distance for relative large windows

where $Q_D^* < 1.3$ (wall fire regime). The dimensionless excess heat release rate is calculated according to equation 8.

A global formula for characterizing the vertical profile of heat flux with presence of side walls based on Lee's model.

$$\frac{\dot{q}_t'' \times Z_{f,D}}{\dot{Q}_{ex} / l_1} \times e^{(0.6\times(\frac{H}{l_1})\times(1-\frac{l_1}{D}))} \propto function(\frac{Z}{Z_{f,D}}) \tag{14}$$

Where $\dot{q}_t''$ is the total heat flux to the façade wall, H is the height of the window, D is side wall separation distance, and Z and $Z_{f,D}$ are the vertical position on the façade and the mean flame height with side wall distance of D.

With the increase in the separation distance of side walls, the new term approaches to $e^{0.6\times\frac{H}{l_1}}$ and is identical to the original model of Lee. This formula is based on the experiments in Lu's study (Lu 2014, pp. 14-22) for $H=B$ and $H>B$ cases. In the same study author propose that it should be also applicable for $H<B$ case, because it based on Lee's original model (Lee et al. 2007).

2.3.5 Heat flux profile with different size of window

In Appendix 1 is presented heat flux profile upon the facade for various window geometric dimensions with different total HRR (Heat Release Rate). The heat flux decreases with height vertically and increases with total heat release rate; and the heat flux is lower for relative larger window.

As for the heat flux profile upon the facade wall above the flame tip, the heat transferred to the facade wall is dominated by convection located in pure buoyancy plume region. So the heat flux profile upon the facade above the flame tip can be calculated by the following convective heat expression

$$\dot{q}'' = h_c(\Delta T) \tag{15}$$

As the convection coefficient for buoyant turbulent plume flow region is nearly a 1/3 power of the temperature rise, Equation can be expressed by

$$\dot{q}'' \propto (\Delta T)^{4/3} \tag{16}$$

(Lee 2006, p. 40).

In high-rise building fires flame can be observed to eject from the window of a room after flashover and then spread to upper floors, leading to catastrophic loss of casualties and properties. Behaviors of façade fire plume ejected out of the window over the building façade have received focused attentions in the last decades. One of the most important parameters is the heat flux upon the building façade wall due to the exposure of ejected fire plumes which directly determines damage to the thermal insulation materials as well as the vertical fire spread along the building façade. (Lu 2014, p. 14).

3 Materials and Methods

Over the last years, the requirements for the thermal insulation of buildings in Finland have been increased. The present day's thermal insulation must have some important features as high thermal resistance and small thickness as far as possible.

According to Dujive (2012, p. 7), glass- and rock wool (also mineral wool) together with Expanded Polystyrene (EPS) are the most suitable insulating materials for application within Passive house renovation. This is because of the fact that for both mineral wool (glass wool and stone wool) and EPS, multiple end-of-life scenarios are available. EPS can be recycled or incinerated, whereas mineral wool can be recycled into new mineral wool, but also into other products such as façade panels or sound insulation. For both EPS and mineral wool recycling facilities are already in place and used in practice. Materials such as PIR do not have these recycling options yet, which leaves incineration as the end-of-life solution. (Duijve 2012, p. 7).

From a health point of view, both EPS and mineral wool should be improved further. Especially the formaldehyde based binders used in mineral wool and the fire retardant hexabromocyclododecane used in EPS should be replaced by other materials on a short term (Duijve 2012, p. 7), but in the first instance insulation materials must meet fire safety requirements. Fire resistance of materials including insulations can be classified according to SFS-EN 13501-1 which will be discussed further.

3.1 European Fire Classification of Materials

Since the beginning of 2007 in Finland, building materials must be tested for their reaction to fire. Testing based data can be used for classification according to SFS 13501-1. This publication includes requirements for building surface materials, such as ceiling to have a certain reaction to fire performance when in direct contact with fire. As shown in Table 1, there are seven main categories of construction materials. (SFS-EN 13501-1:2009, p. 7).

Table 1. European fire classification of buildings materials. (SFS EN 13501-1:2009).

A1 A2	Non-combustible
B	Material of limited combustibility
C	Combusts in a period of 10-20 minutes
D	Combusts in a period of 2-10 minutes
E	Combust in a period of 2 minutes
F	Material provides no resistance to fire

Ranks vary from class A1 to F, depending on the reaction to fire of testing material. In addition to these main groups, SFS-EN 13501-1 also has some additional classifications of material with regard to the production of smoke and formation of flaming droplets/particles. This classification is presented in Table 2.

Table 2. Additional fire classification for materials. (SFS-EN 13501-1).

s1	No/Hardly any smoke production
s2	Limited smoke production
s3	Unlimited smoke production
d0	No flaming droplets/particles occur
d1	Limited droplets
d2	Many droplets

The national building code of Finland E1 set requirements for the external surface of façade wall or for ventilation gap surface, if it is located there. In residential or office buildings of class P2 external walls and the external surfaces of ventilation gaps have to respond to protective cladding requirements, if external wall consists of building materials that are not at least A2-s1, d0-class. (E1 2011, pp. 24-25).

Table 3. Class requirements for surfaces of external walls and ventilation gaps. (E1 2011, table.8.3.4, p. 24).

	Fire class and use of the building					
	P1		**P2**			**P3**
	Buildings of class P1 in general	Residential and office premises with not more than 8 storeys	Institutions	Residential and office premises with 3–8 storeys	Other buildings of class P2	
External surface of external wall	B-s1, d0 [1)]	B-s2, d0 [2)]	B-s2, d0	B-s2, d0 [2)]	D-s2, d2	D-s2, d2
External surface of ventilation gap	B-s1, d0 [1)]	B-s2, d0 [2)]	B-s2, d0	B-s2, d0 [2)]	D-s2, d2	D-s2, d2
Internal surface of ventilation gap	B-s1, d0	B-s1, d0	B-s1, d0	A2-s1, d0	D-s2, d2	-

Symbol in the Table: — = no requirement

Notes to the Table:

1) In buildings of class P1 with not more than 8 storeys, a part of the external surface of the external walls may be of class D-s2, d2, if the constructions surrounding such parts protect the wall surface from the spread of fire. Building materials of class D-s2, d2 may be used to a small extent for the fixing of facade boards in buildings of not more than 8 storeys.

In production and storage buildings of class P1 and assembly and comercial buildings of class P1 with not more than 2 storeys building materials of class D-s2, d2 may be used to the external wall and external surface of ventilation gap, if:
- the height of the building is not more than 20 meters,
- external wall window s and other s openings fill the EI 30 requirement,
- caused by external ignition fire spreading to the wall is prevented effectively enough and
- fire spreading from the facade to the attic and the roof is prevented with EI 30 construction.

2) The use of building materials of class D-s2, d2 is permitted under these provisions:
In buildings with an automatic extinguishing system such as in residential or office buildings of class P1 with not more than 4 storeys, residential or office buildings of lcass P2 with 3-8 storeys and institutional buildings of class P2, materials of class D-s2, d2 may be used for the external surfaces of external walls and the external surfaces of ventilation gaps at the lower floor of the building or for surface at the top and the bottom of exit or escape operating windows and for other openings, except when:
- the spread of fire through ventilation gap is limited sufficiently at least on each floor,
- the spread of fire in horizontal direction to the ventilation gap of the stairwell external wall is blocked,
- the spread of fire across the facade to the attic and roof is blocked in EI 30 structures,
- falls of major parts of the facade structure at fire case is sufficiently prevented and
- buildings or structures will not be placed less than 8 meters from the facade, if the fire spreading doesn't prevented by other methods.

3.2 Types of façade insulation materials

3.2.1 Expanded polystyrene (EPS)

Expanded polystyrene (EPS) is insulation material made from synthetic aromatic polymer. It can be produced by pressing polystyrene grains into molds expanded under steam or in hot water with the help of steam again. (Yucel et al. 2003, p. 3).

Hard polystyrene foam materials contain nearly 98% air. Because of motionless air low thermal conductivity rate, EPS has good insulation characteristics. Other 2% of foam total volume is the foam skeleton. In addition to this, the polystyrene material that transfers the heat is a very insulating material. Because of the fact that Polystyrene Foam Material takes form from very little ($1m^3$ EPS Polystyrene Foam material consists of 3-6 billion cells) closed cells: 0.01-0.1 mm in diameter, the conduction rate of heat by air movement decreases with more little cell volumes thus from the side of insulation technique, it is good insulating material. (Yucel et al. 2003, pp. 3-4). Cell structure of EPS is presented in the following figure.

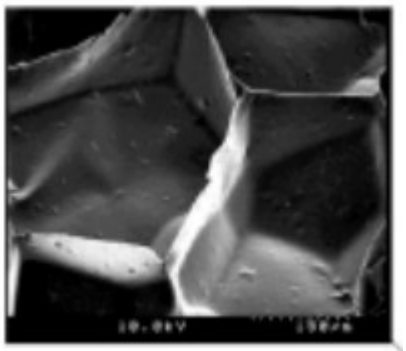

Figure 8. EPS cell structure. (Yucel et al. 2003, p. 3).

More number of laminates can prevent heat rays best. First, the property that takes attention is the unit weight of polystyrene foam material is less. The weight of foam material that is obtained by kinds of methods with pre swelling is varying from 10-100 kg/m3. Also thermal conductivity value varies according to production density. Generally, the standard foam material that is used at construction sites has a density of 10 - 30 kg/m3. (Yucel et al. 2003, p. 3).

The grey EPS with density of 18 kg/m^3 was used for testing in this study. Photos of testing sample taken before the test are presented in Appendix 15. Other parameters that have been determined in the flammability tests are presented in Chapter 4.

3.2.2 Polyisocyanurate (PIR)

The common used thermoset foam used as rigid thermal insulation is polyisocyanurate. It is also referred to as PIR. PIR is essentially an improvement on polyurethane foam. Its chemical content is quite similar to regular polyurethane except that the proportion of methylene diphenyl di-isocyanate (MDI) is higher and a special polyol is used in the reaction instead of a polyether polyol. Catalysts and additives used in PIR formulations also differ

from those used in regular polyurethane. (HuYa, Rigid PIR foam thermal insulation boards, 2015).

Polyisocyanurate insulation products are highly effective, lightweight and many have the ability to bond to most materials. Thermal conductivity of PIR has a typical value of 0.023 W/(m·K) (Celotex GA4000, PIR specification, 2015).

PIR foam panels are often laminated with aluminum foil or fire retardant covering. Prefabricated PIR sandwich panels are manufactured with corrosion protected, corrugated steel facings bonded to a core of PIR foam and used extensively as roofing insulation and vertical walls. (American Chemistry Council, Foam Sheathing Materials and Properties, 2015). Aluminum foil covering protects insulation using its reflective properties, while some retardant coverings protects by increasing its thickness at the high temperature.

In current study samples of PIR with density of 31 kg/m^3 were used for the material testing. Photos of samples can be found in Appendix 15. Firstly, PIR was tested without aluminum covering, and then with fire retardant covering (COV). Results of tests are in Chapter 4.

3.2.3 Stone wool

Stone wool is a fibrous, glassy material which is used as a thermal and acoustical isolator. Untreated stone wool is completely amorphous. Since the main components of stone wool are SiO_2, Al_2O_3, CaO, MgO and FeO, it is an alkaline earth alumosilicate glass. The positive charge of the earth alkaline cations is neutralized by the substitutions of Si^{4+} by Al^{3+} in the tetrahedral sites (Moesgaard & Pedersen 2005). Since the concentration of Al is lower than that of Ca, Fe and Mg, Al occupies tetrahedral positions (Shelby 2005).

A mixture of basalt, limestone, recycling products and dolomite is used as a raw material. Together with additives like olivine, bauxite or slags they are melted in a cupola furnace (Moesgaard & Pedersen, 2005). In the stone wool production plant the raw materials are usually pressed to briquettes before the melting process. During the process an exsolution of two melts occurs: One metallic iron melt which sinks down to the bottom of the furnace and which must be removed frequently and a silicate melt which is the basis for the fibre formation (Kirkegaard & Korsgaard 2004). The silicate melt flows throught an opening out of the tank onto a winder of spinning wheels whose centrifugal force converts the melt droplets into fibres while they freeze into glass (Moesgaard & Pedersen 2005).

The cooling rate accounts for 10^6 K/s (Pakosch 2006). An air flow spins blows the fibres into a spin chamber where they are coated with a phenolic resin which acts as a binder. In the future also inorganic binders might be used (Kirkegaard & Korsgaard 2004). During the finishing process they are sprayed with silane (SiH_4) to improve the coherence between the fibres and their coating. After the coating has dried the stone wool can be cut, packed and sold (Moesgaard & Pedersen 2005).

In this work, the stone wool sample was manufactured by Paroc. The density of the wool was 100 kg/m^3.

3.3 Experimental methods

3.3.1 Large-scale façade fire test ISO 13785-2

Large-scale façade fire test exists to replicate a real fire scenario of fire incoming from an opening at post-flashover stage or when fire is fully developed and limited by ventilation. The major number of full-scale test is in using at this time. The most popular from them are: CAN/ULC S134-92 (CAN/ULC), NFPA 285, (NFPA), the Swedish façade fire test SP-105 (SP Fire 105) and the most recent method ISO 13785-2 (ISO 13785-2:2002). These tests can vary in test duration time and each of them imply different heat flux exposure to the façade specimen.

The most recently added large-scale test is ISO 13785-2, which will be analyzed further in this work. This test was developed by ISO standard association and internationally agreed. Might be expected that this test replace the others available large-scale test mentioned above.

ISO 13785-2, which full name is reaction-to-fire test for facades – part 2: Large scale test, prescribes a test method which can evaluate the effects of fire on the exterior material installed onto the outer wall when heated by the flame issuing from the broken window. (ISO 13785-2:2002).

The ISO 13785-2 standard describes a test facility consisting from combustion chamber, facade specimen with side wall, opening and measurement devices. Combustion chamber has volume in range 20-100 m^3. Both façade specimen and combustion chamber have an opening with following dimensions: 2 m wide by 1.2 m high. Façade wall extend up to 4 m above the top edge of window, therefore the total height of apparatus reaches 5.7 m. Vertical side wall (wing) is 1.2 m wide with same height as main façade specimen. (ISO 13785-2:2002).

According to ISO 13785-2 standard any fuel can be used to produce a window flame which exposes the test specimen to heat flux of 55±5 kW/m^2 at a height of 0.5 m above the opening, and 35±5 kW/m^2 at a height of 1.5 m above the top opening. Heat fluxes are measured at 3.5 m above the top of the window, and thermocouples are installed at the top of the test specimen and at the top of the window opening. Evaluation or performance criteria are not included in the standard. (ISO 13785-2:2002).

3.3.1.1 Fire source

According to ISO 13785-2 (Annex A), propane gas with 95% purity may be applied as fuel for testing. Propane burner consists of perforated steel pipes which positions are uniformly distributed in the room. These four burner pipes with diameter of 100 mm and long of 3700 mm are insulated with 25 mm thick ceramic fiber insulation. Fuel flow rate reaches its maximum after 5 minutes from starting the test. Figure 9 shows the fuel flow rate of the standard propane ignition source during the whole test. (ISO 13785-2:2002, p. 11).

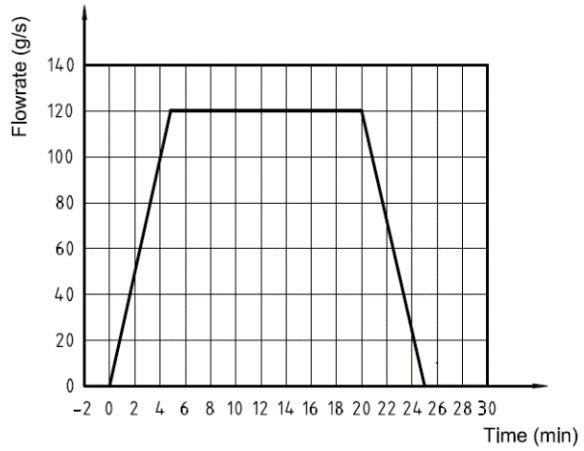

Figure 9. Fuel flow rate. (ISO 13785-2:2002, p. 12).

Width of the combustion room is not the constant by the standard, but positions on burner pipes are schematically look like on the Figure 10.

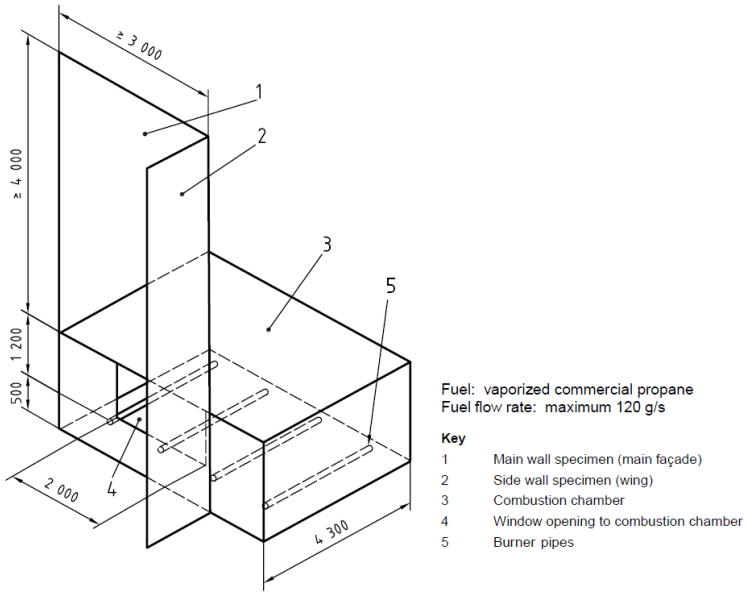

Figure 10. Dimensions of test facilities and ignition source location.

Heat release rate provided by the fire source can be determined by the following equation:

$$\dot{Q} = \chi \dot{m}_{fuel} \Delta H_c \tag{17}$$

(Drysdale 2011, p. 20)

Where mass flow $\dot{m}_{fuel}$ is equal to 120 g/s (ISO 13785-2:2002, p. 5). For propane, the products would comprise only carbon dioxide and water, as indicated in the stoichiometric equation:

$$C_3H_8 + 5O_2 \rightarrow 3CO_2 + 4H_2O \tag{18}$$

The lower heat of combustion value for propane is $\Delta H_c = 46400$ kJ/kg (Drysdale 2011, p. 21). Depending from the source, combustion efficiency may vary for propane from 0.9 to 1.0. For example, Tewarson gives χ=0.9 for the combustion efficiency of propane (Tewarson

1995, p. 53). However, in this case of façade fire testing, almost perfect combustion occurs, so for combustion efficiency is taken 1.0 value. Altogether, with regard to the maximum flow rate of propane gas, heat released by combustion of propane gas is equal to 5.6 MW at the maximum situation.

3.3.1.2 Test facility

ISO 13785-2 test facility consists from combustion chamber, façade test specimen and equipment for measurement. Dimensions of the combustion chamber are 3 m wide by 1.7 m high. The length of combustion chamber is not specified. The façade test specimen with high of 5.7m and wide of 3m has a side wall, so-called 'wing', with same high and wide of 1.2 m. Devices for heat flux and temperature measurement located on the façade wall by following way:

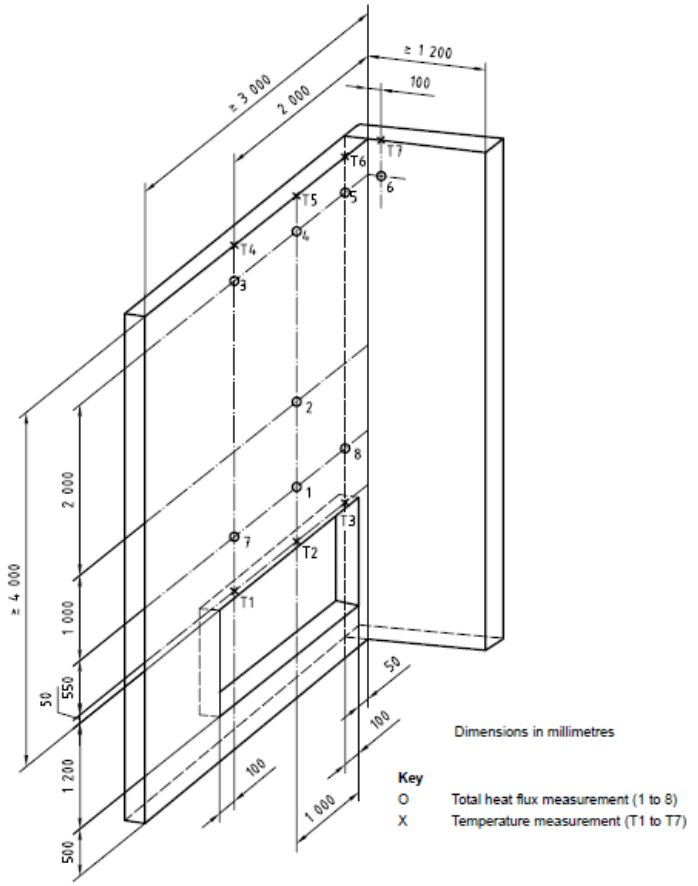

Figure 11. Positions of measuring instruments. (ISO 13785-2:2002, p. 5).

In Figure 11, positions of temperature measuring units are marked with crosses, heat fluxes - by circles. Majority of the devices are located on main façade, but two of them are positioned on the top of side wall. The sensors of the heat flux gauges should be flush with the façade wall. (ISO 13785-2:2002, pp. 2-8).

3.3.2 Flammability tests

3.3.2.1 Thermogravimetric analysis (TGA)

TGA analysis is widely used technique for the determination of burning processes occurring in material under isothermal or non-isothermal conditions. TGA thermal analysis provides determination of weight loss of sample while it is heated. There is a different variation of this test, because except heating test, sample also can be tested isothermally or by cooling in defined atmosphere. Sample size using in TGA test is in range 10-15 mg. (ISO 11358-1:2014).

Performed TGA tests related to this study were made in nitrogen atmosphere. Inert atmosphere helps more accurately define the pyrolysis reaction. Pyrolysis is one of the first step of all thermochemical process occurring in an inert atmosphere.
Pyrolysis is a thermal decomposition process, in which materials complex organic compounds or other chemical bonds break or decompose to gaseous products such as water, carbon dioxide or hydrocarbons. The TGA provide details of the pyrolysis reaction of the material as a function of temperature. (Slopiecka 2011, p. 1687).

The rate of pyrolysis reaction can be abstracted from TGA analysis using the first derivative of the TGA curve with respect to time. This curve is known as the differential mass loss (DTG) curve and it is proportional to the rate of decomposition reaction.

Threshold temperature of decomposition reaction starting, reference temperature related to the peak of chemical reaction rate is the most important parameters, which can be extracted using TGA test analysis.

3.3.2.2 Differential Scanning Calorimetry (DSC)

The experimental data from TGA and DSC referred to this research was received by Simultaneous thermal analysis (STA) test. STA includes application of thermogravimetry (TGA) and differential scanning calorimetry (DSC) and allow performing them at one sample at the same time.

The caloric reactions of the sample can be determined by DSC test. According to this test the rate and degree of heat change can be evaluate as a function of temperature. This is possible because during regulated temperature increasing, DSC test apparatus notices any heat energy uptake, which means material enthalpic changes. This analytical technique is used in understanding of the thermal properties of materials. (Kim & Quintiere 2007).

3.3.2.3 Microscale Combustion Calorimeter (MCC)

Microscale combustion calorimetry (MCC) has recently been developed to measure flammability parameters of very small samples. The sample weight is a few milligrams. The method simulates flaming combustion by pyrolyzing material in a N_2 atmosphere to produce fuel gases which are subsequently oxidized in an O2 rich atmosphere. (US Patent 5981290).

MCC apparatus measures residual oxygen in the combustion gases on the basis of that heat released during flaming can be obtained. According to Walters study (2015), this test method can be also modified to measure carbon dioxide (CO_2) and carbon monoxide (CO) concentrations in combustion products using infrared carbon monoxide and carbon dioxide analyzers

inserted into the gas stream to allow compositional analysis of the combustion gases. (Walters 2015).

The most important flammability parameter of a material measured in the MCC is the heat released during combustion. In the most cases, measuring HRR for a material and determining HRR* for a particular fire test will be more difficult than simply conducting the fire test itself (US Patent 5981290).

3.3.2.4 Cone calorimeter test

The cone calorimeter is a modern device used to study the fire behavior of small square samples (10x10cm) of various materials in condensed phase. The cone calorimeter is a fire testing device based on the principle of oxygen consumption during combustion. It is widely used bench scale instrument in the field of Fire Safety Engineering. This device has been approved by International Organization for Standardization for measuring heat release rate of a sample. (ISO 5660-1:2002).

According to Figure 12, cone calorimeter has a radiant electric heater. Shape of heater is truncated cone, because of that test got its name. Radiant heater can provide constant exposure to the specimen with heat flux up to 100 kW/m^2. Group of thermocouples located in contact with heating coil measure the heater temperature by average value of them. (Ezinwa 2009, p. 17).

Figure 12. The Cone calorimeter. (Ezinwa 2009, p. 18).

Cone calorimeter measures the heat release rate using a method called oxygen consumption calorimetry, developed by Huggett. The heat released from a fuel is directly proportional to the amount of consumed oxygen. According to the Hugget's study, most hydrocarbon fuels have almost the same value for heat of combustion (13.1 MJ/kg with 5% accuracy). The following equation shows, how cone calorimeter software calculates the heat release rate:

$$\dot{q} = (13.1 \cdot 10^3) \cdot 1.10C \frac{0.2095 - X_{O_2}}{1.105 - 1.5X_{O_2}} \tag{19}$$

where $\dot{q}$ is the rate of heat release (kW), C is orifice plate coefficient (kg$^{1/2}$m$^{1/2}$K$^{1/2}$), X_{O2} is measured mole fraction of O_2 in the exhaust air. (Lindholm et al. 2009, p. 5).

Cone calorimeter is also gathers information about ignition time, mass loss and other parameters associated with burning properties of fuel sample. Test is usually performed with differ-

ent heat fluxes over specimen surface (with 35kW/m^2, 50 kW/m^2, etc.). The data collected from this fire test can be used for fire modelling, prediction of real scale fire behavior and pass/fail tests. (Lindholm et al. 2009, pp. 1-2).

3.4 Numerical approach

Both the façade fire test and small flammability tests were modelled using Fire Dynamics Simulator version 6.1 (McGrattan et al. 2012. pp. 1-12). The course of development of large-scale façade fire test simulation is presented in detail in a special chapter dedicated to it (Chapter 6).

The TGA and MCC tests simulations are based on the pyrolysis_1.fds verification test case from the public FDS repository (https://github.com/firemodels/fds-smv/tree/development/Verification). The most important parameters related to pyrolysis modelling in FDS are the reference temperature where the thermal decomposition rate is at its maximum, and the amount of residue after pyrolysis, were taken from experimental data.

The Cone Calorimeter test was also modelled using FDS 6. This test was simulated with non-combustible stone wool and used as a simple thermal conductivity model for evaluating fire protection thickness in the end of this work.

4 Experimental results

Experimental data used for visualization of test results is presented in this chapter. Cone calorimeter and MCC data were received from VTT fire testing laboratory from the tests performed in the spring 2015. TGA and DSC (STA) test were carried out at the Aalto University's Department of Chemistry.

4.1 TGA

The main purpose for which TGA test carried out is determining the mass change of a sample of insulation material over a time during the heating process. The test was run in nitrogen atmosphere with temperature increasing rate of 20 ºC/min up to 800 ºC.

TGA test was conducted for four different kinds of insulation materials: EPS (grey), PIR, COV and Stone wool. Actually, type of insulation marked with abbreviation COV, is not used as separate type of insulation material, usually it is used for covering more flammable types of insulations, for example PIR. Despite that, in TGA test it has been examined separately. The degradation behavior of tested insulation materials is presented in Figure 13.

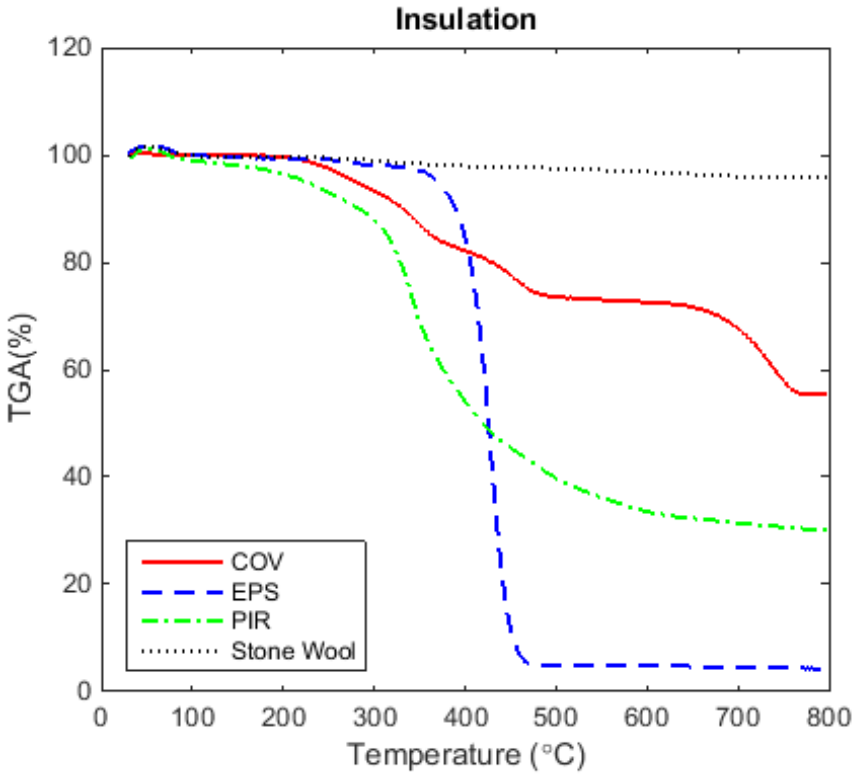

Figure 13. TGA for insulation materials

In the results corresponding to material marked with COV, it is easily to detect thermal decomposition phenomenon. COV insulation passes through three decomposition reactions at temperatures 300 ºC, 450 ºC and 700 ºC.

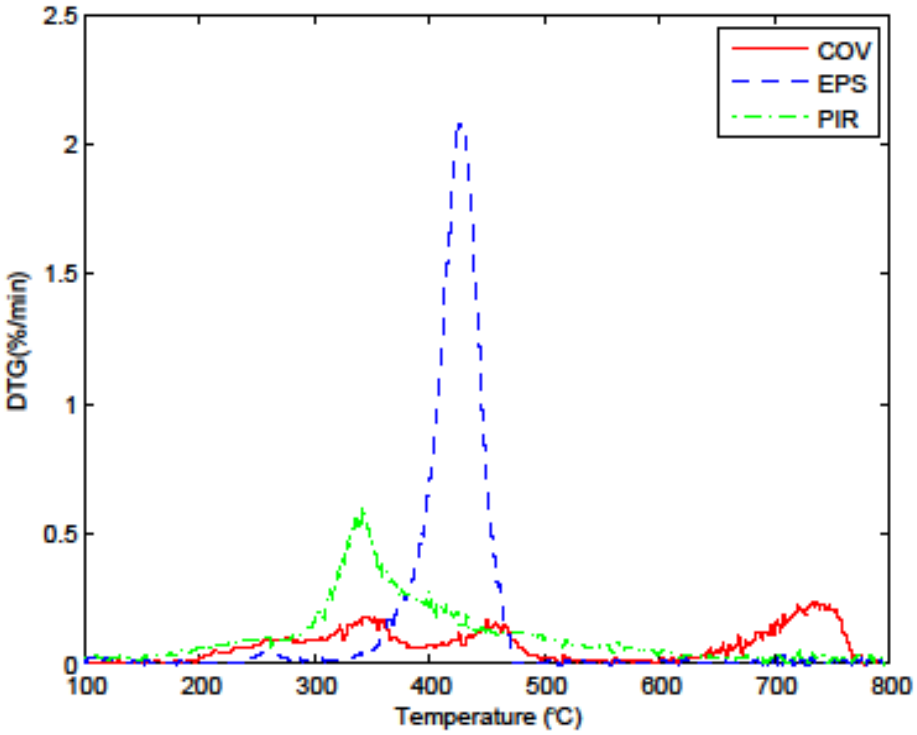

Figure 14. DTG thermal curves for the decomposition of insulation materials.

Thermal degradation of grey EPS presented in Figure 14 occurs by one chemical reaction. Some mass loss is observed already below 300 °C, but extensive mass loss starts at T ≥ 350 °C. Sample of EPS loses mass very rapidly and leaves almost no residue at all.

The PIR insulation starts to degrade at lower temperature than EPS (decomposition observed even at 100 °C temperature). Chemical reaction rate is no so high than it was with EPS sample. PIR insulation sample decompose in the range 300 °C–500 °C.

4.2 DSC

Differential scanning analysis was performed at the same time with the TGA test presented above. The results from the test are presented in Figure 15. First melting point is observed for EPS (grey) at temperature about 220 °C, after that follows the endothermic decomposition reaction with peak at 380 °C temperature. PIR sample starts to degrade at 100 °C. This is difficult to detect, because it is very slow decomposition reaction. More active thermal degradation of PIR in range 200 - 600 °C was observed.

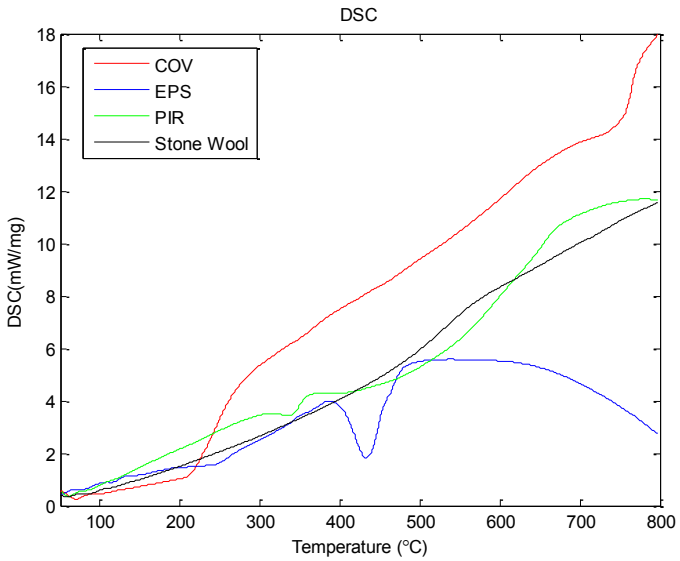

Figure 15. DSC test results for insulation materials

COV marked curve refers to fire retardant covering material. Analysis of COV curve presented in Figure 15 shows that chemical reaction starts at temperature 200 ºC followed by stable phase. COV stays without thermal changing before temperature increases to 700 ºC, where the second reaction was observed.

Stone wool shows very stable behavior in test, there is only one recrystallization phase observed at temperature about 550 ºC.

4.3 MCC

MCC technique was used to assess the flammability characteristics of insulation materials in very small scale. MCC test was performed with two different heating rates 70 K/min and 30 K/min (Figure 16).

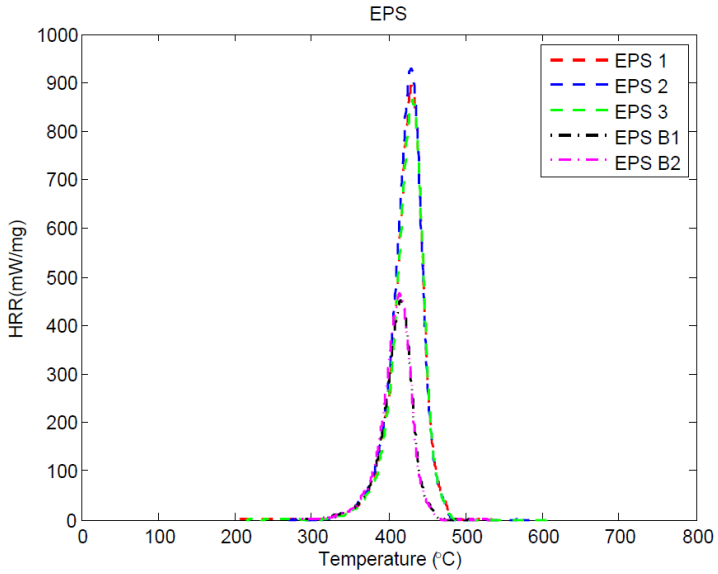

Figure 16. Heat release rate (HRR) as function of temperature for grey EPS.

EPS 1, EPS 2 and EPS 3 named curves are got from the MCC test with heating rate of 66-70 K/min. EPS B1 and EPS B2 curves correspond to the tests with heating rate of 30 K/min. The maximum value of heat release rate during heating of 66-70 K/min is determined to be equal to 867 W/g, 902 W/g and 932 W/g for the first free samples. The samples of EPS from another group gave the following results for maximum HRR: 454 W/g and 468 W/g. The peak of HRR is reached at temperature of 430 ºC for the first group and at temperature 415 ºC for the second.

Microscale combustion test made for PIR-Al demonstrate the following results:

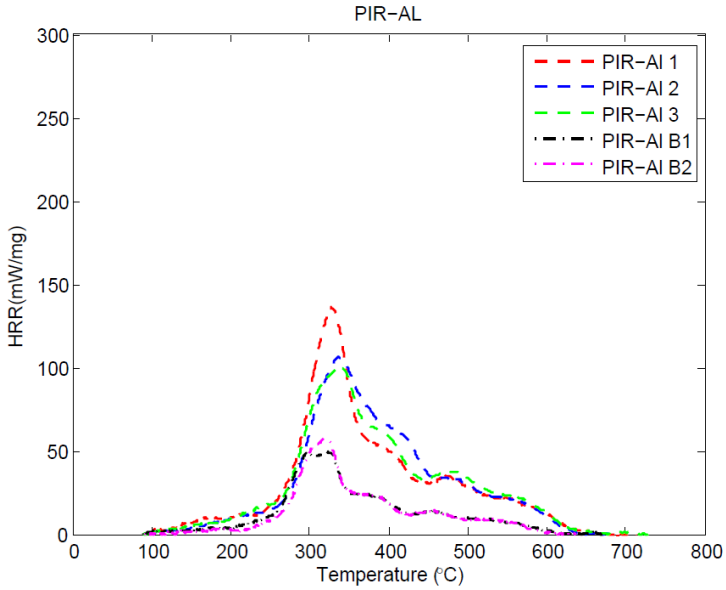

Figure 17. Heat release rate (HRR) as function of temperature for PIR-Al.

The most important results from collected data for PIR-Al are presented in Table 4.

Table 4. MCC test results of PIR-Al.

PIR-Al			
60 K/min		30 K/min	
Max.HRR (W/g)	At Temperature (Celsius)	Max.HRR (W/g)	At Temperature (Celsius)
153	327	55	322
120	337	62	320
110	340		

Peak of heat release rate for PIR-Al is located in the range 320-340 ºC. Results show that test heating rate has a strong influence on them. With increasing of test heating rate, peak of heat release rate shifts to the right (observed at higher temperature) and the peak value of HRR increases although amount of released heat stay almost unchanged. This rule applies to all performed MCC tests.

MCC test results marked with PIR-COV are made with the same PIR foam presented above. COV material has not been tested individually, which explains that results are almost similar to PIR test results. The maximum value of heat release rate is observed at the same temperature, but it was a lower than in test of regular. Gathered data is presented in Figure 18.

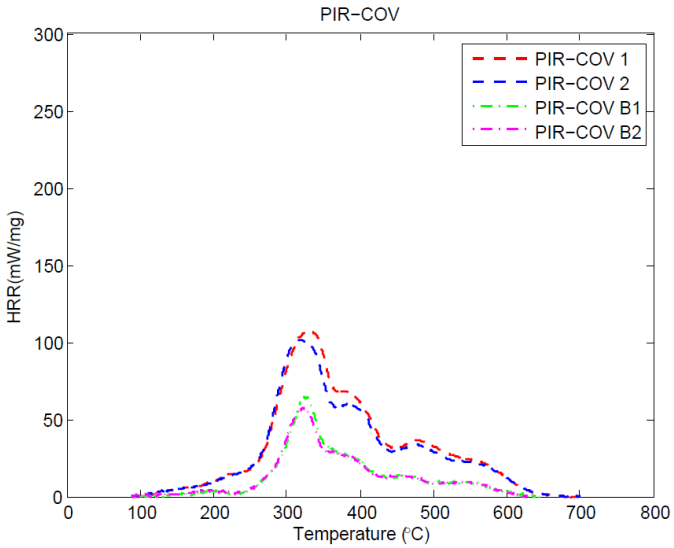

Figure 18. Heat release rate (HRR) as function of temperature for PIR-COV.

Exact values of maximum heat release rates are presented in Table 5.

Table 5. MCC test results of PIR-COV

PIR-COV			
60 K/min		30 K/min	
Max.HRR (W/g)	At Temperature (Celsius)	Max.HRR (W/g)	At Temperature (Celsius)
118	334	73	324
114	320	67	322

Calculating the HRR integral with respect to time, the following results were obtained for heat of combustion (Table 6).

Table 6. Heat of combustion of tested materials.

Heat of combustion (MJ/kg)	
EPS 1	34.8
EPS 2	35.9
EPS 3	33.5
EPS B1	34.6
EPS B2	35.9
PIR 1	14.1
PIR 2	13.7
PIR 3	13.8
PIR B1	13.3
PIR B2	12.4
PIR-COV 1	14.3
PIR-COV 2	13.4
PIR_COV B1	12.8
PIR-COV B2	12.5

4.4 TGA vs MCC

In this part the results between the small-scale tests are compared. Thermal degradation (TGA) test and flammability performance (MCC) test should present the same dependence from temperature in mass loss burning rate (TGA) and heat released during combustion (MCC). Firstly, TGA test with nominal heating rate of 20 ºC/min is compared to MCC test with nominal heating rate of 30 ºC/min. Figure 19 and 20 present comparison for sample of expanded polystyrene (EPS) and polyurethane foam (PIR). Figures include two vertical axes, where the left axis belongs to mass loss rate determined in TGA test, right axis presents heat release rate from MCC test.

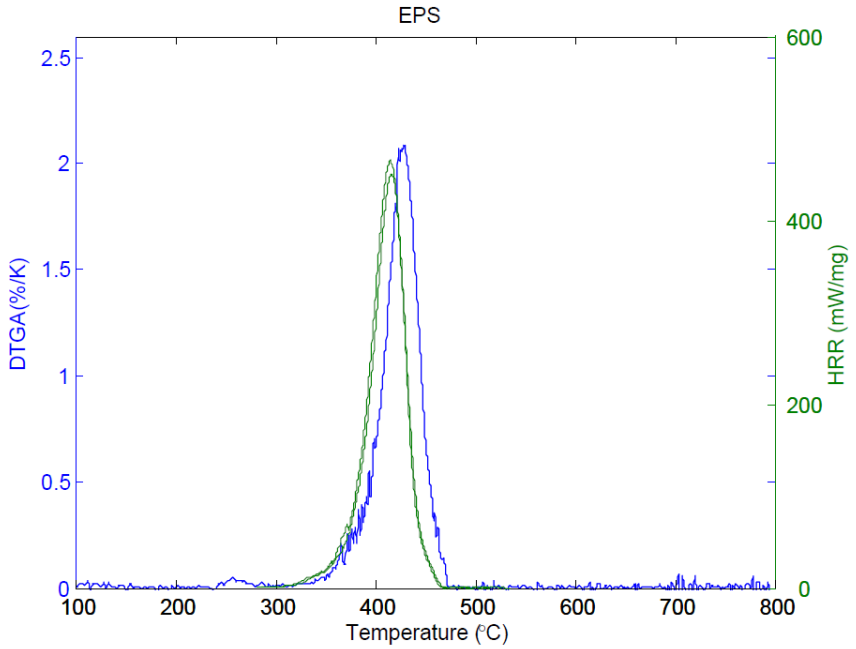

Figure 19. Comparisons of experimental results from TGA (20 K/min) and MCC (30 K/min) tests for EPS insulation.

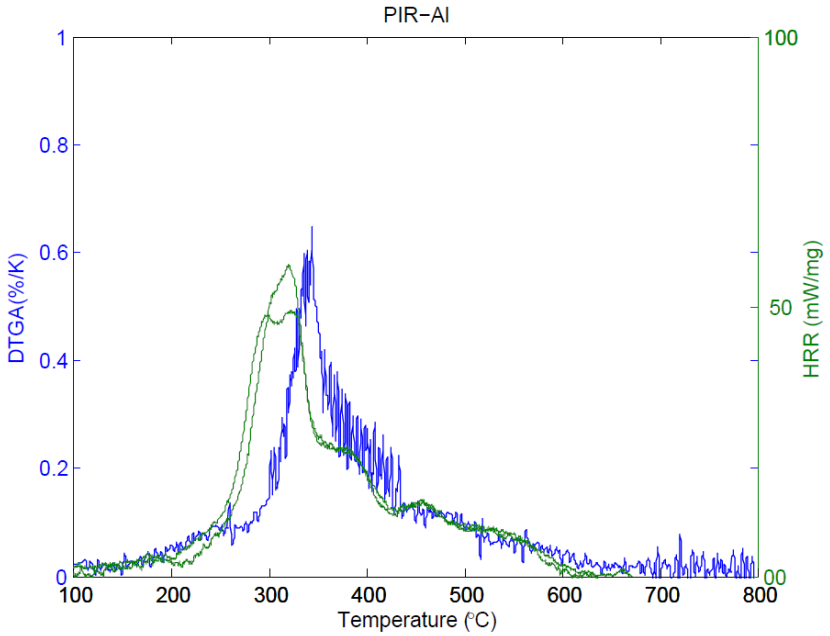

Figure 20. Comparisons of results from TGA (20K/min) and MCC (30 K/min) tests for PIR insulation.

Comparisons to MCC test with heating rate of 60 ºC/min and TGA test with heating rate of 20 ºC/min are presented in Figures 21 and 22.

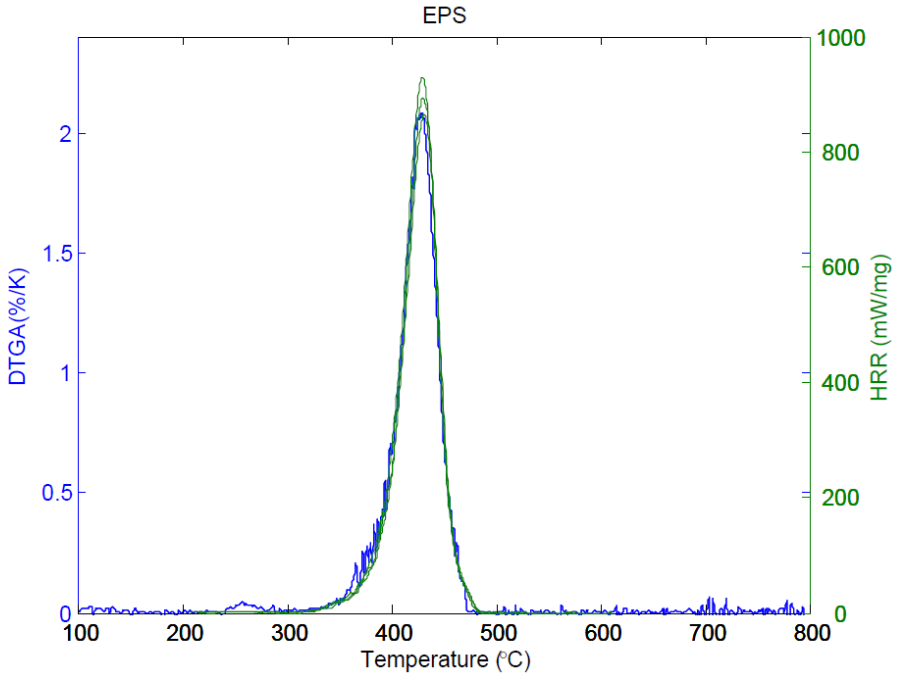

Figure 21. Comparisons of results from TGA (20 K/min) and MCC (60 K/min) tests for EPS insulation.

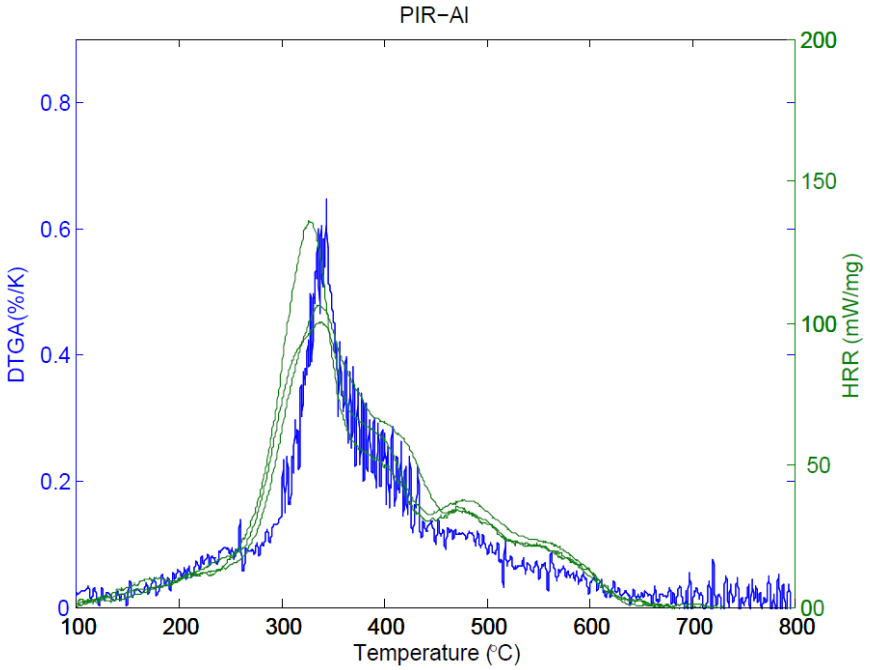

Figure 22. Comparisons of results from TGA (20 K/min) and MCC (60 K/min) tests for PIR-Al insulation.

According to gathered figures, very interesting results are observed; because the superimposition of two sets of data from MCC and TGA tests showed that the MCC test performed with heating rate of 60 ºC/min impose more accurately to the TGA test results, when MCC with heating rate of 30 ºC/min differs greatly (distance between the peaks is 15-20 ºC).

4.5 Cone calorimeter test results

Cone calorimeter test was performed to explore flammability of common façade insulation materials. Observations and measurements from test are collected in this chapter. In Figure 23 are presented residues of tested materials after the Cone Calorimeter test with exposure of 35 kW/m^2.

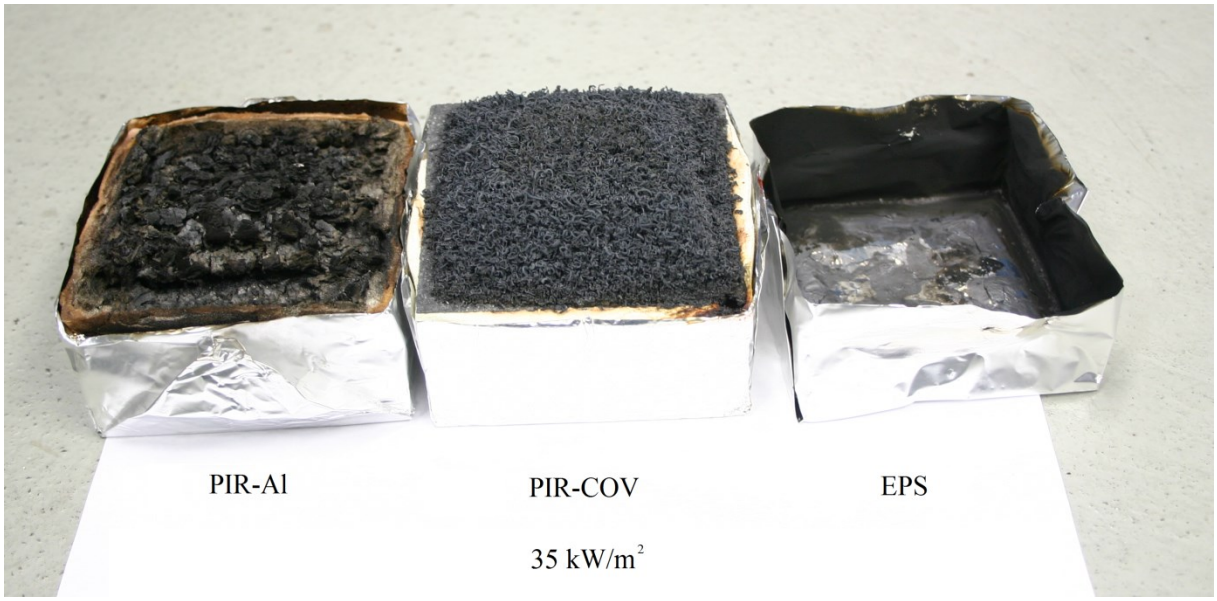

Figure 23. Samples residues remaining after the Cone calorimeter test (35 kW/m^2).

Cone Calorimeter tests of flammable specimens such as PIR-Al, PIR-COV and EPS were performed using steel edge frame. Test with Stone wool was performed without it.

4.5.1 EPS

Two Cone calorimeter tests were performed for EPS with piloted ignition (with radiative heat flux of 35 kW/m^2 and 50 kW/m^2). Both of tests have some general features: In the beginning of test, when temperature of sample starts to increase, low HRR is observed. When temperature of sample is over than 350 ^{o}C, ignition occurs, but before there is very intensive and long fuming phase is observed. Rapid combustion with very sharp heat release rate peak was monitored. Heat release rate as function of time is presented in Figure 24.

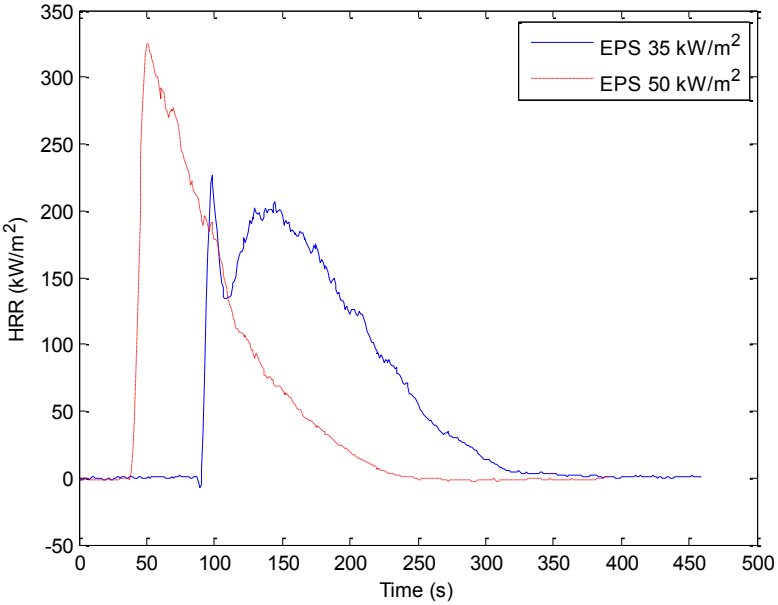

Figure 24. Heat release rate (HRR) as function of time for EPS.

During the fuming phase, EPS was melted, it occurred in 10 seconds after the test starting. After the burning, there was a completely empty cup. Appendix 2 of this thesis presents photos of specimen's condition after cone calorimeter test.

4.5.2 PIR

Polyisocyanurate (PIR) is commonly laminated with aluminum covering, but in Cone Calorimeter test, it was examined without it. This material was also tested by two different exposure levels. In the beginning of test (in first two seconds) sharp HRR peak was observed in each test. Rapid ignition followed by slowly decreasing HRR, before it has been burned out. Figure 25 shows the heat release rate of PIR during this test.

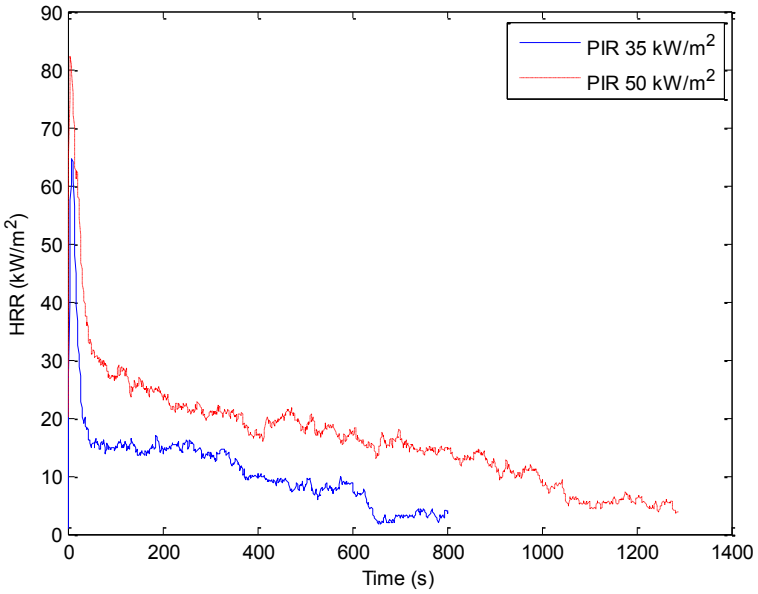

Figure 25. Heat release rate (HRR) as function of time for PIR.

PIR samples did not completely burned out, but charred. In test with radiative heat exposure of 35 kW/m^2, char thickness after the test was about 30 mm, where about 10 mm of material was partially charred. In the test with exposure of 50 kW/m^2, PIR was completely charred. Photos taken after the test can be found from Appendix 2.

4.5.3 PIR-COV

PIR-COV is the common polyisocyanurate (PIR) with fire retardant covering. Thickness of this covering is about 1 mm. Because of PIR covering intensive swelling (up to 20 mm) in few seconds after the test starting, the position of sample in Cone Calorimeter test was changed. This change caused that test was performed for PIR-COV on lower exposure level (25 and 36.2 kW/m^2).

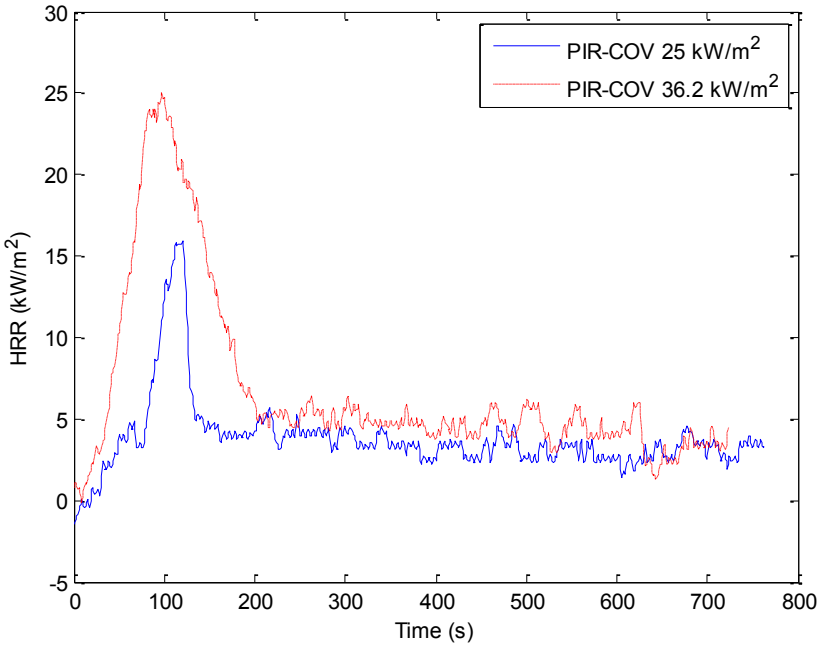

Figure 26. Heat release rate (HRR) as function of time for PIR-COV.

Relative rapid ignition was observed in the beginning of PIR-COV testing. It was followed by even HRR to the end of test. In test with exposure of 25 kW/m^2 char thickness is about 17 mm, in the test with exposure of 36.2 kW/m^2 – about 25 mm from the exposed side. Photos of testing materials residue can be found from Appendix 2.

4.5.4 Stone wool

Stone wool samples were tested on Cone calorimeter in horizontal position (all materials was tested in this way). Three samples were exposed to different radiative heat fluxes for 20 minutes.

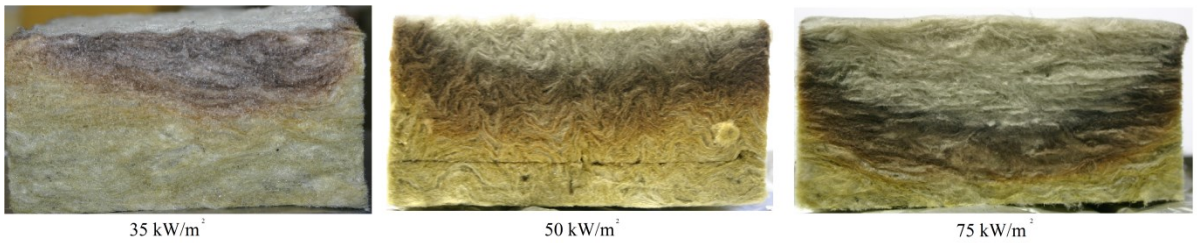

Figure 27. Stone wool photo after heating.

There is visible color changing of stone wool samples after the heating (Figure 27). Sintering of tested stone wool occurred at temperature over than 600 °C. Little mass loss is observed at less temperature, what is probably stone wool binder material burning. Binder material content in stone wool is commonly less than 5% of mass. Figure 28 shows mass loss of stone wool during the test.

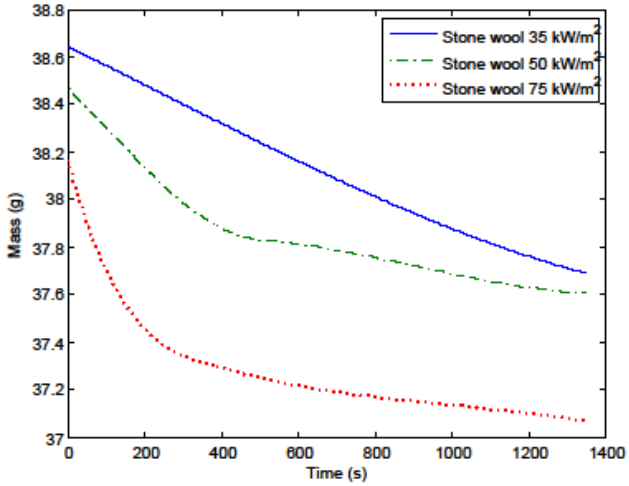

Figure 28. Mass loss of stone wool as a time function.

Thermocouples were installed in stone wool samples before the test. In first test with exposure of 35 kW/m2 thermocouple was set under 15 mm thick stone wool layer. In next two tests thermocouple was installed deeper inside (40 mm) than in first test.

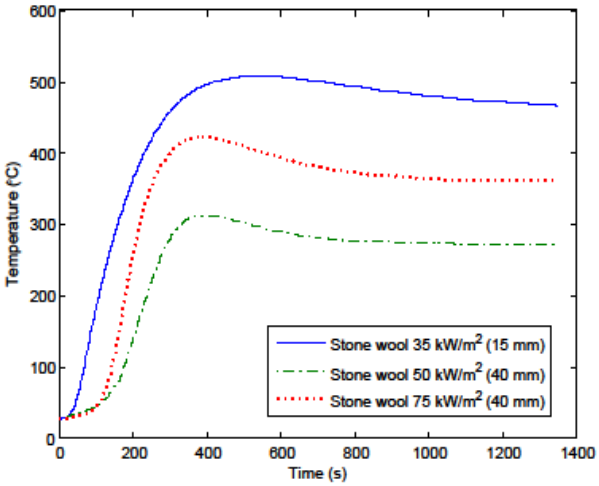

Figure 29. Temperatures inside Stone wool during the test.

Results of temperature measurements are illustrated in Figure 29. Temperature under 15 mm thick stone wool layer increased to this maximum in 5 minutes after that stayed on the almost constant level at temperature close to 500 ^{o}C. Results from the tests with heat flux of 50 kW/m^2 and 75 kW/m^2 show identically same behavior of temperature development inside the material. Temperatures increased to 400 ^{o}C and 300 ^{o}C correspondingly.

4.5.5 Summary of Cone calorimeter tests

The most significant results received from Cone calorimeter tests are in Table 7.

Table 7. Summary of Cone calorimeter tests

		EPS	PIR-AL	PIR-COV
35 kW/m2	Ignition time (s)	92	3	115
	Peak HRR (kW/m2)	226	64.59	15.91
	Peak MLR (g/s)	0.06	0.021	0.01
	Averaged EHC (MJ/kg)	30.92	14.34	10.07
50 kW/m2	Ignition time (s)	41	1	57
	Peak HRR (kW/m2)	325	82.12	25.04
	Peak MLR (g/s)	0.122	0.027	0.0135
	Averaged EHC (MJ/kg)	27.19	17.09	13.27

These results are also presented in graphs, which are located in Appendixes 5, 6, 7, and 8.

5 FDS simulations of flammability tests

5.1 EPS simulations

TGA test was simulated using FDS 6 software with integrated pyrolysis model. According to the experimental results, the EPS pyrolysis leaves about 5 % residue. The kinetics of the pyrolysis reactions were modelled via three parameters: reference temperature, pyrolysis range and heating rate.

Specifically for EPS, behavior of material was examined in test with heating rate 20 ºC/min. Expanded polystyrene has burned with one chemical decomposition reaction, which reference temperature is 430 ºC and pyrolysis range is 95 ºC. The results of made simulation are presented in Figure 30. FDS code used for this simulation can be found in Appendix 11.

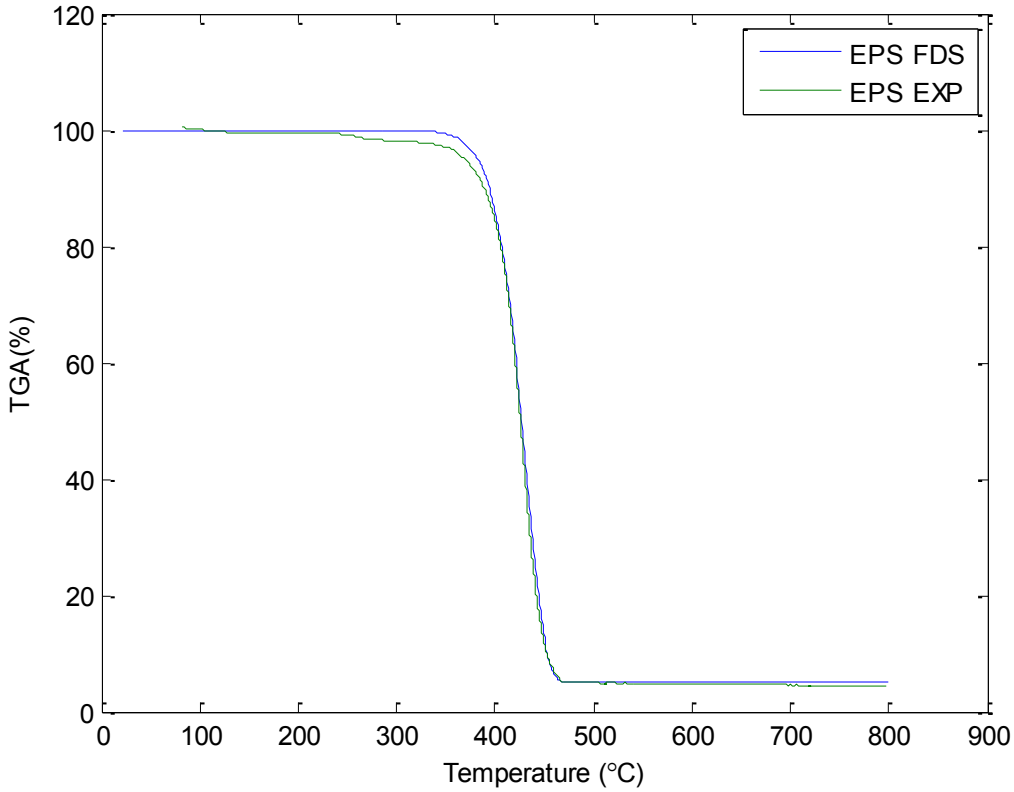

Figure 30. Simulation of TGA test. Mass loss for EPS

The simulated mass loss for EPS fits to the experiment results very well with only single reaction. In FDS 6, program creates separate output file for results of TGA test simulation. This file also includes the results for MCC and DSC tests. Due to another heating rate in MCC tests performed, simulation were made with material properties based on TGA test results (reference temperature and pyrolysis range) and with heating rate corresponding to MCC test. Heat of combustion value was set to 45 MJ/kg. The results are presented in Figure 31.

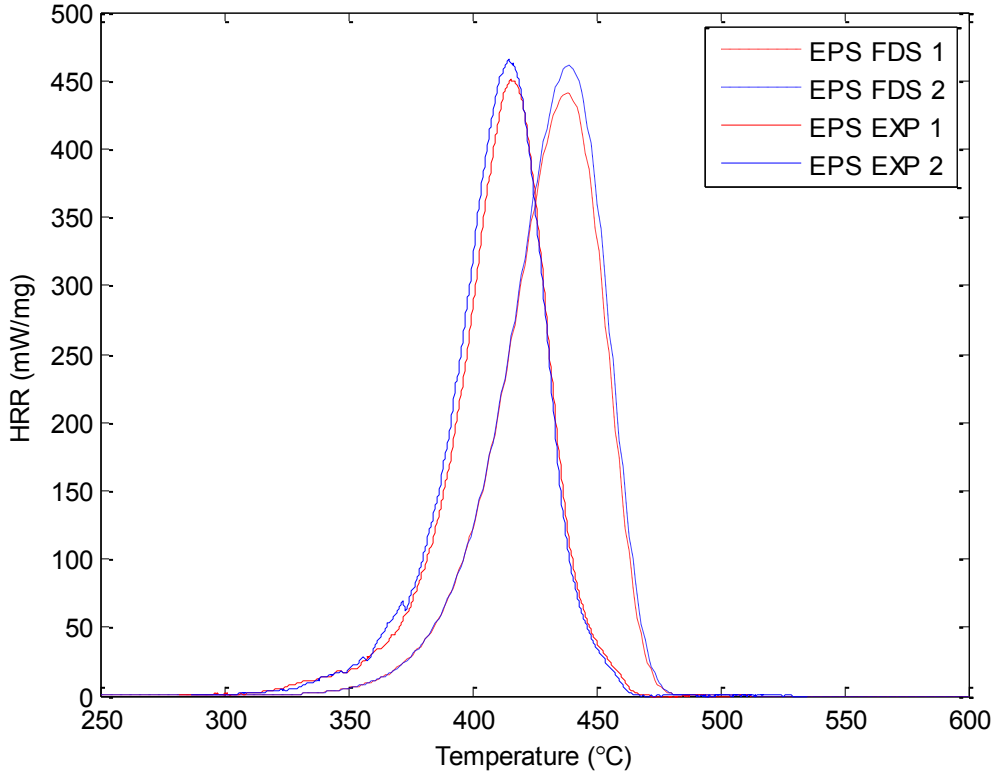

Figure 31. Simulation of MCC test EPS (30 K/min)

The next comparison was made in the same way as was described above, but predictions was made for MCC test with heating rate in range 66-70 K/min.

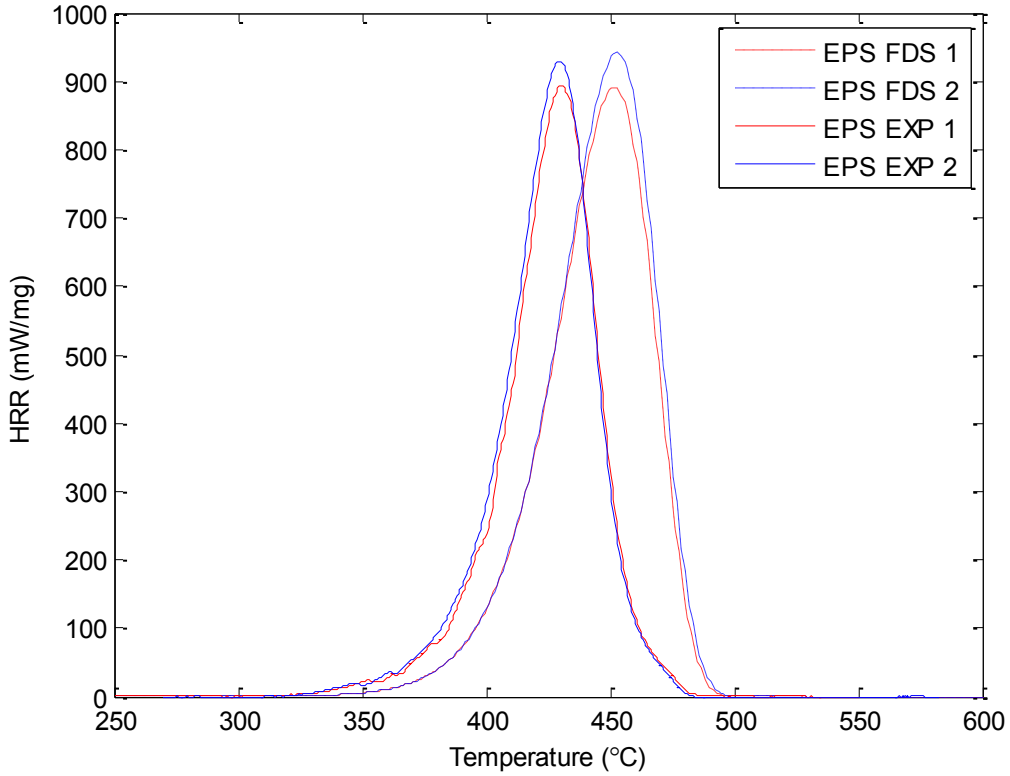

Figure 32. Simulation of MCC test for EPS (70 K/min)

Simulations based on TGA test results show the same behavior of burning and heat released during combustion even though burning peak shifted in both comparisons.

5.2 PIR simulations

According to the experiments results, pyrolysis product of PIR has a residue yield of 30%. Simulation of TGA test was performed with heating rate of 20 ºC/min. Because of all gathered experimental data, it was decided to represent combustion of PIR by three consecutive reactions. The results of made simulation are presented in Figure 33. The FDS input file listing can be found in Appendix 12.

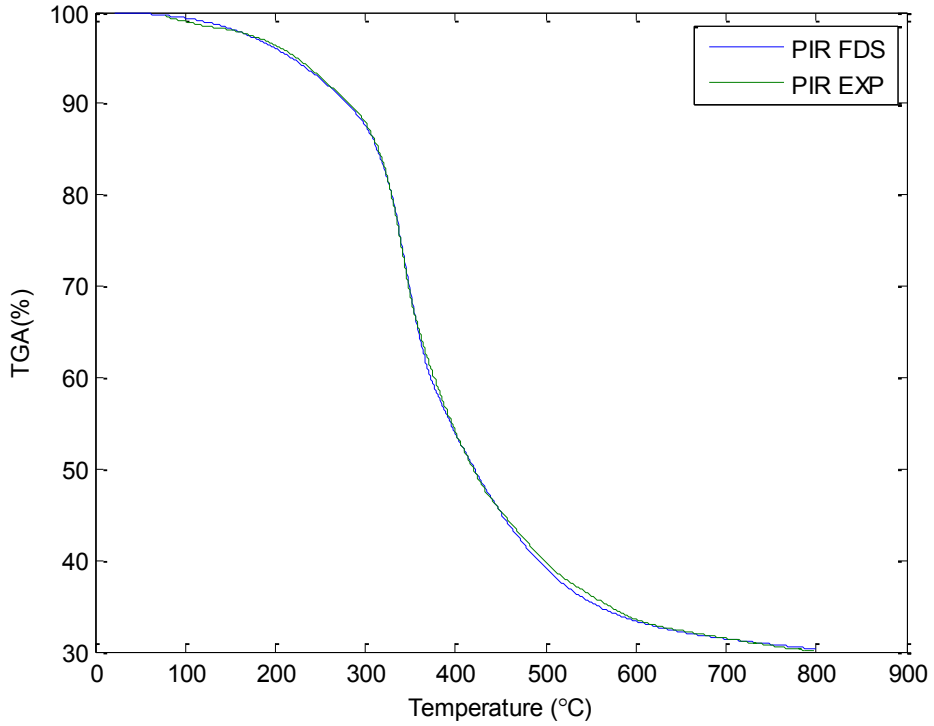

Figure 33. Simulation of TGA test. Mass loss for PIR

The same FDS input was used to simulate MCC test, where heating rate was changed to 30 ºC/min. Heat of combustion for PIR was equal to 25 MJ/kg. Heat release rate got from simulation as function of temperature is presented in Figure 34.

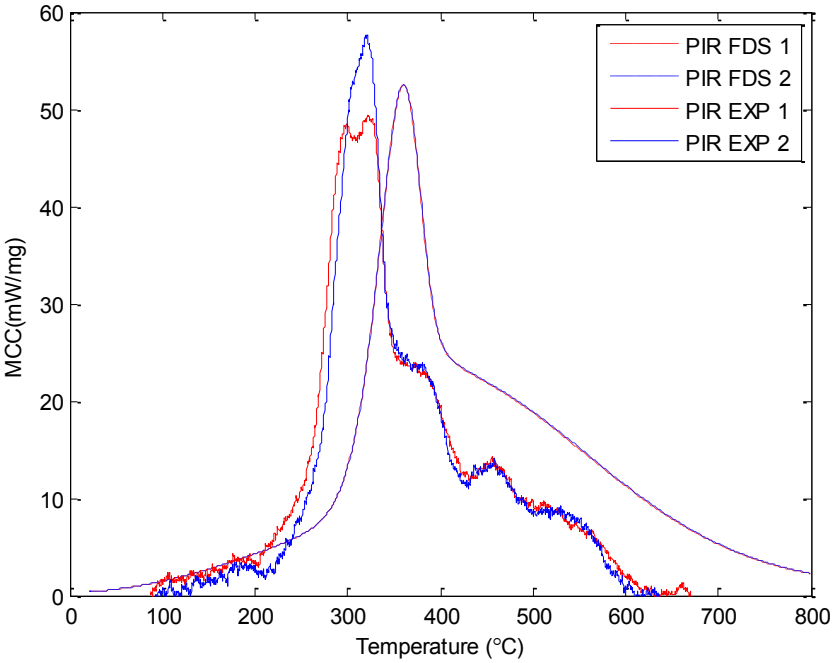

Figure 34. Simulation of MCC test for PIR (30 K/min).

5.3 COV simulations

Simulation of TGA test for COV sample is similar to simulation of PIR sample. According to experimental data three chemical decomposition reactions was found. Results of simulation are presented in Figure 35.

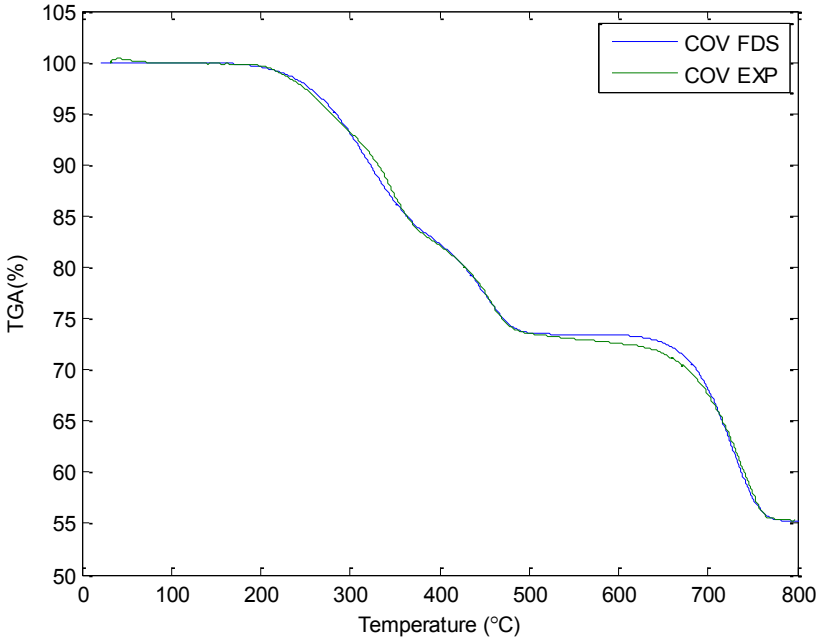

Figure 35. Simulation of TGA test. Mass loss for COV

5.4 Stone wool heating. Cone calorimeter

The cone calorimeter test was simulated to determine the temperature development within the stone wool specimen. Stone wool is non-combustible material; therefore, it was simulated without pyrolysis properties of material (simple thermal conductivity model). Back side insulation was installed under the wool specimen before installing foil covering. After that, specimen was set to the testing steel frame.

For stone wool properties such as density, specific heat capacity were used in simulation the following values: density – 95 kg/m^3, specific heat – 840 J/kgK. Because of conductivity behavior to change its value with temperature increasing, this is presented in simulation as temperature dependent function (Table 8).

Table 8. Thermal conductivity of stone wool
(Rockwool Product catalogue 2013)

T (°C)	10	20	30	40	50	100	150	200	250	300	350	450
λ (W/mK)	0.034	0.035	0.036	0.037	0.038	0.045	0.05	0.055	0.06	0.065	0.07	0.085

Back side insulation was simulated using 13 mm thick Insulfrax S blanket properties (Unifrax 2007). Measured and simulated temperatures are compared in Figure 36. According to simulation and test comparison, simulation tends to the same temperature value as from experiment was received. It is also shows that simulation does not represent real temperature development inside material at the first 1000 seconds. According to the wool manufacturer, the possible reason for the observed discrepancy is related to the exothermic oxidation of wool binders during the first this time.

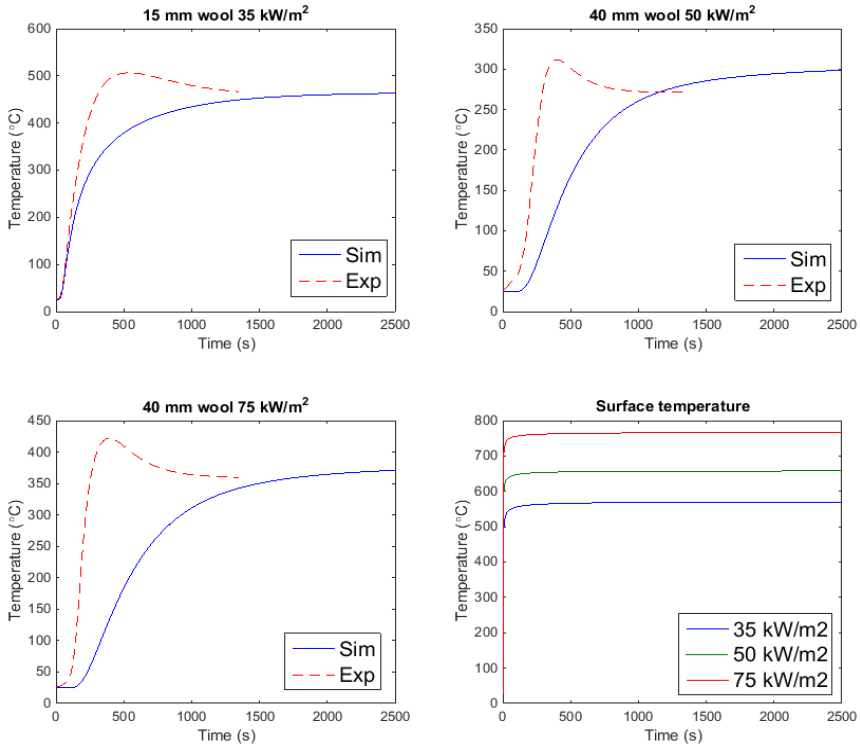

Figure 36. Simulation of Cone Calorimeter test. Temperatures inside the stone wool.

6 FDS simulation of ISO 13785-2 test

6.1 Model description

ISO 13785-2 test model consists from combustion chamber with window and side wall on the façade. Geometry of the model and test facility were presented in Chapter 3.3.1. In general context of compartment fire simulation, the quality of the utilized grid size is commonly assessed using the non-dimensional $D^*/\delta x$ ratio, where D^* is a characteristic fire diameter and δx corresponds to the nominal size of the grid cell. If the value of the $D^*/\delta x$ ratio is sufficiently large, the fire can be considered well resolved. Several studies have shown that values of 10 or more are required to adequately resolve most fires and obtain reliable flame temperatures. (Lin & Ferng 2009, pp. 2243-2250). By NUREG recommendations, $D^*/\delta x$ ratio should be between 4 and 16 to accurately resolve fires. (NUREG 1824, 2007). The characteristic fire diameter D^* is given by following relationship:

$$D^* = \left(\frac{\dot{Q}}{\rho_\infty c_p T_\infty \sqrt{g}} \right)^{2/5} \tag{20}$$

Applying the heat release rate of 5600 kW, density of air of 1.204 kg/m3, specific heat of 1.005 kJ/kgK, ambient temperature of 293 K and gravity of 9.81 m/s2 to Equation 20, we get $D^* \approx 1.9$. Thus, in the current study, for accurate solving of the given problem, cell size should be about 0.1-0.5 m.

It is not necessary to perform ISO 13785-2 test with maximum heat release rate, if the exposure level on façade wall can be achieved with lower HRR. Standard gives the indicative values for heat flux immediately above the window and for temperatures at the height of 600 mm above the window. The façade wall at steady state phase of the test should be exposed to 55±5 kW/m^2 and temperatures must be at least 800^{o}C.

Therefore, the grid size must be recalculated for the lowest possible heat release rates of burner. Table 9 shows the recommended limits for grid cell size for ¼, ½, ¾ and maximum HRR of burner.

Table 9. Grid cell size dependence from HRR.

5.6 MW	25 %	50 %	75 %	100 %
D^*	1.10	1.45	1.70	1.91
$\delta x = D^*/4$	0.27	0.36	0.43	0.48
$\delta x = D^*/16$	0.07	0.09	0.11	0.12

In regard to fulfilling the $D^*/\delta x$ criteria, 0.1 m cell size is selected for numerical simulation of this study case.

He in its study (He 2010, pp. 245-246) has concluded that the accuracy and validity of the numerical simulation of building fires can be domain dependent as well as grid dependent. He conducted a parametric study and suggested a correlation between the hydraulic diameter of the vent opening and the effective domain extension.

$$D_h = 4 \cdot \frac{A}{P_o} \tag{21}$$

(He 2010, p. 231).

P_o and A are perimeter and area of opening. In our case, when window has dimensions 2 m by 1.2 m, hydraulic diameter is equal to 1.5. For the ventilation controlled fire effective domain extension factor should be 1 and effective domain extension can be evaluated by

$$D_e = \eta_e \cdot D_h \tag{22}$$

(He 2010, p.231).

Therefore, the domain of extension in front of main window up to 3 m is more than enough.

Experimenting with different parameters (chapter 6.4) related to radiation such as amount of radiation angles was found that calculated values of temperature and heat flux both on the façade and inside the combustion chamber remain almost unchanged. Therefore, in further simulations 100 radiation angles are used which in FDS is the conventional value for that.

6.2 Model validation

This part of study has been carried out for predicting the behavior of fire test based on ISO 13785-2 'Reaction-to-fire tests for facades – Part 2: Large-scale test'. The experiment performed in Tokyo University is described by Yoshioka et al. (2012).

Applying the large-scale façade apparatus of ISO 13785-2 with a non-combustible façade, temperature and incident heat flux were measured in the proximity of the exterior of the façade located above the window opening from where the flame originates, in order to measure the heat fluxes that outer wall surface will receive when there is no combustible materials located in the façade wall. (Yoshioka et al. 2012).

The test apparatus consisted of the combustion chamber and the façade test specimen. Combustion chamber walls and ceiling were made from 6 mm steel plates and 50 mm ceramic fiber boards from exterior to interior side. Floor of combustion chamber was constructed from outside as follows: 6 mm steel plate, 50 mm ceramic fiber board and 25 mm ceramic fiber blankets. The dimensions of the combustion chamber were $3 \times 4.3 \times 1.7$ meters for width, length and height, respectively. The façade specimen, in its turn, consisted from main wall with dimensions 3×5.7 m (width and height) and from 1.2 m wide side wall with the same height. The façade wall specimens were constructed in in the same manner as combustion chamber walls: 25 mm ceramic fiber blankets on the surface exposed to fire and 25 mm calcium silicate boards connected to the steel frame.

There were three series of tests performed with propane gas used as fire source. Each series of tests was done with some modifications implemented to the standard ISO test. First group of tests marked with I-letter was done with regular façade window and at the same time with one distinctive feature (one rear side opening opened). According to the ISO 13785-2, it is possible to make vents on the opposite to the façade front side for making passive ventilation more effective. Combustion chamber construction was designed with four these openings. I-marked test were performed with one rear side vent opened. Alternatively, second group of test marked with ①-sign were performed with all four vents opened. In the last group of test

marked with ②-sign all of supplemental openings were closed, but the exposure to the façade was checked with different façade window dimensions. Further information is presented in Table 10 below:

Table 10. Experimental conditions.
(Yoshioka 2012, p. 7).

Case	Fire source	Heating Load	Test duration	Gas flow (m3/h)	HRR (MW)	Open-ing			Vents at rear of cham-ber
						B(m)	H(m)	B/(H/2)	
I-1	City gas	1/2 of ISO	5 min	225	2.8	2	1.2	3.3	3: Closed 1: Open
I-2	City gas	3/4 of ISO	5 min	337.5	4.2	2	1.2	3.3	3: Closed 1: Open
①-1	City gas	1/4 of ISO	5 min	112.5	1.4	2	1.2	3.3	All (4) open
①-2	City gas	1/2 of ISO	5 min	225	2.8	2	1.2	3.3	All (4) open
①-3	City gas	3/4 of ISO	5 min	337.5	4.2	2	1.2	3.3	Former: All open Latter: 2 closed
②-1	City gas	1/8 of ISO	5 min	56.25	0.7	2	0.2	20	All (4) closed
②-2	City gas	1/4 of ISO	5 min	112.5	1.4	2	0.5	8	All (4) closed
②-3	City gas	1/2 of ISO	5 min	225	2.8	2	1	4	All (4) closed

Each series of tests was simulated in the same manner as experiment was conducted. For tests marked with ①-sign this means that all of three parts of that test was held by one continuous or unseparated simulation. The same rule applies for other tests too.

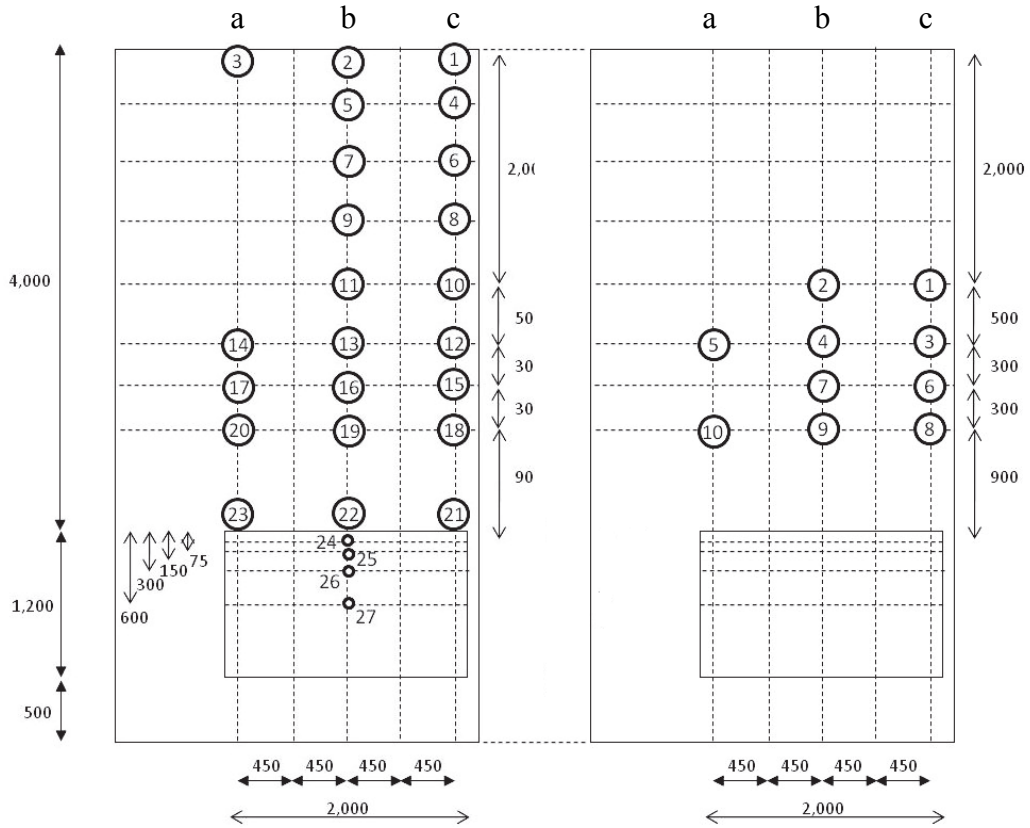

Figure 37. Positions of thermocouples (left) and heat flux meters (right) on façade (unit: mm)
(Yoshioka 2012, pp. 6-7).

Experiments were performed with more thermocouples and heat flux meters for the best reliability of output data than ISO 13785-2 standard requires. However, thermocouples and heat flux meters were arranged slightly differently compared to the standard as shown in Figure 37.

Simulations of three series of tests were performed with the heating load described in Table 10 and using real geometry and material properties. Thermocouples were simulated using the FDS's built-in thermocouple models, with bead diameters 3.2 mm and 1.6 mm. The temperatures measured by majority of thermocouples did not fall below 40°C even after the cooling stage of previous test. It was decided to put the value of 40°C for ambient temperature in simulation. The radiative fraction was set to 0.2. Particularly, for experiment this value can be defined by burner properties. Experiment was conducted with different gas fuel supply rates. The Table 11 shows burning rates and released heats during simulation.

Table 11. HRRs and burning rates as function of time for simulated tests.

Test series I
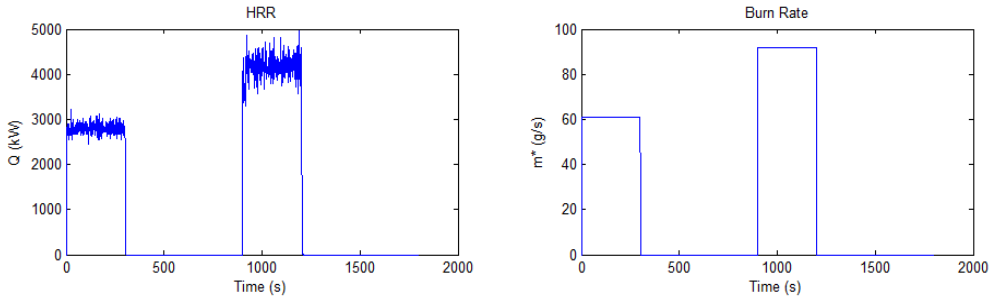
Test series ①
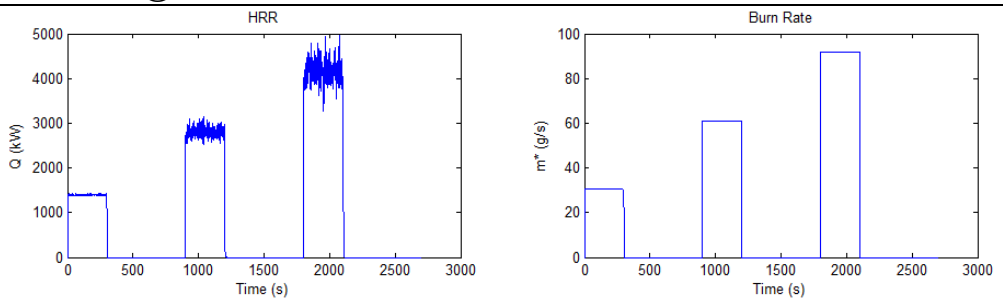
Test series ②
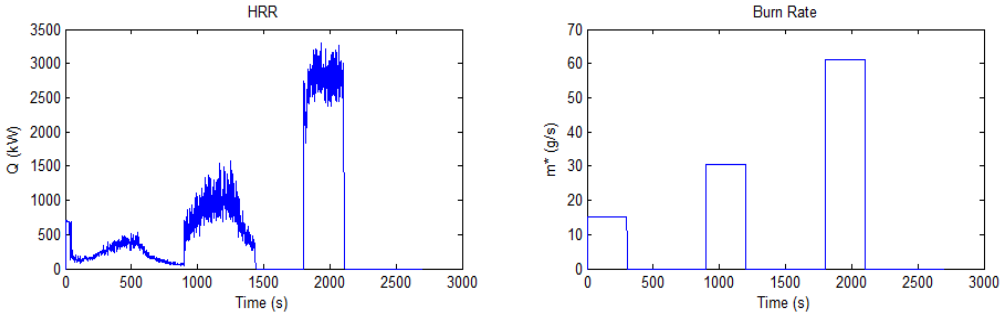

Results for the tests converge with data and experimental conditions. Heat release rate for the tests marked with ②-sign is not like a constant. This is because in last series of test very small façade window opening was used. Due to the lack of oxygen coming through a window, the full amount of supply fuel did not burn, extending the burning time. Burning occurs in those tests even when the fuel supply is switched off until the remaining fuel has burned out.

6.2.1 Simulation results of tests I-1-2

Simulation of test with regular façade window and one rear side opening gave the following results for heat flux (Figure 38). Heat flux meters HF10 and HF9 are located 900 mm from top edge of window, HF5 and HF4 are located 1500 mm from top edge of window.

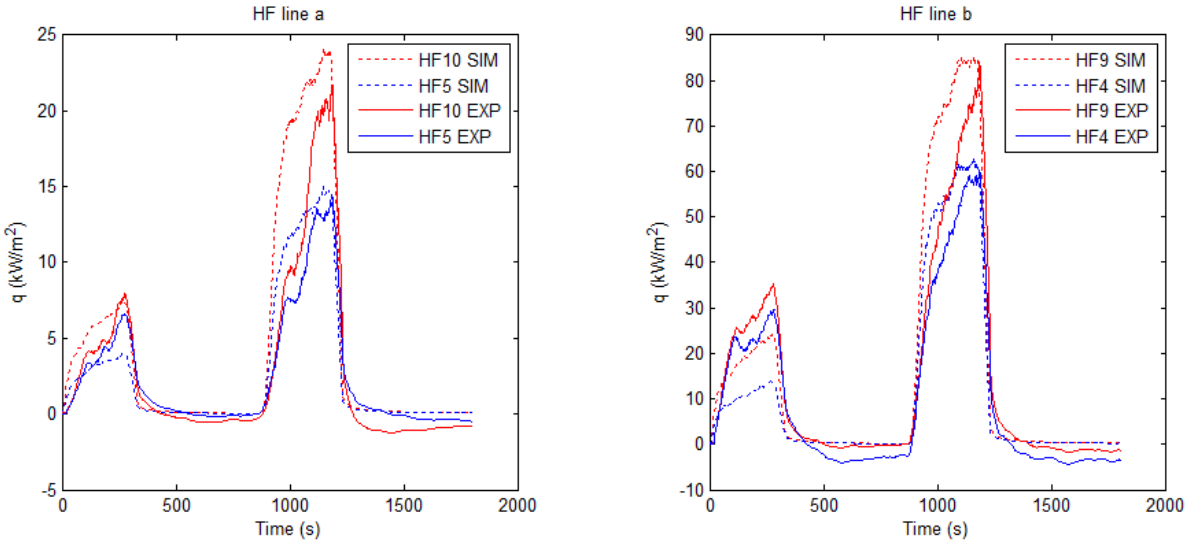

Figure 38. Test I-1-2. Experiment vs. Simulation. Heat fluxes on façade.

Temperature development during the same test and simulation is presented in Figure 39. Thermocouples T23 and T22 positioned 50 mm above the window and, T3 and T2 are located 4000 mm above the window. In all four measurement locations, the simulated temperatures are in good agreement (deviation < 10 %) with the measurements.

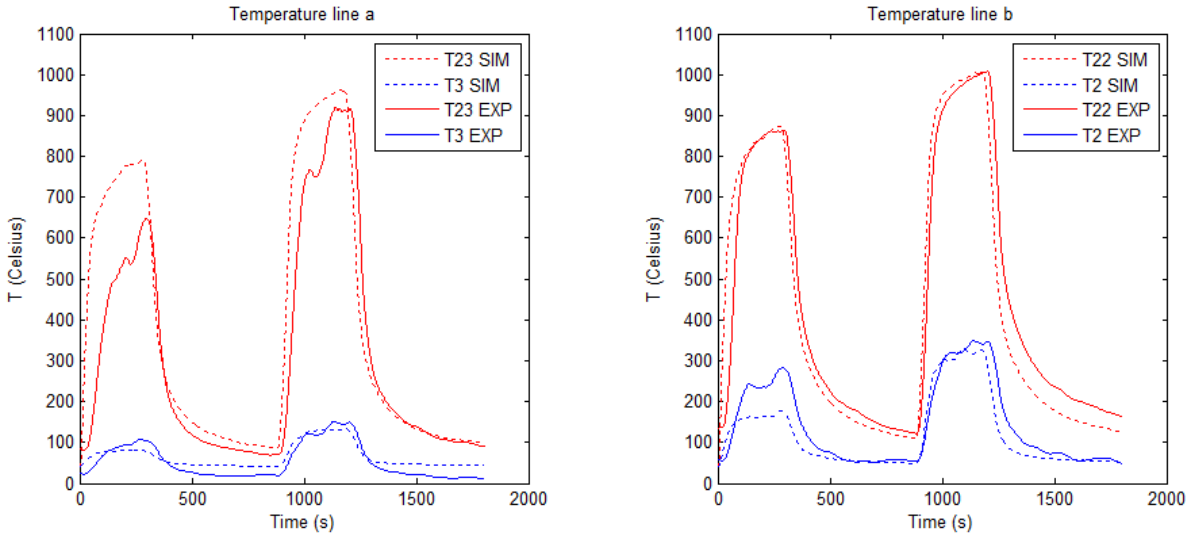

Figure 39. Test I-1-2. Experiment vs. Simulation. Temperatures on façade.

6.2.2 Simulation results of tests ①-1-2-3

The simulation of the test with four rear side openings and different fire load gave the following results for heat flux (Figure 40) and temperature (Figure 41).

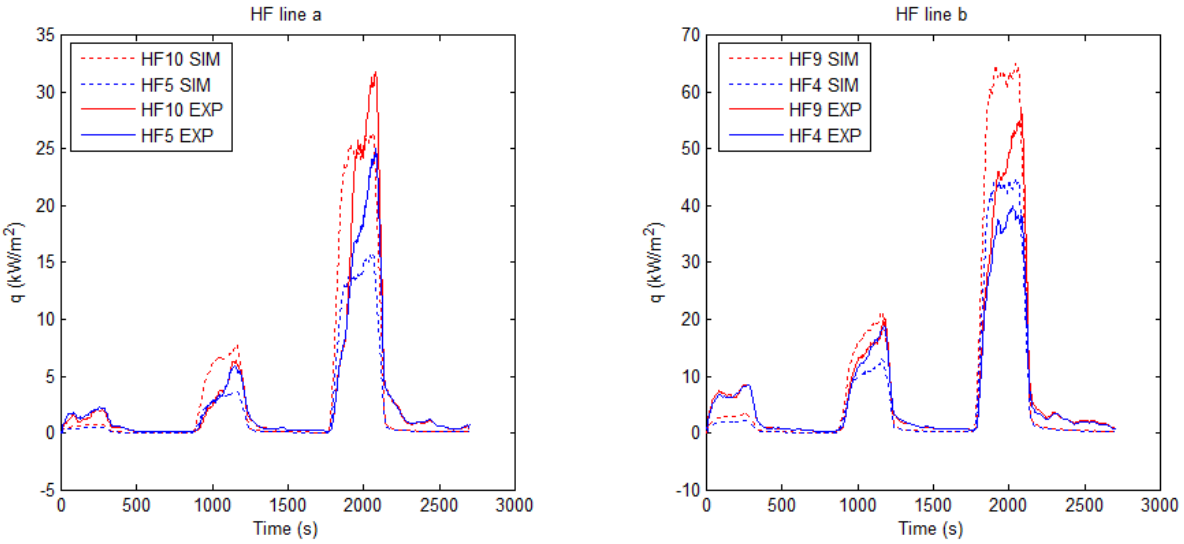

Figure 40. Test ①-1-2-3. Experiment vs. Simulation. Heat fluxes on façade.

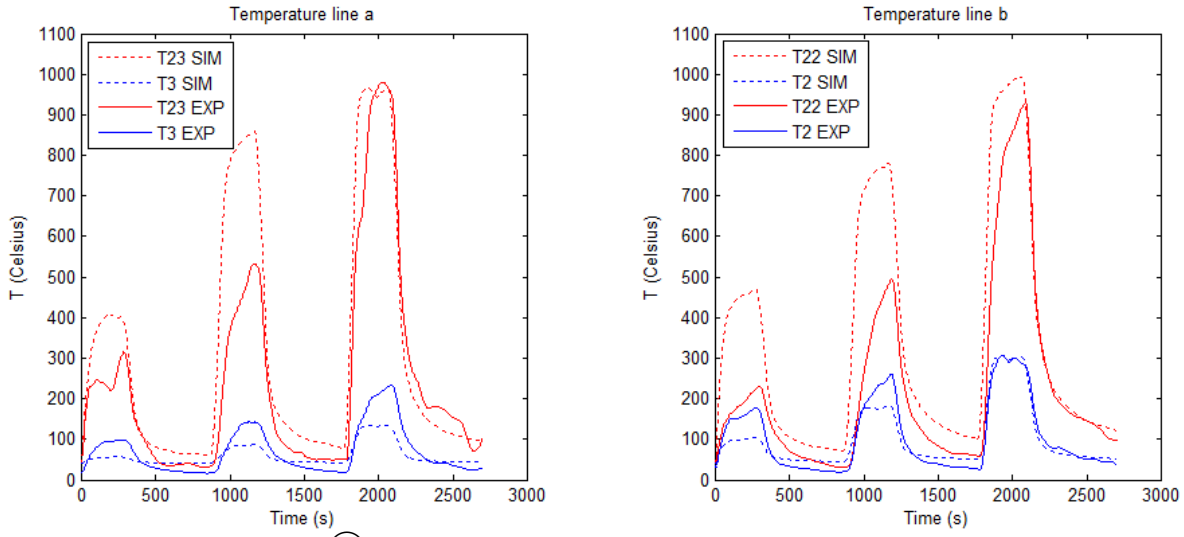

Figure 41. Test ①-1-2-3. Experiment vs. Simulation. Temperatures on façade.

Heat flux predictions on façade with very small fire load (25% of ISO maximum fire load) are significantly less than experiments results. At the same time temperature of gas coming from combustion chamber through façade opening has a larger value compared to experimental data. The difference between simulation and experiment decreases with increasing of fire load.

6.2.3 Simulation results of tests ②-1-2-3

This simulation made for case without any rear side openings and different main window dimensions. Width of façade window stays without changing. The height of façade window for these tests is 0.2 m, 0.5 m and 1 m. Heat flux and temperature predictions on façade are presented in Figures 42 and 43.

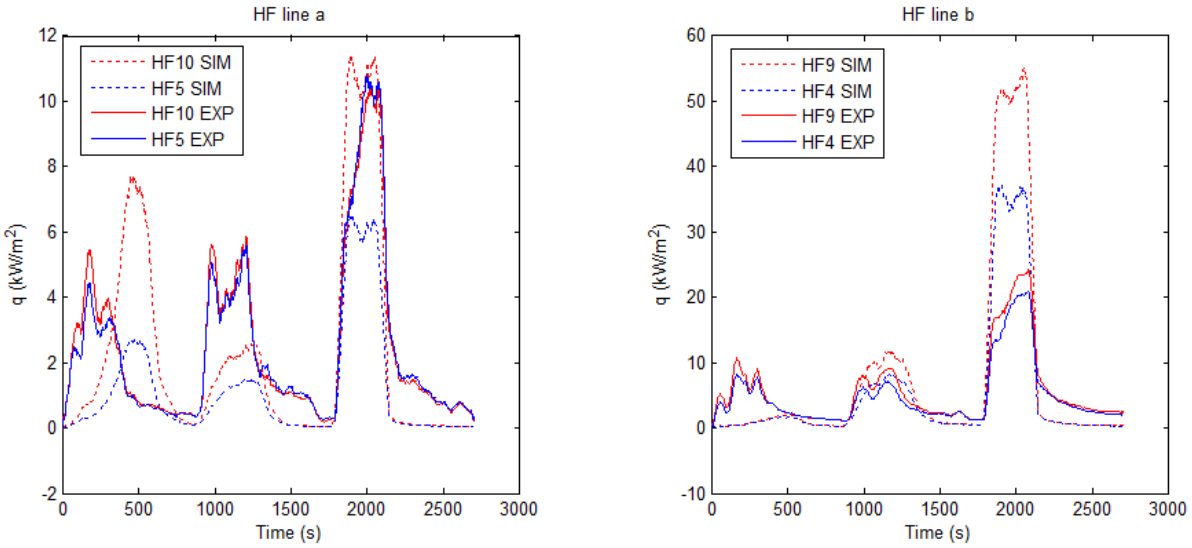

Figure 42. Test ②-1-2-3. Experiment vs. Simulation. Heat fluxes on façade.

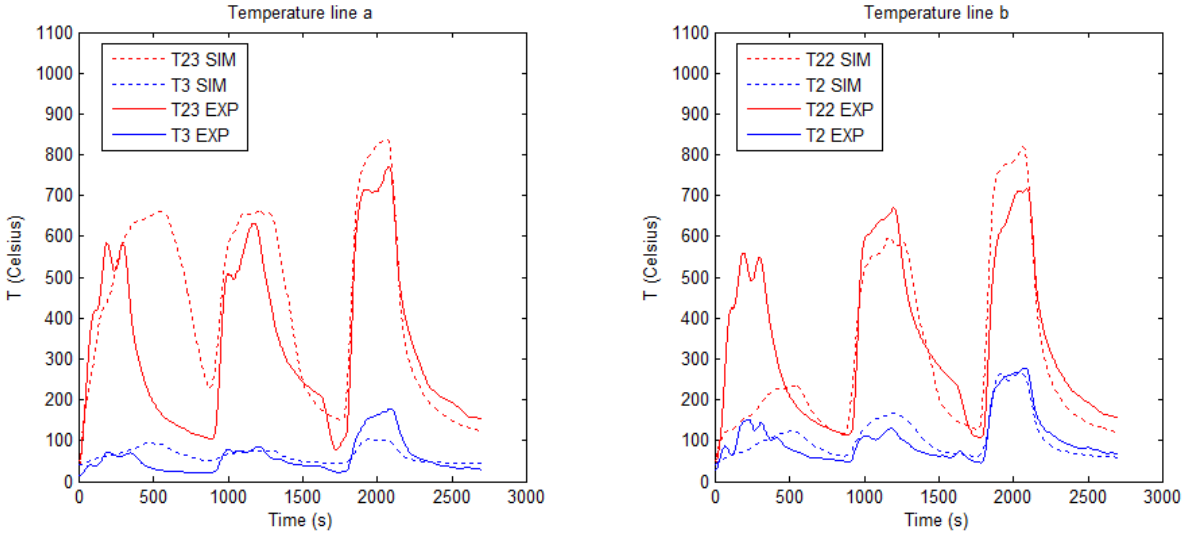

Figure 43. Test ②-1-2-3. Experiment vs. Simulation. Temperatures on façade.

This series of tests does not match requirements of right ISO 13785-2 test realization. In ISO 13785-2 façade window opening is defined as 2 m x 1.2 m opening with 0.1 m uncertainty.

6.2.4 Summary of the validation results

All three sets of experiments have several arrays of heat flux meters and thermocouples on façade and inside chamber. The large amount of data is here summarized by comparing the observed peak values of the measurements and predictions. Firstly, measured and predicted temperatures inside combustion chamber are compared in Figure 44. The horizontal axis corresponds to temperatures received from experiment and vertical axis corresponds to prediction of that value measured in simulation. Total experimental relative standard deviation of 0.07 is assumed, following NIST thermocouple reference tables (NIST 1999).

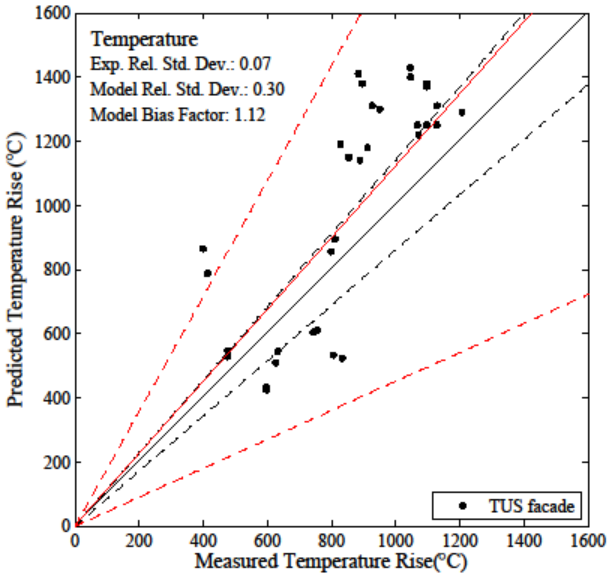

Figure 44. Summary of temperature predictions inside the combustion chamber

When measured temperatures in chamber increase over 900 °C, FDS over-predicts these temperatures. For tests with small fuel flow rates, when temperatures inside chamber achieve not more than 800 °C, FDS gives under-predicted results.

Positions of heat flux meters and thermocouples used during the validation are marked with red circles in Appendix 16. Heat flux predictions from the points are presented in Figure 45. Predictions of temperatures on façade for all three sets of data are presented in Figure 46.

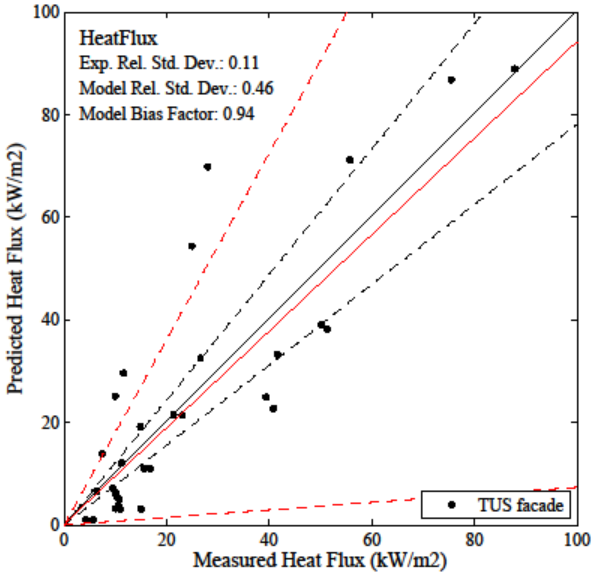

Figure 45. Summary of heat flux predictions on façade.

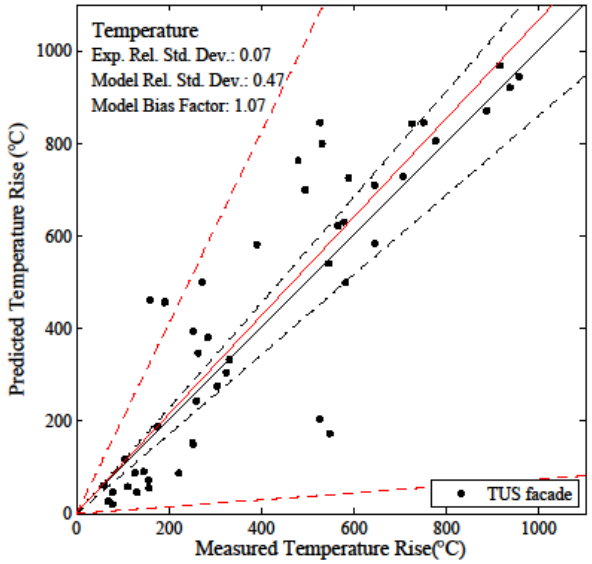

Figure 46. Summary of thermocouple temperature predictions on façade

There was observed that mostly dispersed results are coming from simulations of test with small fire load (less than 2.8 MW) or when a temperature on façade does not exceed 800 °C. Excluding these tests from validation graphs results will come to the form presented in Figures 47, 48 and 49. Figure 47 presents comparisons of temperatures inside chamber between simulation and experiment, where horizontal axis corresponds to experiment results and vertical axis – to simulation results.

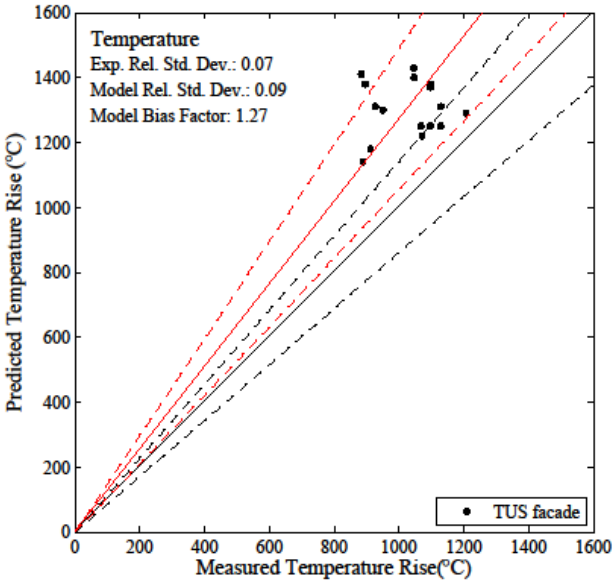

Figure 47. Summary of chamber inside temperature predictions for experiments with temperatures on façade over 800 °C.

Temperature measured by thermocouples in simulations is larger than in experiment, although the size and positions of thermocouples was the same. Excluding tests with small fuel flow rates, the relative standard deviation for heat fluxes on façade becomes smaller. These results are presented in Figure 48.

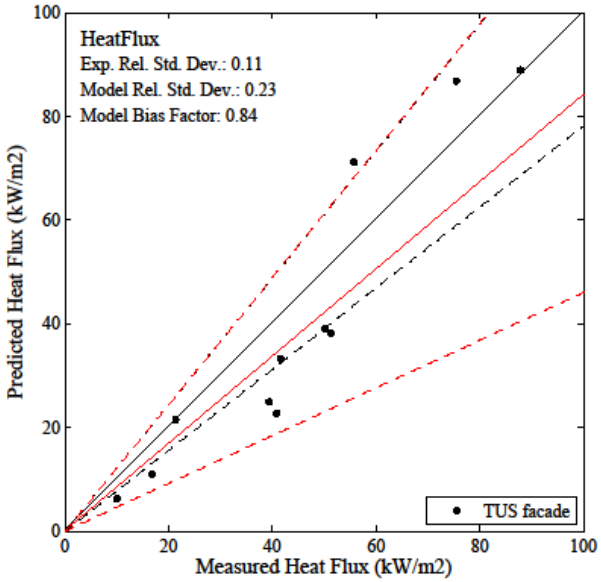

Figure 48. Summary of heat flux predictions on facade for experiments with temperatures on façade over 800 ºC.

Comparison of temperatures on facade between experiment and simulation with small fuel flow rates excluded is presented in Figure 49. Excluding the test that are not represent ISO 13785-2 thermal exposure requirements, the model bias factor closer to 1 and the model relative standard deviation comes smaller (decreased from 0.47 to 0.35) for temperature prediction on façade wall.

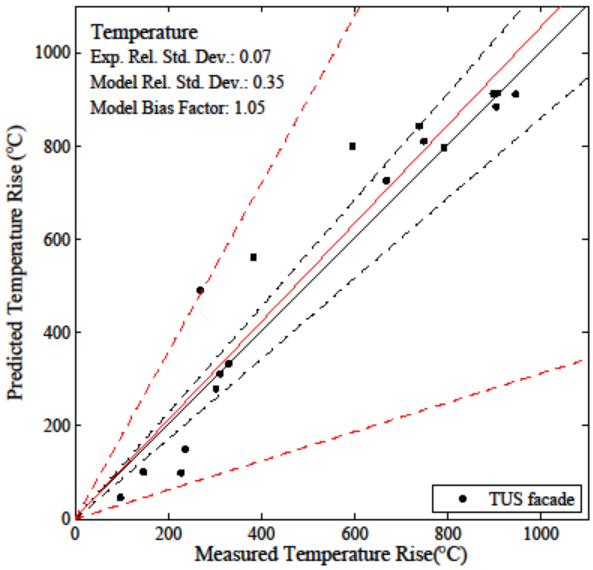

Figure 49. Summary of thermocouple temperature predictions on facade for experiments with temperatures on façade over 800 ºC.

6.3 Sensitivity study

6.3.1 Room dimensions

According to the ISO 13785-2 standard, the internal volume of combustion chamber can vary from 20 to 100 m^3. The dimensions of the combustion chamber defined as 4300 mm for depth and 1700 mm for height. Therefore, the width of the chamber can vary from 2736 mm to 13679 mm. To determine the influence of this parameters, numerical simulation were performed with extreme values of the allowed chamber width.

Simulations were made with the following characteristics:

- Maximum heat flux corresponds to fuel supply flowrate of 120 g/s.
- Fuel flowrate increased linearly from zero to maximum flowrate in first 5 minutes of simulation.
- Simulation was extended for two minutes with maximum flowrate
- First case corresponds to simulation with combustion room width of 3 m.
- Second case corresponds to simulation with combustion room width of 13 m.
- Others characteristics of chamber was identical for both cases.

The figure below presents heat flux development for the all-time of simulation (summary 420 seconds). Heat flux meters (HF1, HF7 and HF8) are located above the higher edge of the window opening on 0.6 m height. HF1 measures heat flux on centerline, HF7 on left side and HF8 on right side of the window that is close to the side wall.

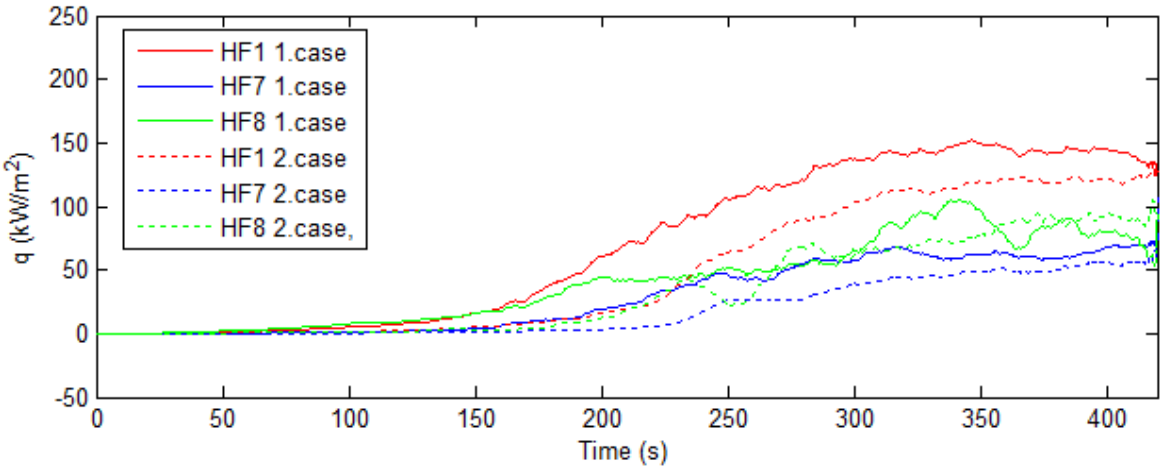

Figure 50. Heat fluxes at height of 600 mm above the window.

First case (3 m wide combustion chamber) values of heat flux meters HF1 and HF7 are higher than for the second case for the whole simulation period. The biggest difference between two cases occurs in interval 200-250 seconds, when HRR still is increasing, after that the smaller difference was observed.

The large difference between two cases at first seconds (time interval 150-350 s) is caused by difference in time, when flashover in compartment occurs. The smaller chamber requires less heat to move into fully developed fire stage. The percentage difference between the results is the modulus of difference between two values divided by the average value of those two val-

ues. The biggest difference in heat fluxes was observed on HF1. The percentage difference of HF1 is showed in Figure 51.

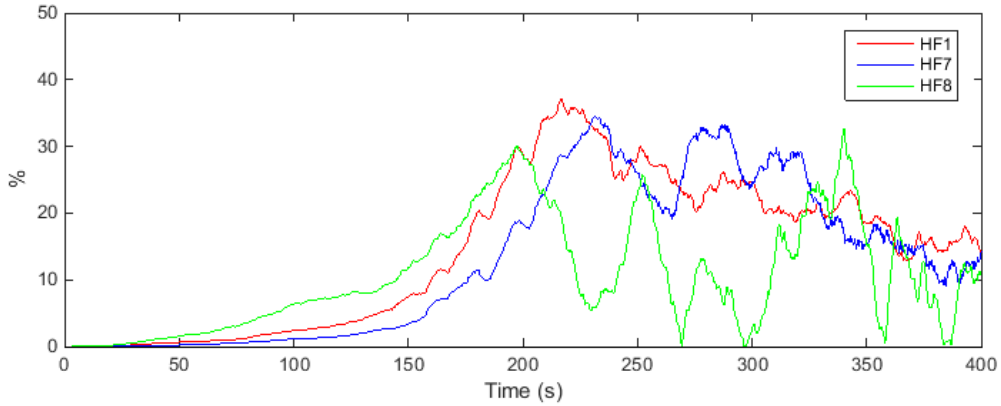

Figure 51. Percent difference for HF1, HF7 and HF8.

Predicted temperatures measured by thermocouples placed on the façade are presented in Figure 52. Thermocouple marked with T2 is located at the window centerline. Thermocouples T1 and T3 are placed on the left and right side above the window. Positions of thermocouples correspond to positions in Figure 11.

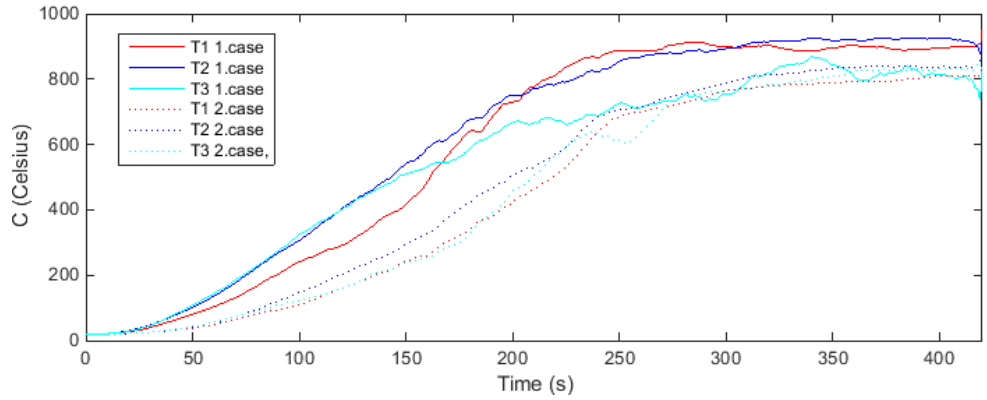

Figure 52. Temperatures immediately above the window.

For the first case, temperature at thermometer T2 reaches an average value of 920 ºC, the corresponding value of second case is 830 ºC. Similar to the heat flux, the temperatures differs more in the beginning of the test. After that, difference decrease almost linearly to 10% value. Percentage difference of temperature predictions between cases is presented in Figure 53.

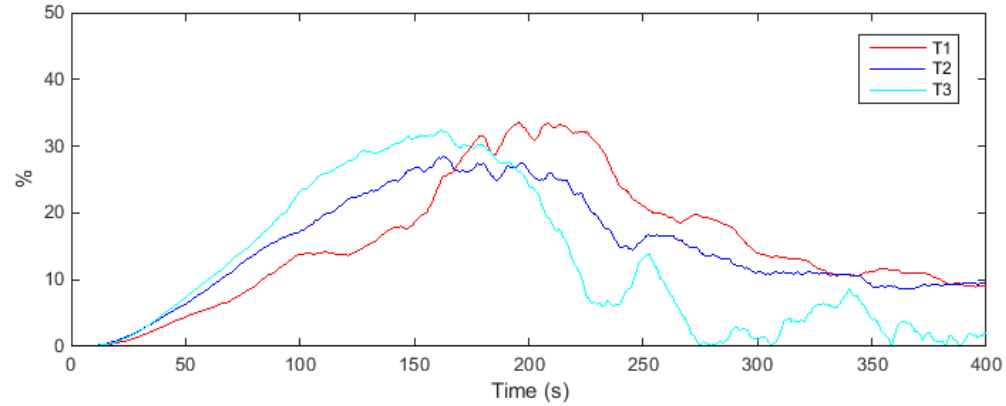

Figure 53. Percent difference for T1, T2 and T3.

6.3.2 Additional ventilation

Additional openings on the back wall of the chamber are permitted in order to allow natural ventilation. There is no specific prescription in ISO for these openings. (ISO 13785-2:2002). To identify this criteria influence, simulation was performed for combustion chamber with ventilation factor increased by 10% by adding additional opening to rear wall of combustion chamber. 10% is responsible for about additional opening with dimensions 0.5 m width and 0.6 m height.

The amount of ventilation in a fire compartment is described by ventilation factor:

$$F_v = A\sqrt{H} \tag{23}$$

where A is the area of the window opening and H is the height of the window opening. These parameters for two or more openings can be calculated with following equation:

$$H = (A_1H_1 + A_2H_2 + ...)/A \tag{24}$$
$$A = A_1 + A_2 + ... = B_1H_1 + B_2H_2 + ... \tag{25}$$

(Drysdale 2011, p. 365, 410).

Calculation results for multiple openings and primary situation with only one façade window opening is demonstrated in Table 12:

Table 12. Comparison of ventilation factors.

Ventilation factor			
Facade window only		Additional opening 0.5x0.6	
A	H	A	H
2.4	1.2	2.7	1.13
F_v		F_v	
2.629		2.874	

Ventilation factor increases by 10% (9.3%) adding an opening in back side of the chamber. The next simulations were made to determine the influence of the additional ventilation opening to the heat fluxes and temperatures on façade. Description of simulations compared in this part is:

- Maximum heat flux corresponded to fuel supply flowrate of 120 g/s.
- Fuel flowrate increased linearly from zero to maximum flowrate in first 5 minutes of simulation.
- Simulation was performed for two minutes with maximum flowrate
- First case corresponds to simulation with normal ventilation factor defined by façade window opening with dimension 2 m x 1.2 m.
- Second case corresponds to simulation with ventilation factor increased by 10 percent.
- Others characteristics of chamber was identical for both cases.

The heat flux results gathered from simulation are presented in Figure 54.

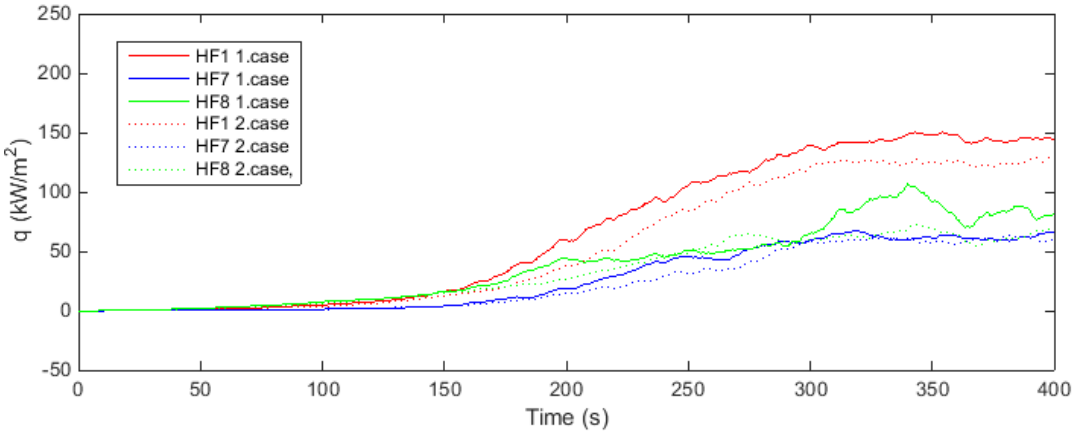

Figure 54. Heat fluxes at height of 0.6 m above the window.

Heat flux values on façade received from test without additional ventilation is the bigger than the heat flux values predicted in simulation with opening in rear wall. This is actually for all-test time. Percentage difference of heat flux predictions between cases is presented in Figure 55.

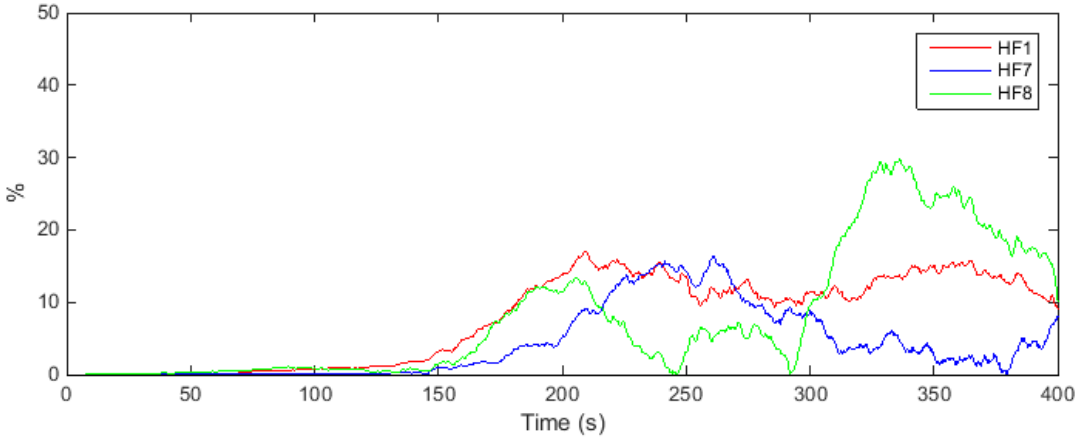

Figure 55. Percent difference for HF1, HF7 and HF8.

Temperatures measurements have done 50 mm above the top edge of window. Results of examined cases with respect to temperature are presented in Figure 56:

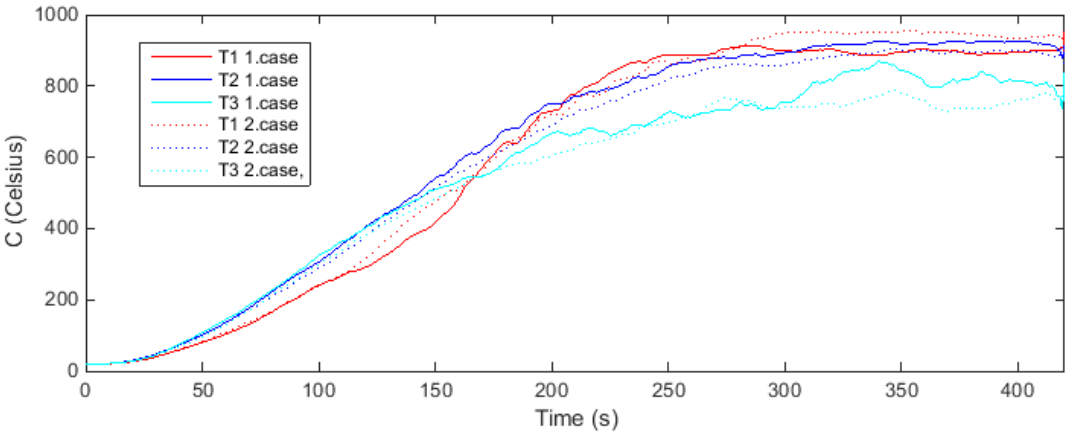

Figure 56. Temperature immediately above the window.

The following percent difference of temperature predictions was observed (Figure 57):

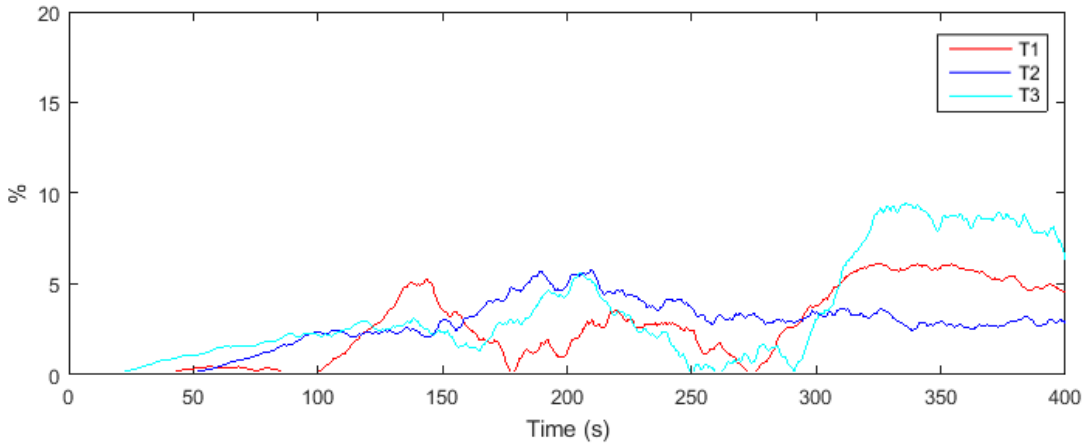

Figure 57. Percent difference for T1, T2 and T3.

6.3.3 Façade window dimensions

According to ISO standard façade window dimensions are specified as 2±0.1 m width and 1.2±0.1 m height. In Table 13, presented how ventilation factor (F_v) changes with different combinations of these parameters. Calculations made using equation 2.

Table 13. Ventilation factors for different façade window dimensions.

Ventilation factor					
Facade window 2x1.2 m Case 1.		Facade window 2.1x1.3 m Case 2.		Facade window 1.9x1.1 m Case 3.	
A	H	A	H	A	H
2.73	1.30	2.40	1.20	2.09	1.10
F_v		F_v		F_v	
3.11		2.63		2.19	

As Table 13 demonstrates, ventilation factor with window size of 2.1×1.3 m is 18.4 % more than with normal window (2.0×1.2 m). In its turn, the ventilation factor with smaller window (1.9×1.1 m) is 16.6 % less than ventilation factor specified by normal window.

Here are presented results for first seven minutes of ISO test simulation. Making heat flux-time curves used ‘moving average ‘smoothing with time interval of 2.6 sec.

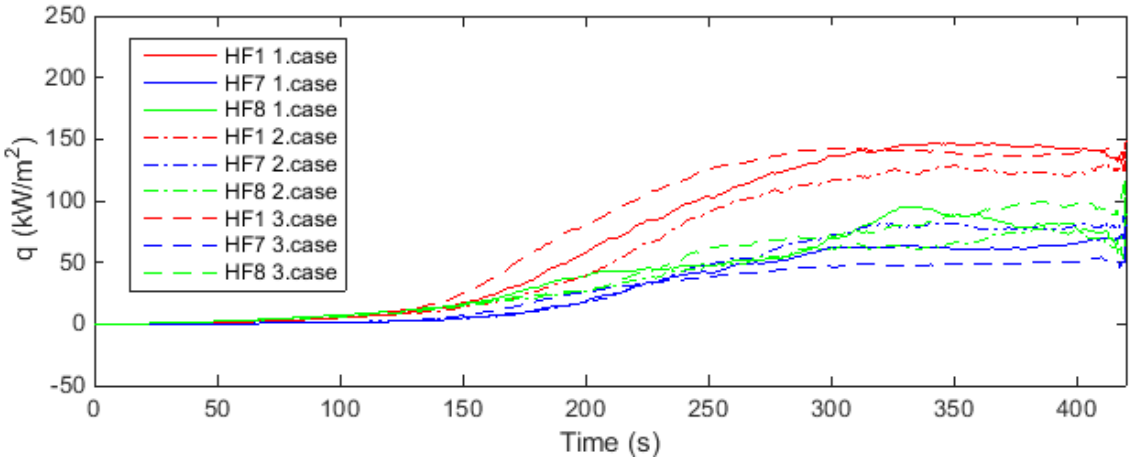

Figure 58. Heat flux 0.6 m above the window.

The percent difference between cases made separately for second and third case with respect to the first case results (window with dimensions 2.0×1.2 m).

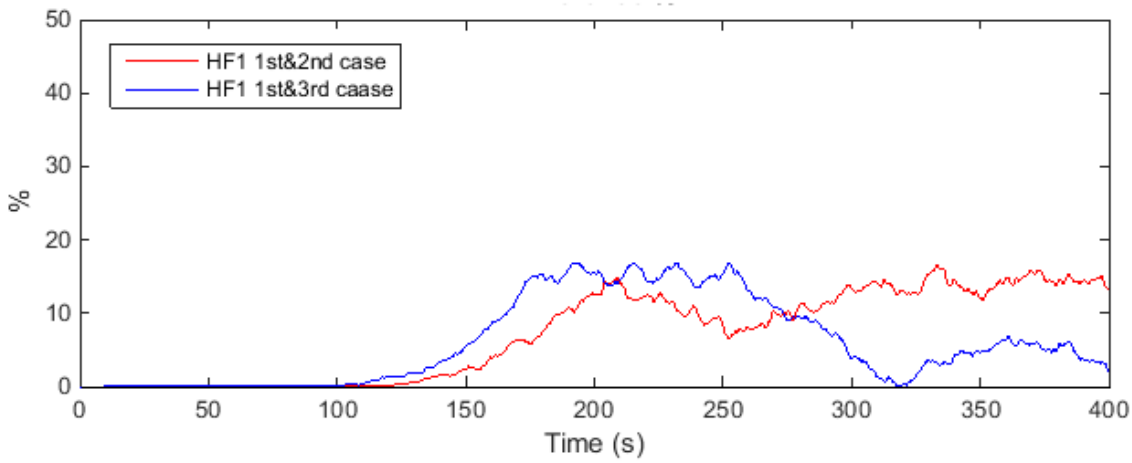

Figure 59. Percent difference of HF1 results for 1st,2nd and 3rd case.

Similar procedure was done for temperature predictions on façade. Values of temperature are taken at 50 mm height from window top edge.

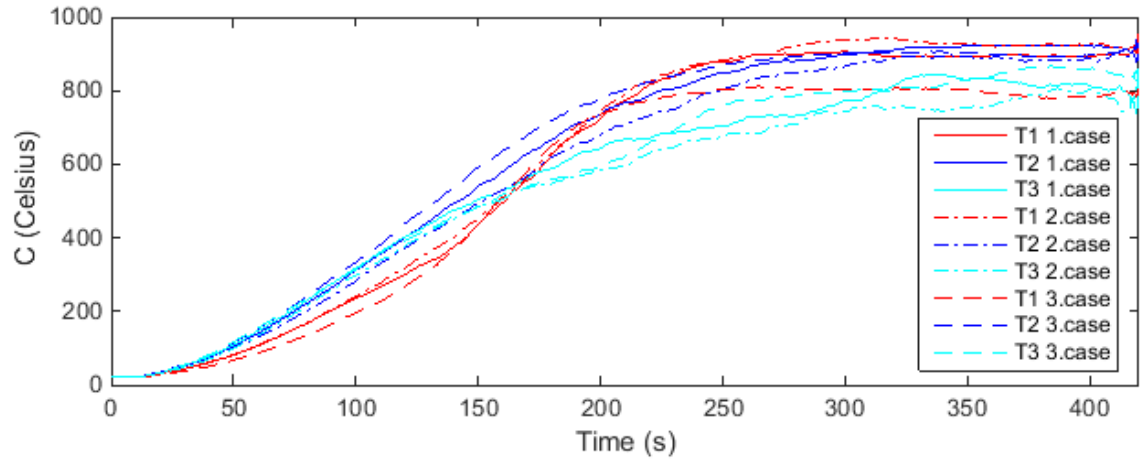

Figure 60. Temperature at centerline immediately above the window.

The percent difference of temperature predictions between two cases calculated with respect to test with normal size façade window opening (2.0×1.2 m).

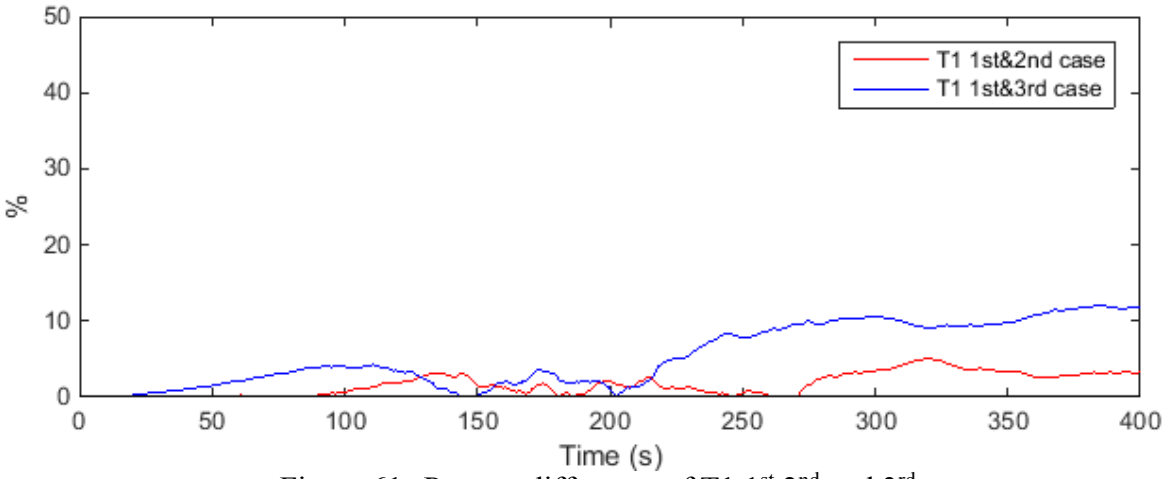

Figure 61. Percent difference of T1 1st,2nd and 3rd case.

Behavior of temperature development and its maximum does not differ greatly with façade window dimensions decreasing or increasing by 0.1 m in height or in width. In next chapter maximum values of heat fluxes and temperatures on façade are compared for all performed sensitivity tests.

6.3.4 Summary of sensitivity simulations

Sensitivity parameters can be divided into three groups. First group of parameters is test arrangement. Parameters as room geometry, openings and their dimensions, air temperature in the test and wall material properties relate to this group. Second group of parameters describe burning process itself. Third group includes common parameters affecting the numerical solution accuracy. In chapter 6.3.4 are collected figures of maximum heat fluxes and temperatures observed during sensitivity simulations.

6.3.4.1 Test arrangement

Room width parameter

Simulations were performed with chamber width of 3 m and 13 m. Maximum heat flux determined during the test is presented on Figure 62.

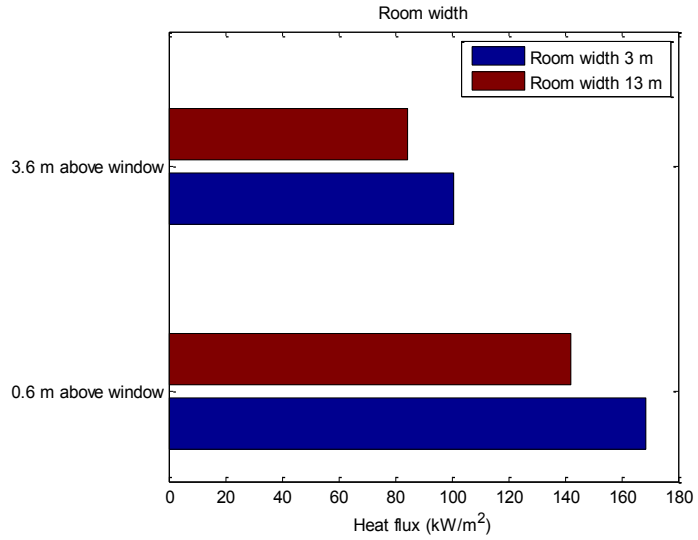

Figure 62. Sensitivity of the maximum heat fluxes to the room width.

Wall temperature measured at 50 mm and 4000 mm above the window opening was at its maximum according to Figure 63.

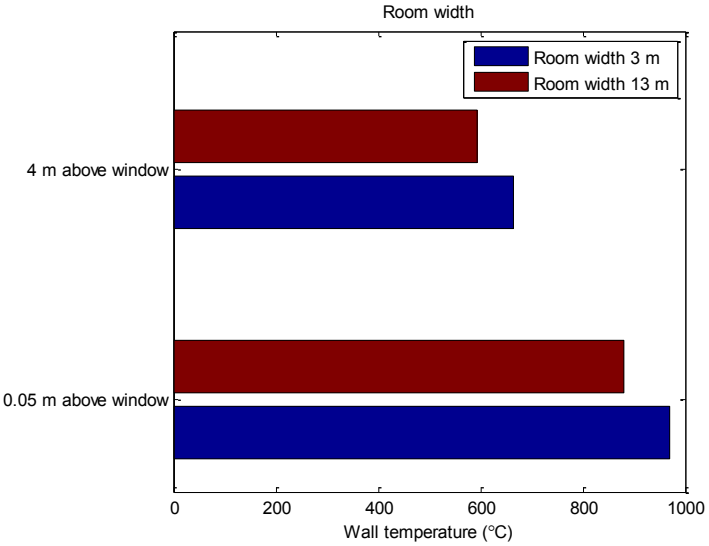

Figure 63. Sensitivity of the maximum temperatures to the room width.

The relative standard deviation for results of heat fluxes at 0.6 m height above the window is 12 % and for temperatures at 50 mm above the window – 6%.

Additional ventilation parameter

Adding an additional opening in rear side caused ventilation factor of room increasing by 10 %. Maximum heat fluxes at 600 mm and 3600 mm are presented in Figure 64.

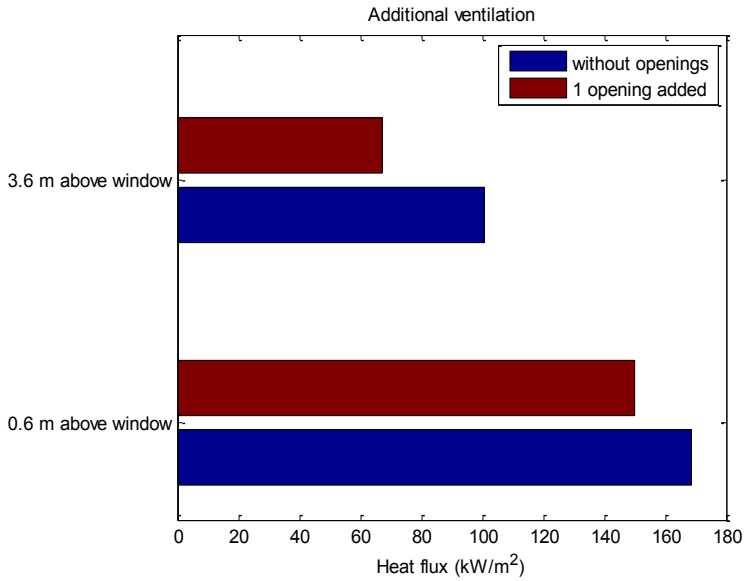

Figure 64. Sensitivity of the maximum heat fluxes to the additional ventilation opening.

Simultaneously, temperatures of the façade wall increased to values presented in Figure 65.

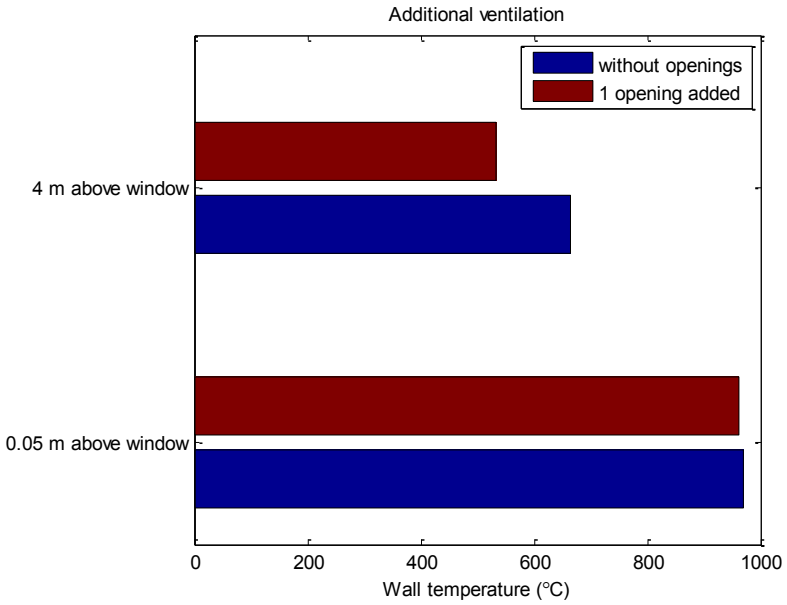

Figure 65. Sensitivity of the maximum temperatures to the additional ventilation opening.

In presence of rear side opening heat fluxes on façade wall are less than in situation with enclosed chamber. Same behavior is observed in temperature comparisons although maximum temperature at 50 mm level above the window remains almost unchanged.

The relative standard deviation for results of heat fluxes at 0.6 m height above the window is 8.4 % and for temperatures at 50 mm above the window – 0.5%.

Façade window dimensions

Comparisons of maximum heat fluxes with different façade window dimensions are presented in Figure 66. Façade opening, named in figure as small window, has dimensions 1.9 x 1.1 m,

normal window – 2 x 1.2 m and large window – 2.1 x 1.3 m. The relative deviation for results of heat fluxes at 0.6 m height above the window is about 1.3%.

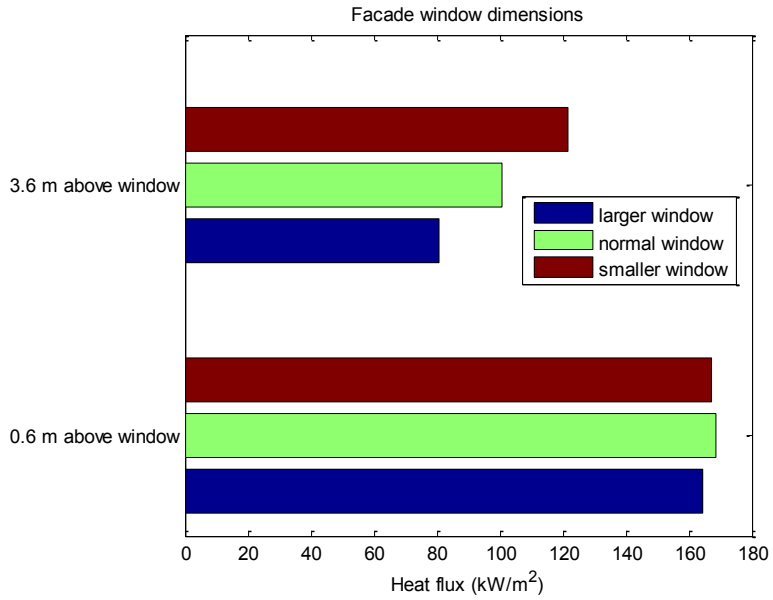

Figure 66. Sensitivity of the maximum heat fluxes to the main window dimensions.

Maximum wall temperatures measured in simulations for this case are presented in Figure 67. The relative deviation for results of temperatures at 50 mm height above the window is about 2.1%.

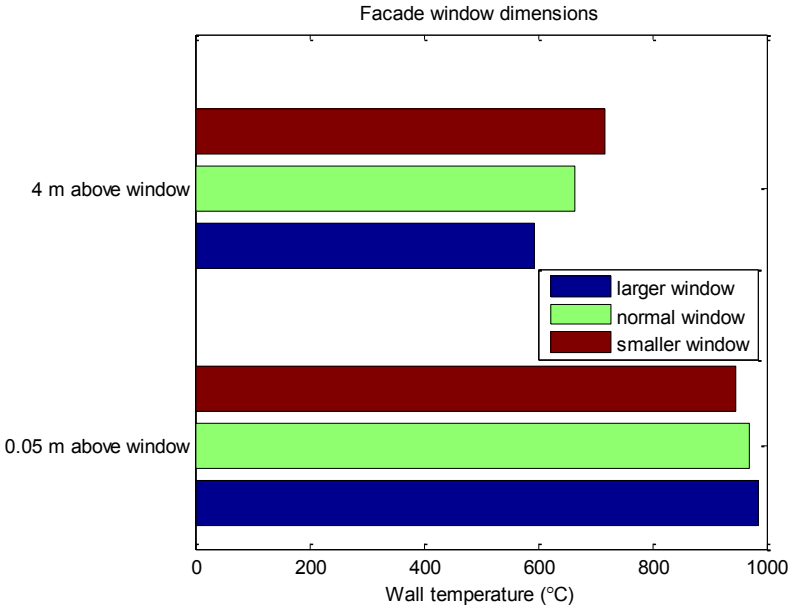

Figure 67. Sensitivity of the maximum temperatures to the main window dimensions.

Heat fluxes above the window are larger in simulation with the smallest window. It appears because in this case less oxygen pass to the combustion chamber and burning mostly occurs on façade. Despite that maximum heat fluxes at 0.6 m above the window are almost the same because of heat flux meters position being inside plume region all time.

Chamber wall material properties

Material of chamber walls can make influence to heat fluxes on façade. According to ISO 13785-2, different types of material can be used. However, wall should be covered with high temperature resistant insulation material. In simulation, concrete and insulation board were covered with 25 mm ceramic fiber blanket. In Figures 68 and 69 maximums of heat fluxes and temperatures is presented.

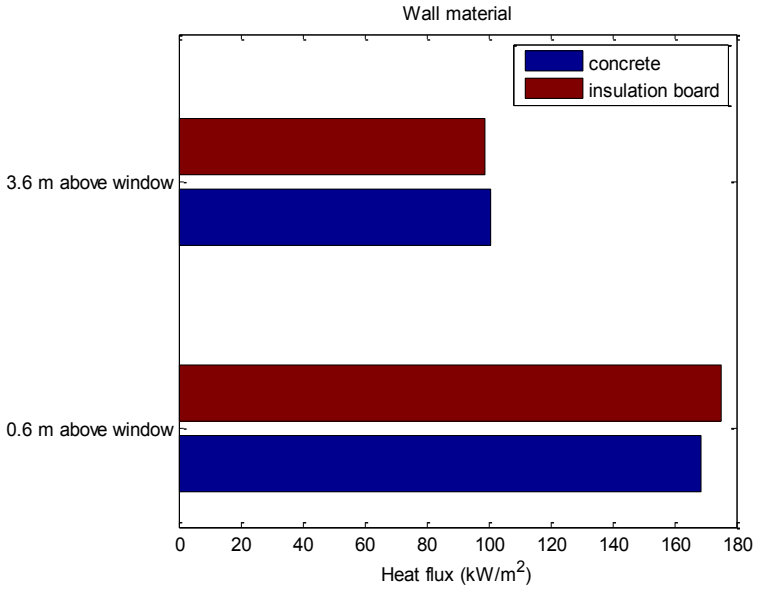

Figure 68. Sensitivity of the maximum heat fluxes to the wall's material.

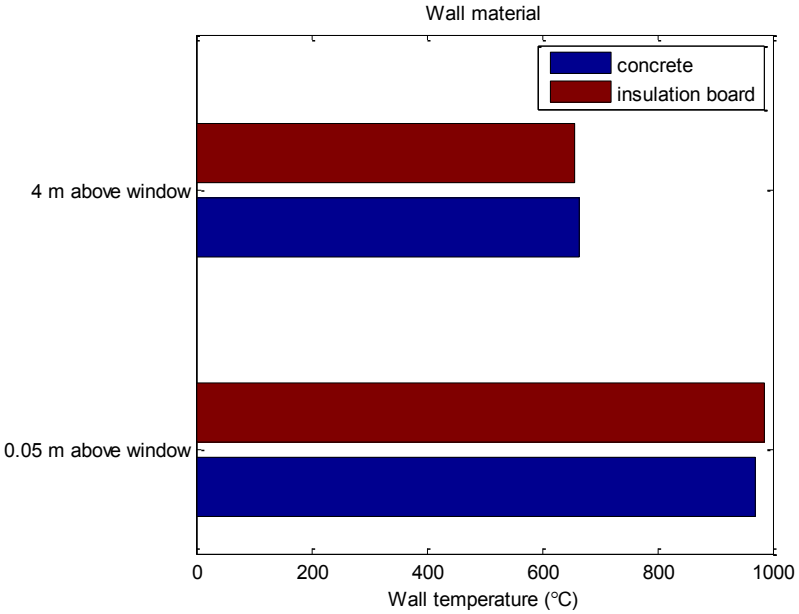

Figure 69. Sensitivity of the maximum heat fluxes to the wall's material.

According to these results it can be concluded that the material of the chamber walls has no influence on the maximum heat fluxes and temperatures on façade, if it is covered with thin high temperature insulation layer. The relative difference for results of heat fluxes at 0.6 m height above the window is 2.6 % and for temperatures at 50 mm above the window is 1.2%.

Air temperature parameter

Since this comparison, for determining parameter's influence to heat flux and temperature on façade, model from validation study was used (model of test ①-1-2-3). More accurate model description is presented in Chapter 6.2.

During experiment air temperature in large hall (laboratory) can increase, especially under the ceiling. For that case simulation was performed with different air temperatures 20 °C and 40 °C.

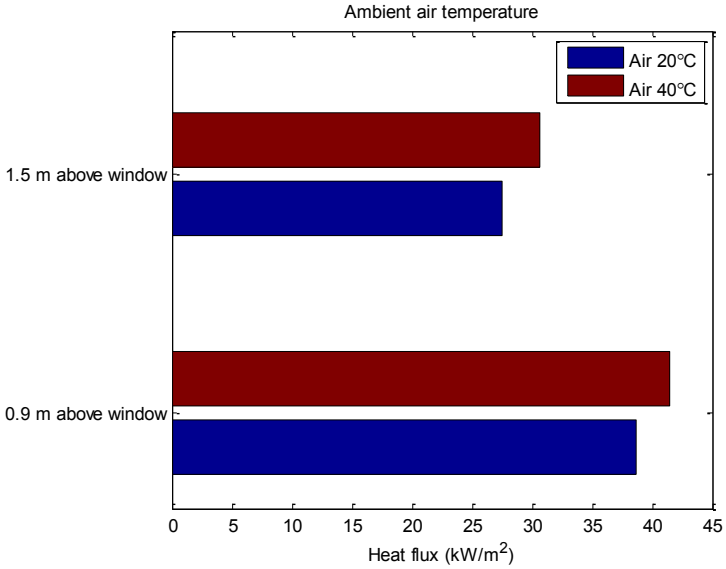

Figure 70. Sensitivity of the maximum heat fluxes to the ambient temperature

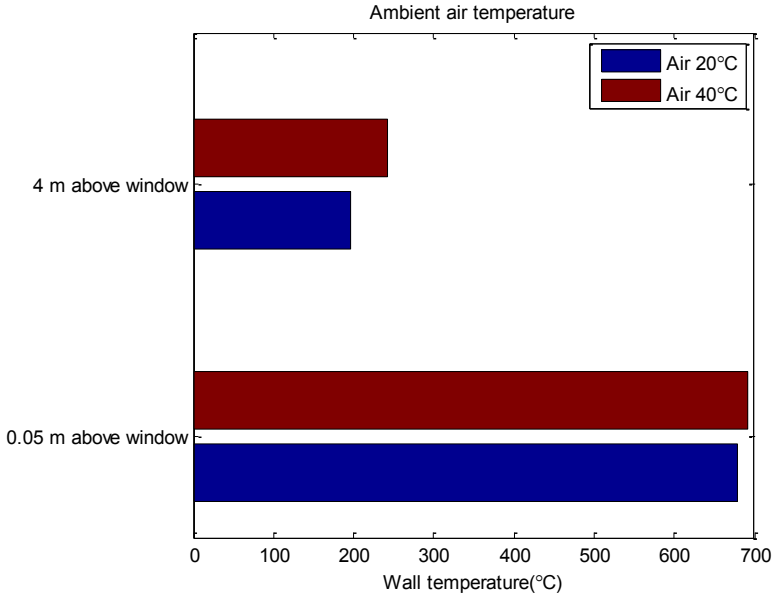

Figure 71. Sensitivity of the maximum temperatures to the ambient temperature.

The relative difference for results of heat fluxes at 0.9 m height above the window is 7.5 % and for temperatures at 50 mm above the window is 1.6%.

Position of the combustion chamber

Position of the chamber with respect to the façade window is not defined in standard. In this simulations test ①-1-2-3 was performed with different positions of the chamber. In Figure 72, sketches of compared tests are presented. 'Left' means that the combustion chamber was located on the left side of the facility, as far as it possible when the window right side and the right wall of chamber match. 'Right' means the opposite location of chamber. 'Center' means that the chamber is placed symmetrically with respect to the window.

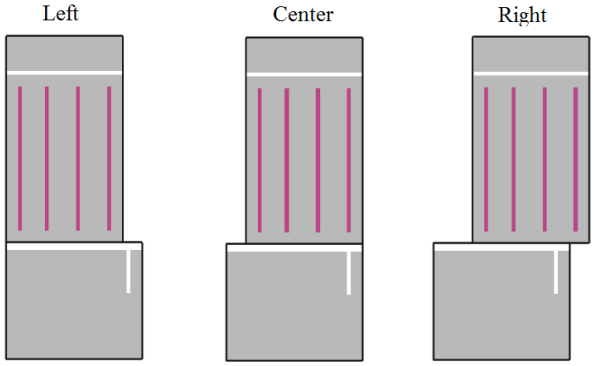

Figure 72. Different positions of combustion chamber with respect to façade window

The results of maximum heat fluxes and temperatures are presented in Figures 73. There are three columns that are corresponding to the three vertical lines on the left, center, and right side above the window. These line positions are the same as in Figure 37.

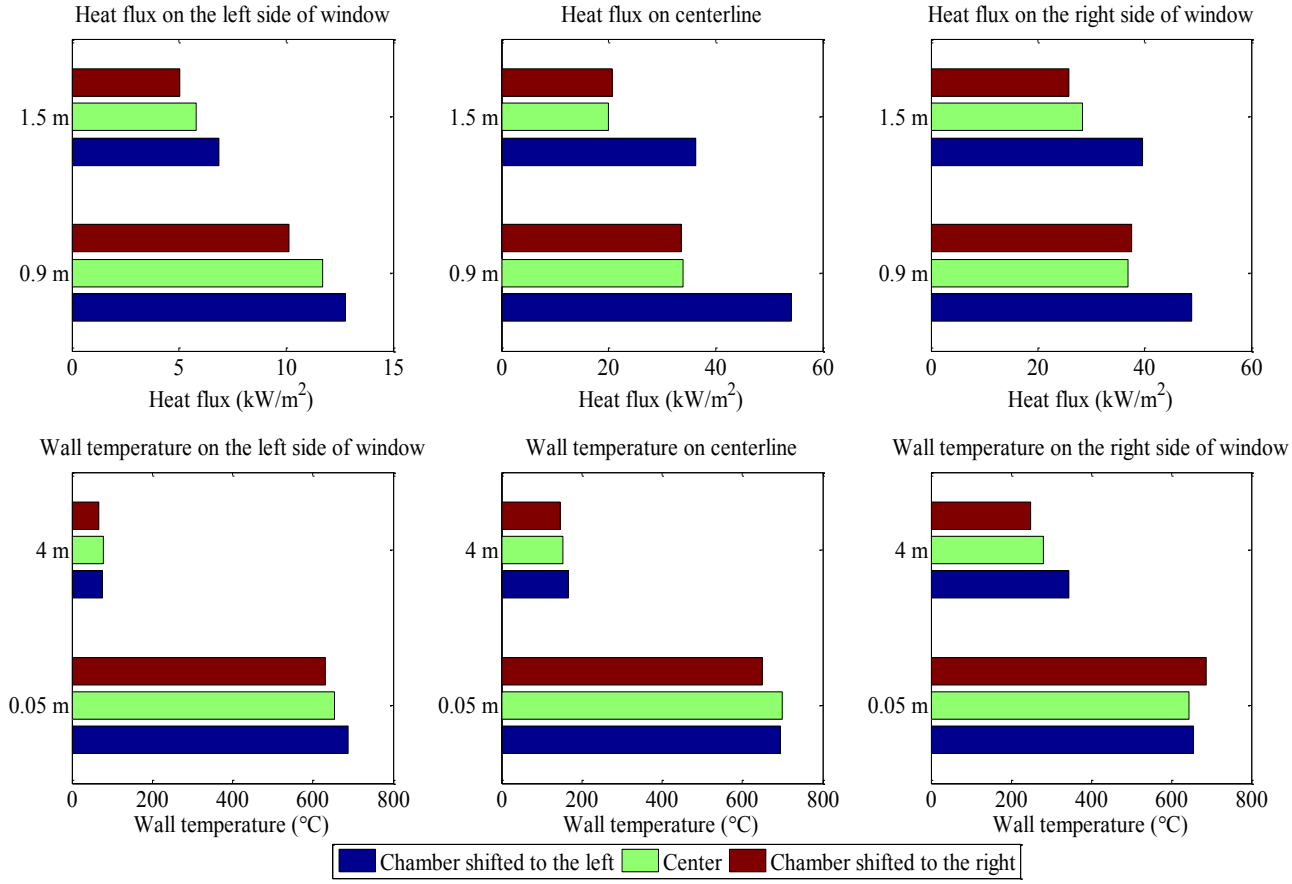

Figure 73. Sensitivity of the maximum heat fluxes and temperatures to the main window position on the left, center and right side of the window

Average value of results from Figure 73 at a certain height is calculated for heat flux and wall temperature. These results are presented in Figure 74.

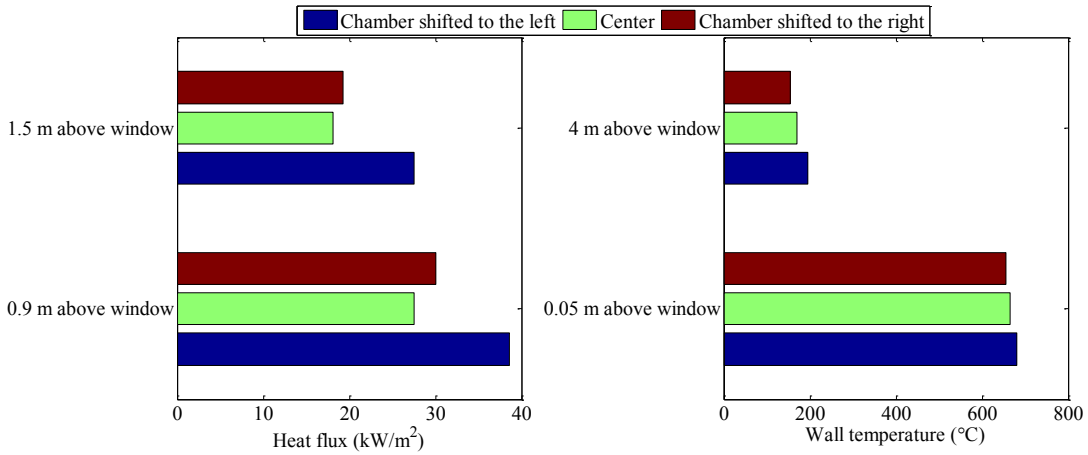

Figure 74. Sensitivity of the maximum heat fluxes and temperatures to the main window position

The relative deviation for results of heat fluxes at 0.9 m height above the window is 18 % and for temperatures at 50 mm above the window is 1.8%. The case with combustion chamber shifted to the left shows larger results for heat flux and wall temperature than other two cases. The simulations with chamber on the center and chamber shifted to the right side show insignificant difference between compared points. The position of the chamber can affect to the plume direction on the façade. Thus, the plume in case with chamber on the center is more vertically-directed than in case with chamber shifted to the left.

6.3.4.2 Model parameters – Physical

Influence of model parameters was investigated during simulations related to the validation study that is presented in chapter 6.2. Maximum values of the heat fluxes and temperatures are taken from test ①-1-2-3 simulation.

Radiative fraction

The default value of the radiative fraction in FDS is 0.35. It means that 35% of the combustion energy will be assigned to the thermal radiation source term (FDS6 User's Guide). This parameter depends on chemical structure of burning material. For natural gas flames roughly 80% of the heat release is convected away and roughly 20% of heat release is radiated (Kashivagi 1998, p. 177).

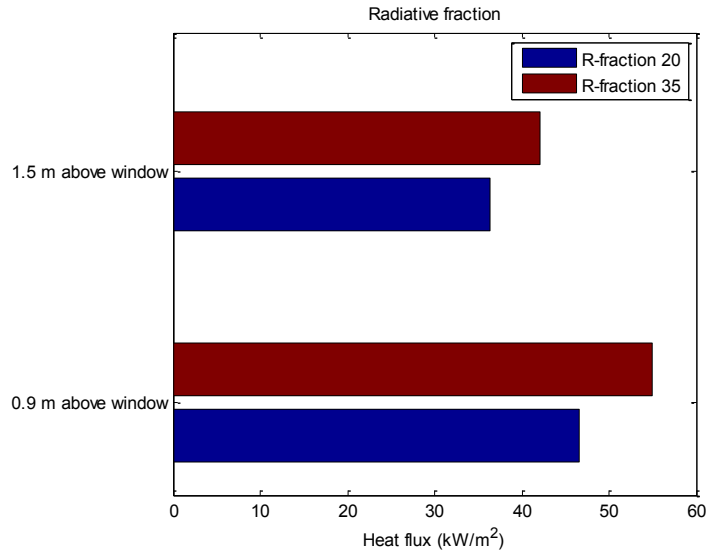

Figure 75. Sensitivity of the maximum heat fluxes to the radiative fraction.

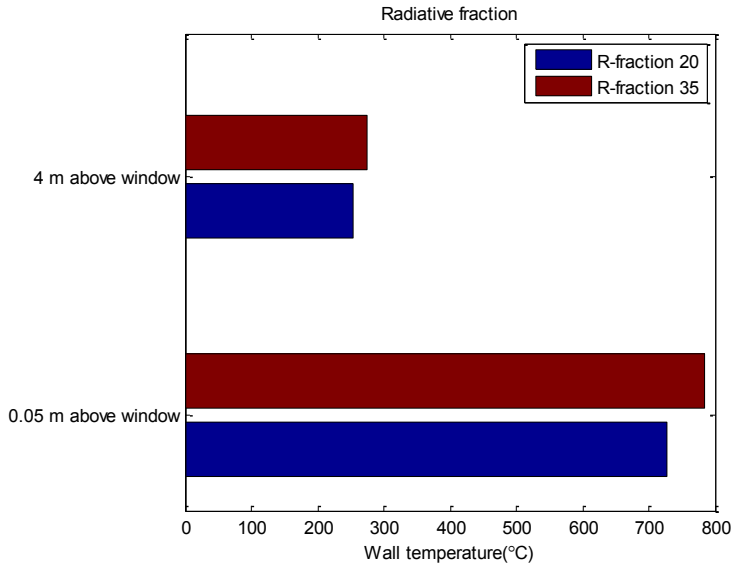

Figure 76. Sensitivity of the maximum temperatures to the radiative fraction.

The relative difference for results of heat fluxes at 0.9 m height above the window is 11.7 % and for temperatures at 50 mm above the window is 5.3%.

Soot yield parameter

Soot amount released in burning firstly depends from chemical content of fuel. In addition, soot yield changes according to fuel to air ratio. (Xie 2010, p. 14). Therefore, soot yields are different as for growth stage of compartment fire development as for post-flashover stage.

However, only one value of soot yield can be used in a single FDS simulation. Therefore, the same simulation cannot represent the different fire stages very well. The sensitivity of the predicted heat fluxes and temperatures to the choice of the soot yield was thus studied by performing two simulations with soot yield values of 1.5% and 5%. In Figures 77 and 78 maximum heat fluxes and temperatures on façade are presented for these simulations.

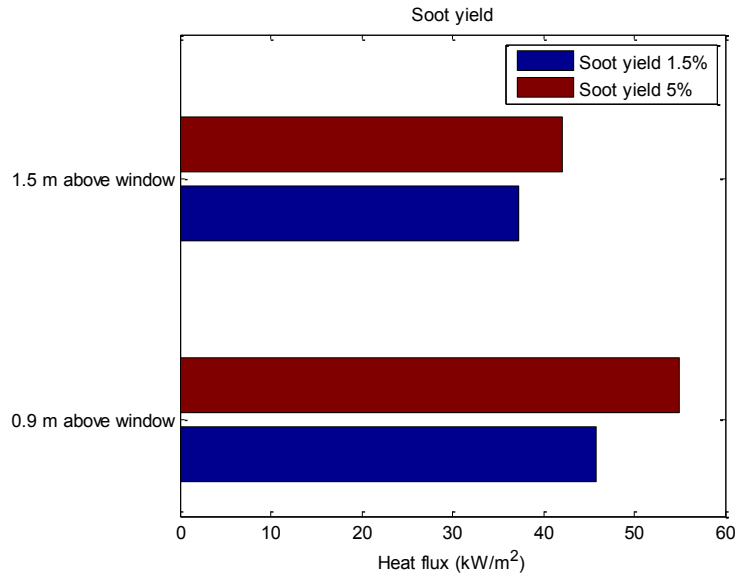

Figure 77. Sensitivity of the maximum heat fluxes to the soot yield.

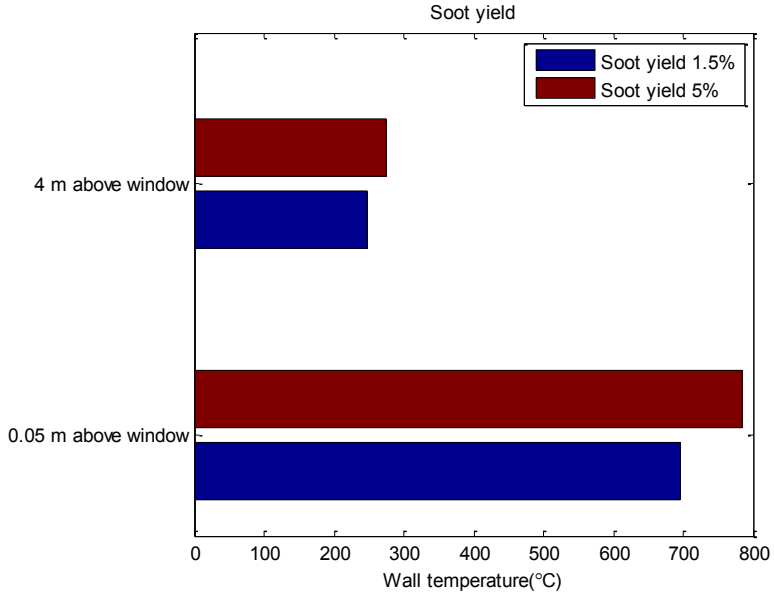

Figure 78. Sensitivity of the maximum temperatures to the soot yield.

Higher soot yield gives higher heat fluxes and wall temperatures on façade. Differences between results are decreasing with height from the window opening on façade wall. The relative difference for results of heat fluxes at 0.9 m height above the window is 12.8 % and for temperatures at 50 mm above the window is 8.4%.

6.3.4.3 Model parameters – Numerical (FDS)

Sensitivity of the model to parameters presented in this part is studied using the simulations of test ①-1-2-3 presented in validation study (chapter 6.2). The maximum of heat fluxes and temperatures observed during the test ①-3 are presented in figures below.

Cell size parameter

Numerical model was tested with different size of mesh cells. According to calculations from Chapter 6.1, it is rational to use the cells in range 50 mm – 100 mm. Influence of changing that parameter is presented in Figures 79 and 80.

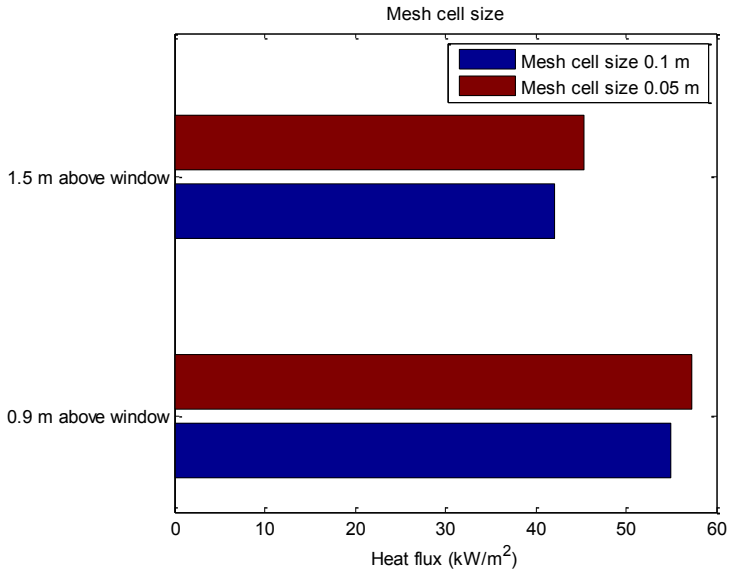

Figure 79. Sensitivity of the maximum heat fluxes to the model cell size.

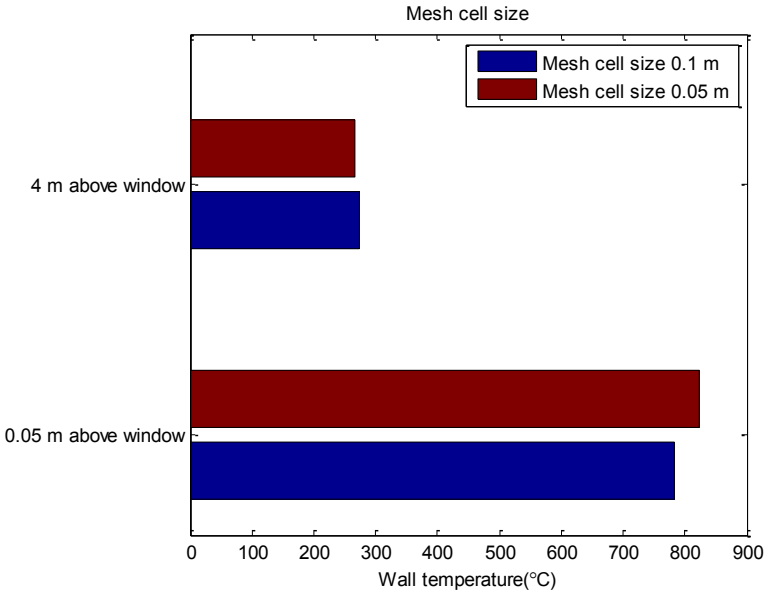

Figure 80. Sensitivity of the maximum temperatures to the model cell size.

Results from the figures above show that the mesh cell size variation from 50 mm to 100 mm does not affect large difference between heat fluxes and temperatures. It should be noted that cell size should be decreased with smaller fire load. The relative difference for results of heat fluxes at 0.9 m height above the window is 2.9 % and for temperatures at 50 mm above the window is 3.5%.

Number of radiation angles

Radiation transport equation can be solved in FDS with different number of radiation angles. Tighter discretization of angles can improve the accuracy of results especially in region locat-

ed relatively far from fire source. By default, FDS uses 100 radiation angles value. Simulations were performed with 1000 and 100 angles to determine the influence of this parameter. A comparison of heat fluxes on façade is presented in Figure 81 and comparisons of temperatures on façade in Figure 82.

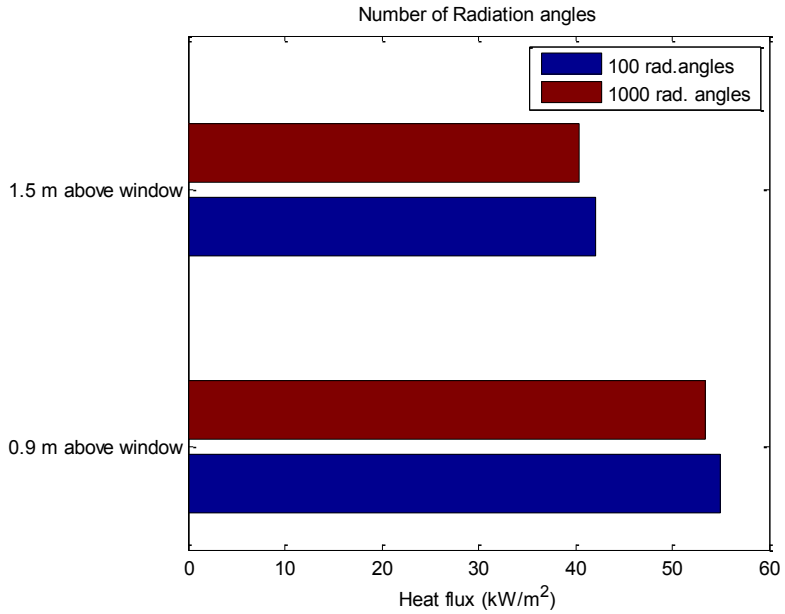

Figure 81. Sensitivity of the maximum heat fluxes to the number of radiation angles.

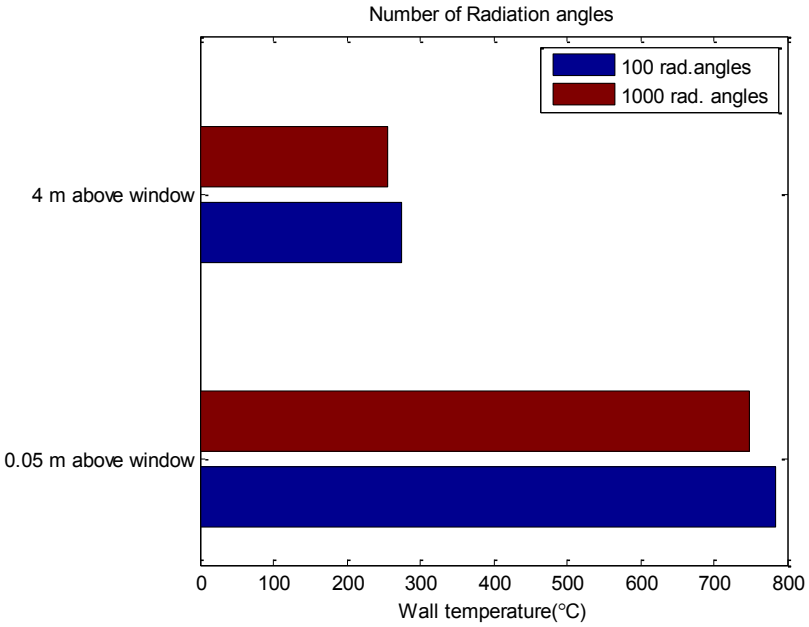

Figure 82. Sensitivity of the maximum temperatures to the number of radiation angles.

Simulations performed with more number of radiation angles shows about identical results, although the heat fluxes and temperatures from model with 1000 radiation angles are little bit less than it in model with 100 radiation angles. The relative difference for results of heat fluxes at 0.9 m height above the window is 2 % and for temperatures at 50 mm above the window is 3 %.

Solid cell size parameter

In FDS, solid phase cells size and distribution inside layer can be defined differently from mesh cells. Making a solid cell half the size gives the following results for heat fluxes and temperatures on façade wall (Figures 83 and 84).

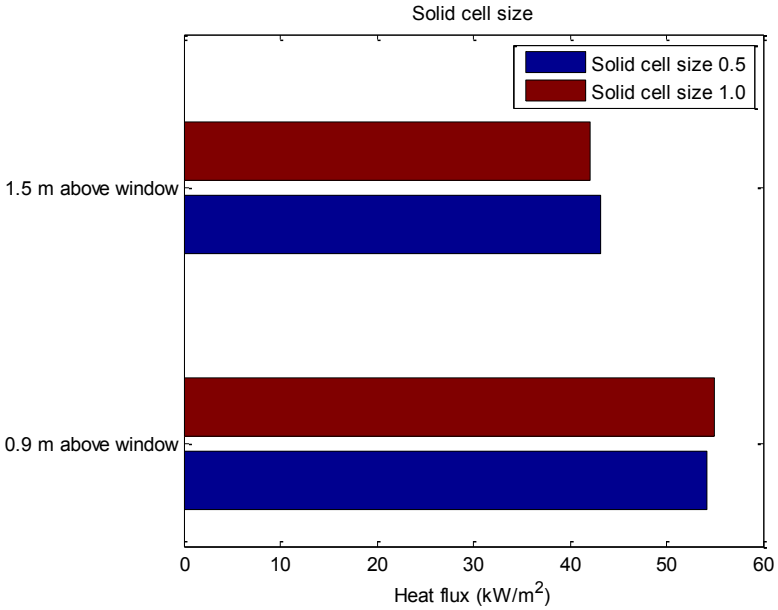

Figure 83. Sensitivity of the maximum heat fluxes to the solid cell size parameter.

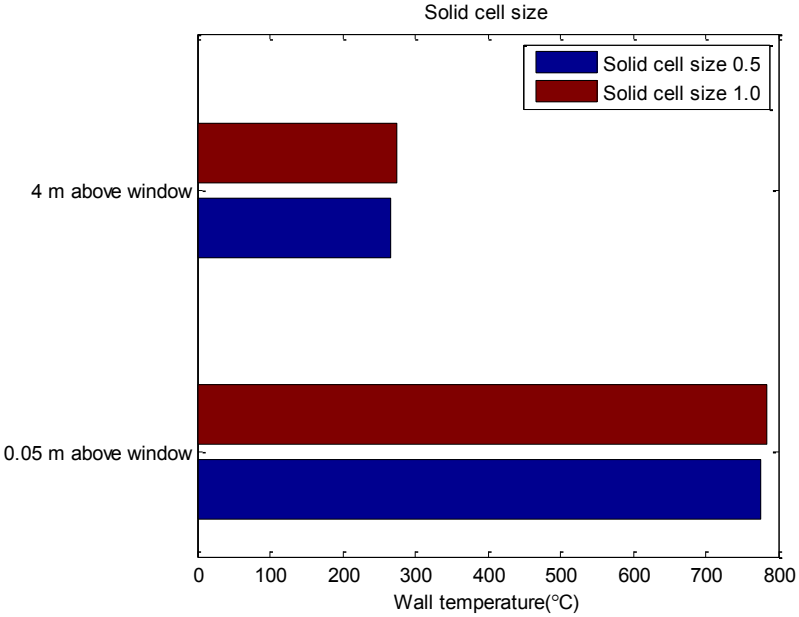

Figure 84. Sensitivity of the maximum temperatures to the solid cell size parameter.

Adding CELL_SIZE_FACTOR comment to the FDS code to all solid structures in model causes minor changing to maximum heat fluxes and temperatures on façade. The relative difference for results of heat fluxes at 0.9 m height above the window is 1 % and for temperatures at 50 mm above the window is 0.7 %.

6.4 Fire protection of façade insulation materials

In this section, the developed and validated model for the ISO 13785-2 scenario is used to study the fire protection requirements for the combustible insulation materials. Fuel flow rate was simulated according to ISO 13785-2. It increased linearly from zero to its maximum in 300 sec after that façade specimen was exposed to constant fire load for 20 minutes after which fuel flow rate was decreasing in 300 sec. According to standard, exposure should be about 55±5 kW/m^2 at 0.6 m height above the window and 35±5 kW/m^2 at 1.6 m height above the window. This exposure level was reached in simulation with maximum fuel flow rate being 63% of the maximum fuel flow rate allowed by the ISO 13785-2 standard. An example of FDS input is presented in Appendix 3. The average value of heat flux meters HF1, HF7, HF8 was in approved interval from 50 – 60 kW/m^2, and HF2 was in interval from 30 - 40 kW/m^2. Positions of that heat flux meters are presented in Chapter 6.2 in Figure 37. Simulation was performed with non-combustible wall made from stone wool that got the same properties of conductivity and specific heat used in simulations of Cone Calorimeter test described in Chapter 5.4.4.

In the simulation process, gauge heat fluxes were measured in different points above the façade window opening. Devices were evenly distributed above the window on with 100 mm horizontal and vertical spacings. Chamber location in relation window location and maximum heat flux at random time step presented in Figure 85.

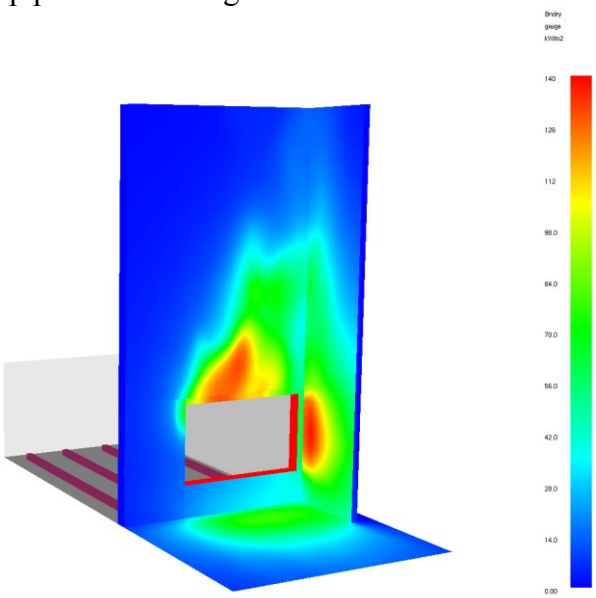

Figure 85. Smokeview figure of gauge heat flux on façade wall. Chamber shifted to the left.

After 300 sec of testing, HRR remains constant, and the heat fluxes on the façade remain constant too if localized, fluctuating plumes are not taken into account. Average heat fluxes measured above the window are represented in Figure 86. Side wall is not shown on the figure, but it is located on the right edge. Left figure corresponds to the case with shifted position of combustion chamber as in Figure 85. Right figure is related to the results of simulation with symmetrically located combustion chamber.

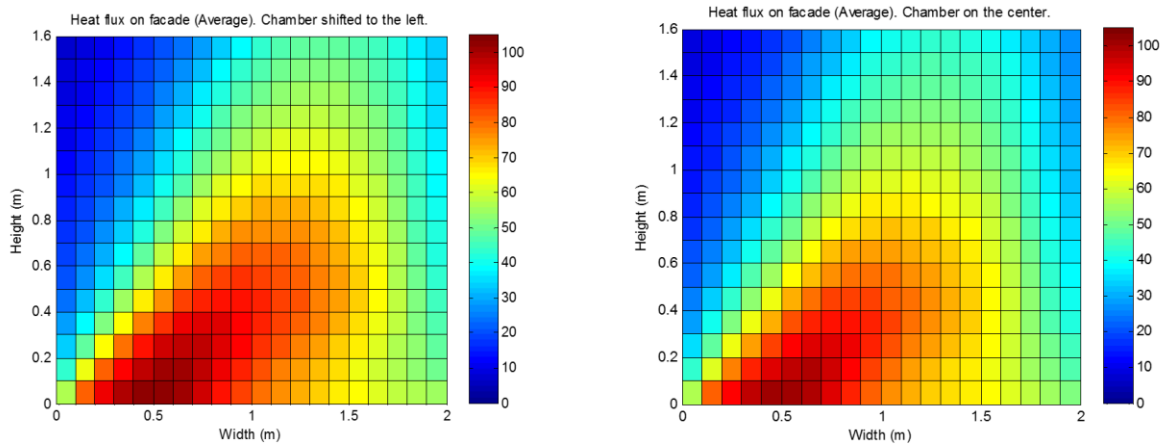

Figure 86. Average heat flux on façade during simulation (constant fuel rate). Chamber shifted to the left (left figure), chamber on the center (right figure).

The largest heat flux results are observed in region from 0 mm to 400 mm above the window (Figure 86). Horizontal position of region with the largest heat flux is slightly shifted to the left side from central axis of window in both cases, because of side wall and combustion chamber geometry influence.

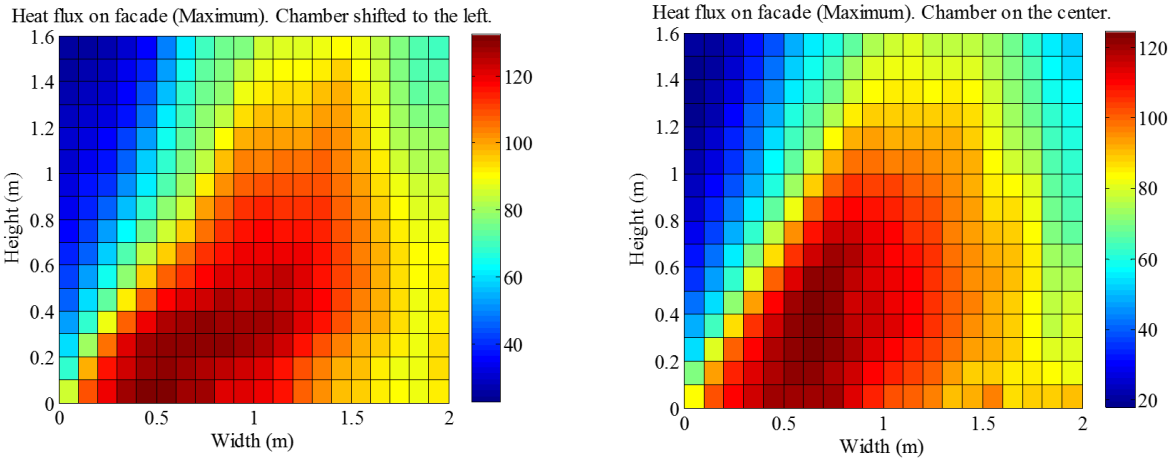

Figure 87. Maximum heat fluxes on façade during the whole simulation time. Chamber shifted to the left (left figure), chamber on the center (right figure).

Maximum heat fluxes through the whole test for each point are presented in Figure 87 (different time step, global maximum for each point separately). According to these results it can be concluded that direction of largest plumes is dependent from the chamber positioning, although position of chamber does not affect so dramatically to the average heat flux exposure.

The simulation with chamber shifted to the left was chosen for further study of wall surface and internal temperature. Façade wall temperature at time step of 700 seconds from the simulation start has the following distribution according to the Figure 88.

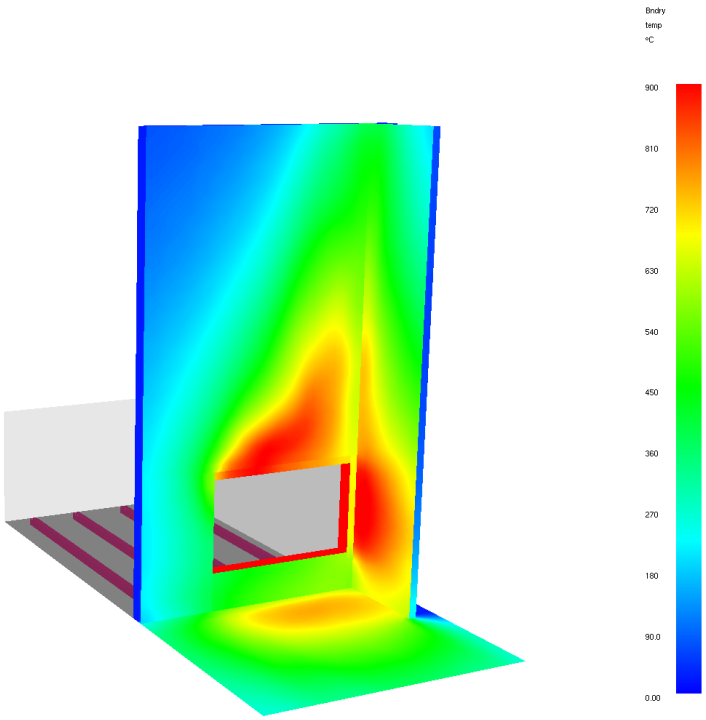

Figure 88. Smokeview figure of wall temperature on façade.

In same time, when heat flux remains almost constant (average heat flux at testing time), temperature is continuously increasing. The temperature distribution on the surface and inside façade wall is presented on Figures 89 and 90. Figure 89 shows temperature after 7 minutes of testing; and Figure 90 after 20 minutes of testing, before the fire HRR starts to reduce.

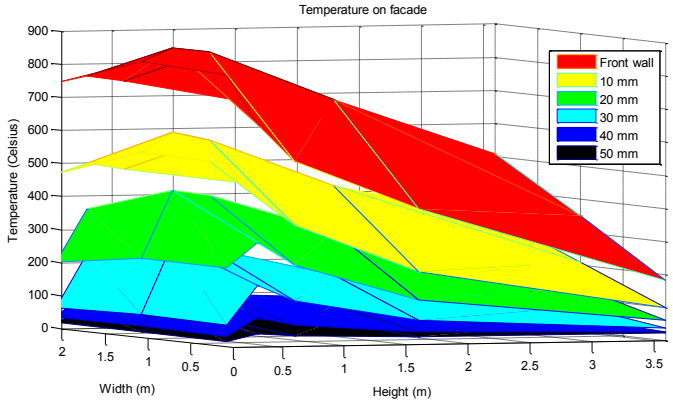

Figure 89. Maximum temperature on façade during simulation (7 min of testing)

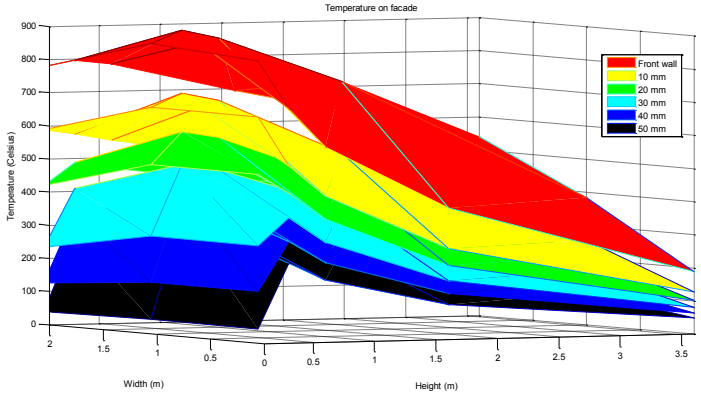

Figure 90. Maximum temperature on façade during simulation (20 min of testing)

In order to obtain more accurate results of temperature at different depths inside the insulation and at different points on the façade, the following actions have been done:

a. The gauge heat flux histories on each measurement device were recorded and saved.
b. Separate cone calorimeter simulation input files were generated for each location. The files were identical except for the sample external flux time histories (ramps).
c. The simulation was performed for all files.
d. The internal wall temperatures were recorded for each case and mapped back to the geometry of the façade wall.

In Figure 91, results of wall surface maximum temperature received from Cone Calorimeter test simulations are presented.

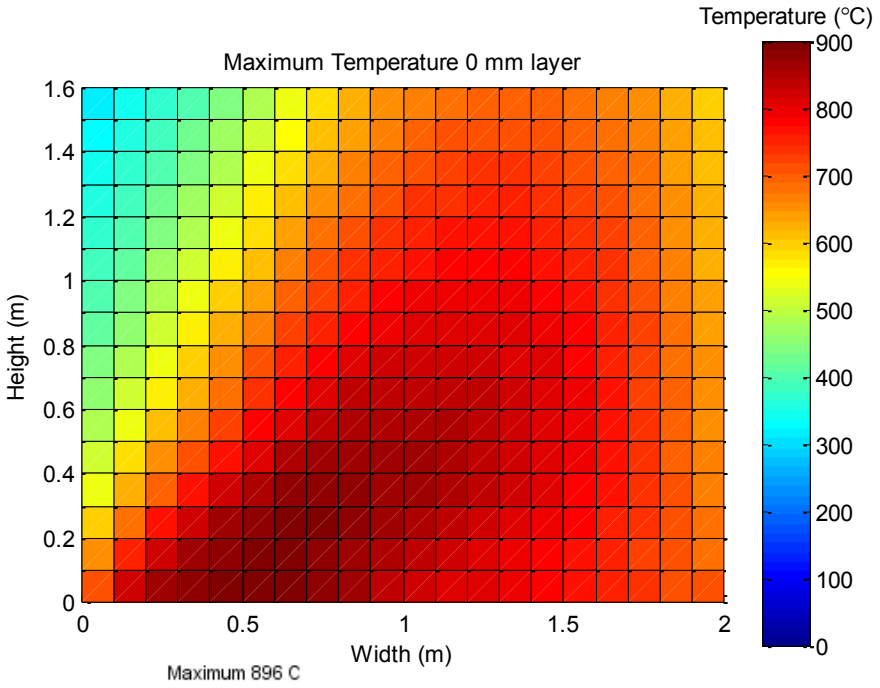

Figure 91. Results of Cone Calorimeter test simulations. Wall temperature.

Maximum temperatures inside the wall were measured every 5 mm. account. In Appendix 9, temperatures on different layers are collected. Layer covered with 60 mm thick stone wool layer has the following temperature (Figure 92):

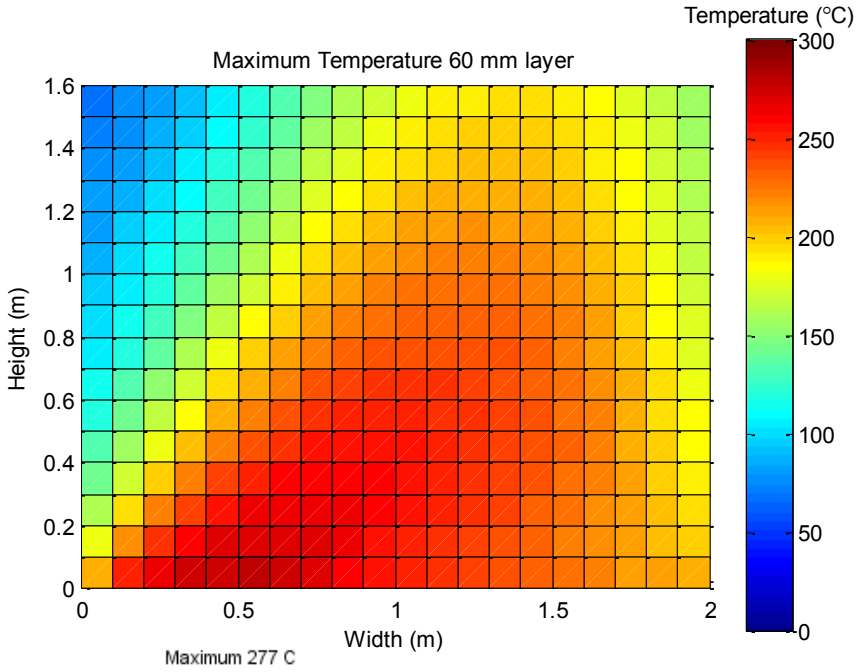

Figure 92. Results of Cone Calorimeter test simulations. Temperature inside wall (60 mm).

According to Figure 92, maximum temperature on layer covered with 60 mm wool does not increase over 300 ºC. Increasing wool covering layer by 10 mm (Figure 93), maximum temperature on the layer does not exceed 200 ºC.

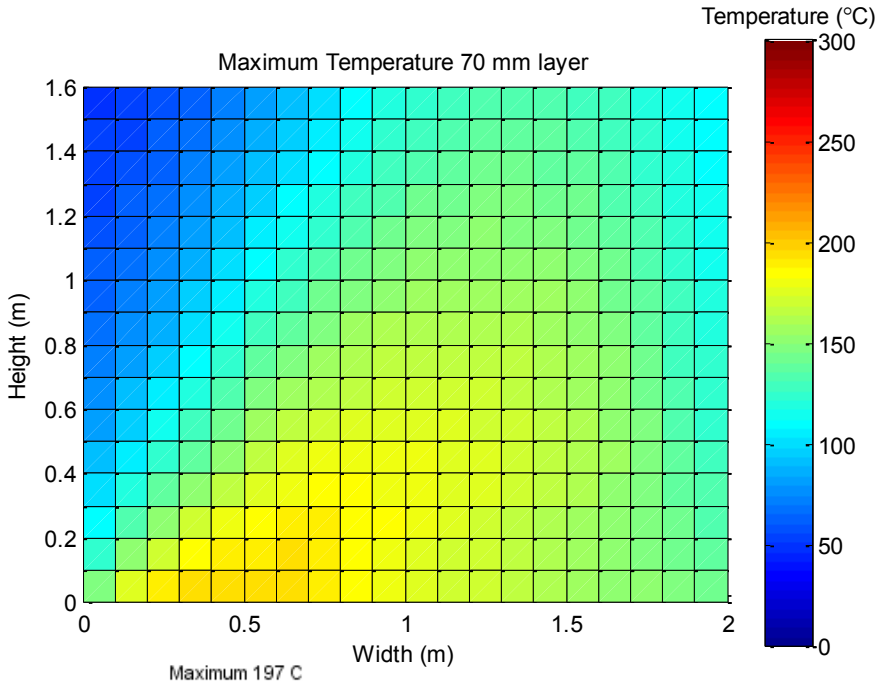

Figure 93. Results of Cone Calorimeter test simulations. Temperature inside wall (70 mm).

When stone wool covering comes to 90 mm, maximum temperature of the layer is less than 100 ºC as it shown in Figure 94.

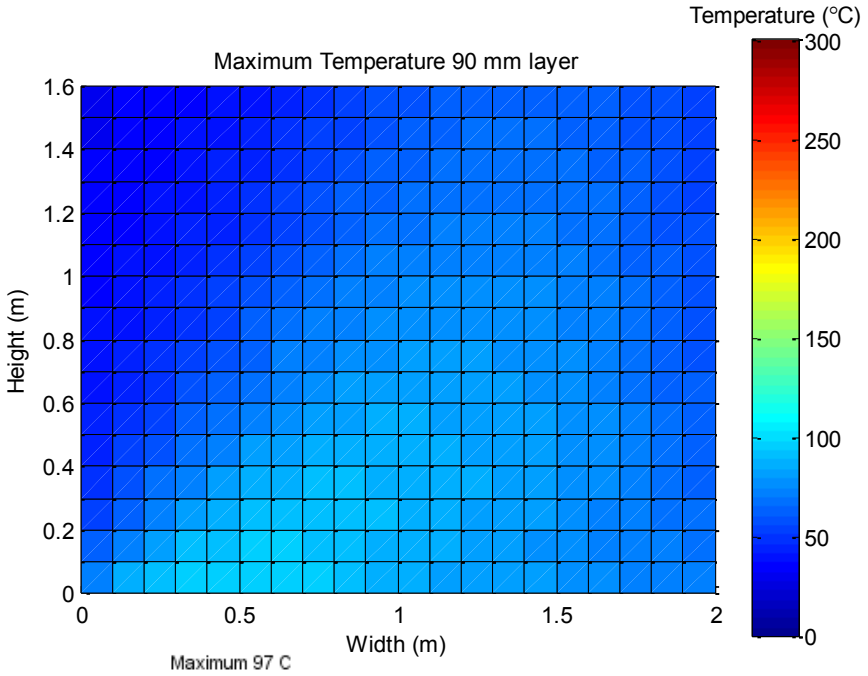

Figure 94. Results of Cone Calorimeter test simulations. Temperature inside wall (90 mm).

According to Figures 92, 93, 94 and results of flammability tests described in Chapter 5.3, can be made the assumption that is required thickness of stone wool covering for resisting flammable insulation materials. Expanded polystyrene (EPS) starts melting at 220 ºC and starts burning at 300 ºC temperature. PIR has not melting temperature but it starts to degrade at 100 ºC at slow rate, with faster degradation reactions taking place at 300 ºC. Results of required stone wool thickness are presented in Table 14.

Table 14. Required Stone wool thickness for protecting flammable insulation materials.

	Required Stone wool thickness against	
EPS	Melting (200 ºC)	70 mm
	Burning (300 ºC)	60 mm
PIR	Slow degradation/burning (100 ºC)	90 mm
	Fast degradation/burning (300 ºC)	60 mm

7 Discussion

The main task of this thesis was to investigate the sensitivity of the ISO 13785-2 test fire exposure on the details of the test setup. The main task was to prepare a validated model for the ISO 13785-2, to characterize insulation materials for simulation purposes, and to demonstrate the use of CFD in façade fire test simulation.

Validation of Large-scale test was performed by the simulation of specific fire test of non-combustible façade conducted in TUS (Tokyo University of Science) laboratory which results was published in Journal of Fire Science and Technology in 2012. In the test series, a range of different heat release rates was used. After the validation, the model was used for investigating heat fluxes at different heights above the opening and temperatures at different depths.

Sensitivity studies were done for two types of parameters: physical measures and properties of the test scenario, and the numerical model parameters. Among the first group of parameters are the combustion room and façade window dimensions and positioning, additional ventilation, wall's material, ambient temperature, radiative fraction and soot yield. The numerical model parameters are the number of radiation angles, model mesh and solid cell sizes. The most important parameters were the façade window dimension and the rear side ventilation conditions (Chapter 6.3). The smallest façade window gave the highest heat flux and temperature predictions. The existence of rear side ventilation decreases the thermal exposure level on the façade wall.

Simulations performed with 3 m and 13 m wide combustion chamber shows that the larger thermal exposure can be achieved with the smaller chamber with the same fire load. Chamber wall material has no influence to the heat fluxes and temperatures on façade, if the walls are covered with high temperature thin insulation layer. Ambient air temperature has the small influence to the exposure on the façade: increasing of that value increases the thermal exposure level. Apparently, position of the combustion chamber does not change the thermal exposure level, but change the fire plumes locations, that causes the differences between the results. The simulations with different radiative fractions show that the larger value gives the larger heat flux and temperatures predictions on the façade. Similarly, with increasing of soot yield value, thermal exposure on façade increases.

Model sensitivity to the numerical model parameters is sufficiently low. Simulations with two different mesh sizes (50 mm and 100 mm cells) look almost identical. The solid cell size parameter and the number of radiations angles of 100 and 1000 angles do not changed predictions at all.

It is concluded that modelling of Large-scale fire test should be accomplished with sufficiently small mesh size (not more than 0.1 m), the number of radiation angles does not to be increased from its default value, and radiation fraction should be set to value in range from 20% to 30%. It should be noted that in this study radiation fraction value of 20% gave the best agreement with the experimental results. The comparisons between simulations and experiments with heat fluxes and temperatures what are sufficient large for material fire testing show that the model provides results with relative standard deviation of 0.23 for heat flux and 0.35 for temperature, and model bias factor of 0.84 for heat fluxes and 1.05 for temperatures. The relative standard deviation between numerical results and the experiment was larger with small burning rates than with high burning rates. There was observed that with fire load more

than 50% of maximum approved fire load (5.6 MW), simulation always gives over-predicted values for temperatures in enclosure.

Studying the flammability characteristics of common wall insulation materials shows that the expanded polystyrene (EPS) starts to melt at 220 ºC and to burn at temperature over 300 ºC. Polyisocyanurate (PIR) starts reacting at approximately 100 ºC. Model constructed on basis of heat release rate from ISO 13785-2 test simulation and common stone wool thermal characteristics presented that to prevent EPS from melting, a 70 mm layer of stone wool is needed at region of 0-400 mm above the window opening. PIR insulation needs 90 mm thick fire protection to be defensed from thermal exposure at the same region.

8 Conclusion and Future Work

The work described in this thesis has been concerned with the creation, investigation and validation of numerical model for Large-scale fire facade test ISO 13785-2 using FDS 6. In the simulations, the heat exposure conditions on façade wall suitable for material testing were reached by simulation with 63% of the maximum HRR allowed by the standard. According to the sensitivity study, many factors can affect this value, such as chamber dimensions, additional ventilation, window dimensions and positioning. It means that the burners should be calibrated for each implementation of the ISO 13785-2 test setup. The created model can be used to determine the most advantageous test setup.

Using the created model, the sensitivities of the thermal conditions to the test and model parameters were studied. According to sensitivity study, the most important parameters were the façade window dimension and the rear side ventilation conditions.

The numerical model is always has an uncertainty in predictions in comparison to real fire results. The validated model provides the predictions with known accuracy. Using the accuracy and prediction the probability of expectations can be determined. The uncertainties of the FDS predictions of the façade heat fluxes were determined. Model bias factor for heat flux predictions on façade wall is 0.84, and for temperatures is 1.05. The uncertainty of predictions of temperatures inside the chamber is greater. Temperature predictions inside the chamber should be further investigated.

The validated model can be used for assessment of façade insulation materials fire resistance in the test conditions. This tool helps to investigate many materials for creation suitable classification for façade insulation building products.

References

American Chemistry Council, Inc. 2015. Foam Sheating Materials and properties. [10.5.2015]. http://fsc.americanchemistry.com/Materials-and-Properties

ASTM D 7309-11. 2011. Standard Test Method for Determining Flammability Characteristics of Plastics and Other Solid Materials Using Microscale Combustion Calorimetry ASTM D 7309-11. American Society for Testing and Materials (International): West Conshohocken, PA.

Babrauskas, V. 2002. The SFPE Handbook of Fire Protection Engineering. The Cone Calorimeter. Third Edition. National Fire Protection Association.

Blagojevich, M. 2011. A new curve for temperature-time relationship in compartment fire. Thermal Science, vol. 15, n. 2. pp. 339-352.

CAN/ULC-S134-92. 2013. Standard Method of Fire test of Exterior Wall Assemblies. Canadian Codes and ULC standards.

Chen, B. & Lu, S. & Li, C. & Yuan, M. 2012. Analysis of compartment fires with a ceiling vent. The 9th Asia-Oceania Symposium on Fire Science and Technology. University of Science and Technology of China, Hefei.

Cheng, H & Hadjisophocleus, G. 2012. Experimental study and modelling of radiation from compartment fires to adjacent buildings. Fire Safety Journal, vol. 10, pp. 43-62.

Delichatsios, M & Ryan, J. 2013. Vertical separation Distance in Multi-Storey Buildings. Building Test Expo 2013. Fire Safety Engineering Research and Technology Centre.

Drysdale, D. 2011. Fire Science and Combustion, An Introduction to Fire Dynamics, Third Edition, John Wiley & Sons, West Sussex, England.

Duijve, M. 2012. Comparative assessment of insulating materials on technical, environmental and health aspects for application in building renovation to the Passive house level. Master thesis report.

E1 Finish National Building Code. 2011. Building's fire safety. Ministry of the Environment.

Ezinwa, J. 2009. Modelling full-scale fire test behaviour of polyurethabe foams using Cone Calorimeter Data. Department of Mechanical Engineering. University of Saskatchevan.

Giraldo, M & Avellaneda, J. & Lacasta, A. & Rodriguez, V. 2012. Computer-simulation research on building-façade geometry for fire spread control in buildings with wood claddings. World conference on Timber Engineering. Auckland.

Gorbett, G. 2008. Computer fire Models for fire investigation and reconstruction. International symposium on Fire Investigation Science and Technology. pp. 23-34.

Guoqiang, L & Wang, P. 2013. Advanced analysis and Design for Fire Safety of Steel Structures. pp. 7-33.

Hartin, E. 2008. Fire Behavior Indicators and Fire Development – Part 1. www.firehouse.com

He, Y. 2010. Effects of Computational Domain on Numerical Simulation of Building Fires. Journal of Fire Protection Engineering, vol. 20, n. 4. pp. 225-251.

Himoto, K. & Tsuchihashi, T. & Tanaka, Y. & Tanaka, T. 2009. Modelling the trajectory of window flames with regard to flow atachment to the adjacent wall. Fire Safety Journal 44. pp. 250-258.

Huang, H. & Ooka, R. & Liu, N. & Zhang, L. & Deng, Z. & Kato, S. 2009. Experimental study of fire growth in a reduced-scale compartment under different approaching external wind conditions. Fire Safety Journal, vol. 4. pp. 311-321.

HuYa. Rigid Polyisocyanurate foam thermal insulating boards, laminated with flexible Aluminum Foil. 2015. Technical Data Sheet. HuYa PIR Insulation Factory. http://www.huyapir.com/downloads/TechnicalDataSheet.pdf

Unifrax LLC. 2007. Insulfrax S Blanket. Product Information Sheet.

ISO 11358-1:2014. Thermogravimetry (TG) of polymers – Part 1: General principles. International Organization for Standardization.

ISO 13785-2:2002. Reaction-to-fire tests for facades – Part 2: Large-scale test. International Organization for Standardization.

ISO 5660-1:1993. Fire tests - Reaction to fire – Part 1: Rate of heat release from building products - (Cone calorimeter method). International Organization for Standardization, Geneva, Switzerland.

Jansson, R. & Anderson, J. 2012. Experimental and numerical investigation of fire dynamics in a façade test rig. Conference: Fire Computer modelling.

Kashivagi, T. & Gilman, J. & Nyden, 1998. M. Polymer Combustion and New Flame Retardants. National Institute of Standards and Technology.

Kawagoe, K. 1958. Fire Behavior in Rooms, Report 27. Building Research Institute, Ministry of Construction, Tokyo, Japan.

Kim, M & Quintiere, J. 2007. Predicting polymer burning using TGA/DSC. Department of Fire Protection Engineering. University of Maryland. pp. 115-124.

Kirkegaard, L. & Korsgaard, M. 2004. Impact of redox state and pre-oxidation on diffusion, crystallization, and high temperature behavior of iron containing alumino-silicate glass fibres. Master Thesis. Aalborg University.

Klopovic, S & Turan, Ö. 1998. Flames venting externally during full-scale flashover fires: two sample ventilation cases. Fire Safety Journal, vol.31. pp. 117-142.

Kolbrecki, A. 2015. Model of fire spread out on outer building surface. Technical Sciences Journal, vol. 63, n. 1. pp. 135-144.

Korhonen, T. & Hietaniemi, J. 2005. Fire safety of Wooden facades in Residential suburb Multi-storey Buildings. VTT Building and Transport.

Law, M. 1991. Fire grading and fire behavior. Fire Safety Journal, vol. 17. pp. 147-153.

Lee, Y. 2006. Heat Fluxes and Flame Heights in External Façade Fires. PhD Thesis, FireSERT. University of Ulster.

Lee, Y. & Delichatsios, M & Silcock, G. 2007. Heat fluxes and flame heights in facades from fires in enclosures of varying geometry. Proceedings of the Combustion Institute. vol. 31 Issue 2. pp. 2521-2528.

Lee, Y. & Delichatsios, M. & Ohmiya, Y. & Wakatsuki, K. & Yanagisawa, A. & Goto, D. 2009. Heat fluxes on opposite building wall by flames emerging from an enclosure. Proceedings of the Combustion Institute 32. pp. 2551-2558.

Lindholm, J. & Brink, A. & Hupa, M. 2009. Cone Calorimeter – A Tool for Measuring Heat Release Rate. Åbo Akademi Process Chemistry Centre.

Lu, K. & Hu, L. & Tang, F. 2014. Heat flux profile upon building facade with side walls due to window ejected fire plume: An experimental investigation and global correlation. Fire Safety Journal, vol. 11. pp. 14-22.

Ma, Z. 2000. Fire Safety Design of Composite Slim Floor Structures. Helsinki University of Technology, Laboratory of Steel Structures.

McGrattan, K. & McDermott, R. & Floyd, J. & Hostikka, S. & Forney, G. & Baum, H. 2012. Computational fluid dynamics modelling of fire. International Journal of Computational Fluid Dynamics, pp. 1-12.

McGrattan, K. & McDermott, R. & Hostikka, S. & Floyd, J. Fire Dynamics Simulator (Version 6) User's Guide. NIST.

Moesgaard, M. & Pedersen, H. 2005. Investigation of the Crystallization Process occuring in Stone Wool Fibres during High Temperature treatments. Project Paper. Aalborg University.

Mowrer, F. and Williamson, R. 1990. Methods to Characterize Heat Release Rate Data.
Fire Safety Journal, vol. 16, no. 5. pp. 367–387.

NFPA 285. 2012. Standard fire test method for evaluation of fire propagation characteristics of exterior non-load-bearing wall assemblies containing combustible components. National Fire Protection Association. USA.

NIST. 1999. Revised Thermocouple Reference Tables, Type K. Monograph 175.

Ohmiya, Y & Yusa, S. & Suzuki, J. & Koshikawa, K. & Delichatsios, M. 2003. Aerothermodynamics of fully involved enclosure fires having external flames.

Oleszkiewicz, I. 1989. Heat transfer from a window fire plume to a building façade. HTD, vol. 123. pp. 163-170.

Oleszkiewicz, I. 1990. Fire and Combustible Claddings. Construction Canada, Jul-Aug. pp. 16-21.

Pakosch, D. 2006. Impact of the pre-heat treatment on the crystallisation behaviour of iron containing alumino-silicate glass fibres. Student Research Report. Aalborg University.

Putorti, A. 1998. Computer Fire Models. Fire Safety Engineering Division, Building and Fire Research Laboratory, National Institute of Standards and Technology.

Lyon, R. & Safronava, N & Quintiere, J. & Stoliarov, S. & Walters, R. and Crowley, S. 2014. Material properties and fire test results.

Rockwool Product catalogue. 2013. ProRox SL980.

SFS-EN 13501-1: 2009. Fire classification of construction products and building elements. Classification using test data from reaction to fire tests. Finish standardization association.

SFS-EN 1363-1: 2012. Fire Resistance tests. General requirements. Finish standardization association.

Shelby, J. 2005. Introduction to Glass Science and Technology. 2nd edition. The Royal Society of Chemistry. Cambrigde. ISBN 978-0854046393.

Slopiecka, K & Bartocci, P. & Fantozzi, F. 2011. Thermogravimetric analysis and Kinetic study of poplar wood pyrolysis. Third International Conference on Applied Energy. Perygia, Italia. pp. 1687-1698.

SP Fire 105. Method for fire testing of façade materials. Department of Fire Technology. Swedish National Testing and Research Institute.

Statistic system of the Finish rescue services. PRONTO. https://prontonet.fi

Stern-Gottfried, J. 2010. Experimental Review of the Homogeneous Temperature Assumption in Post-Flashover Compartment Fires, Fire Safety Journal, 45, 4, pp. 249-261.

Sun, J. & Hu, L. & Zhang, Y. 2013. A review on research of fire dynamics in high-rise buildings. Theoretical & Applied Mechanics Letters, 3(4). doi:10.1063/2.1304201.

Tang, F. & Hu, L. & Delichatsios, M. & Lu, K. & Zhu, W. 2012. Experimental study on flame height and temperature profile of buoyant window spill plume from an under-ventilated compartment fire. International Journal of Heat and Mass Transfer, 55. pp. 93-101.

Tewarson, A. 1995. SFPE Handbook of Fire Protection Engineering. SFPE Boston. MA. pp. 3-115.

U.S. Patent 5981290. 1999. Microscale Cobustion Calorimeter. Lyon, R. & Walters, R. publ. 11.09.1999. 9 p.

Wade, C. 2003. Future directions in fire testing of building products. BRANZ Ltd. Porirua City, New Zealand.

Walters, R. & Safronava, N. & Lyon, R. 2015. A microscale combustion calorimeter study of gas phase combustion of polymers. Combustion and flame, vol. 162, pp. 855-863.

White, N. 2014. Fire Hazards of Exterior Wall Assemblies Containing Combustible Components. Informational Bulletin.

Xie, H. & Chen, S. 2010. Simulation of combustion Process and Soot Yield in Propane/Air Laminar Diffusion Flame by Self-Defined Scalar Method. International Journal of Chemical Reactor Engineering, vol. 8.

Yamaguchi, J. & Tanaka, T. 2005 Temperature profiles of window jet plume. Fire Science Technology, vol. 24, no. 1. pp. 17-38.

Yoshioka, H. & Ohmiya, Y. & Noaki, M. and Yoshida, M. 2012. Large-scale Facade Fire Tests Conducted Based on ISO 13785-2 with Noncombustible Facade Specimens. Fire Science and Technology, vol. 31, no. 1. pp. 1–22.

Yoshioka, H. 2014. Façade tests on fire propagation along combustible exterior wall systems.

Yucel, K. & Basyigit, C. & Ozel, C. 2003. Thermal insulation properties of expanded polystyrene as construction and insulating materials. pp. 1-5.

Zhang, C & Li, G. 2012. Fire Dynamic Simulation on thermal actions in localized fires in large enclosure. Advanced Steel construction, vol. 8, n. 2. pp. 124-136.

Zhang, X & Hadjisophocleous. 2012. An improved two-layer zone model applicable to both pre- and post-flashover fires. Fire Safety Journal, vol. 53. pp. 63-71.

Appendix 1. Heat flux profile upon the wall for different window dimensions.

(Tang & Hu et al., 2015, p. 21).

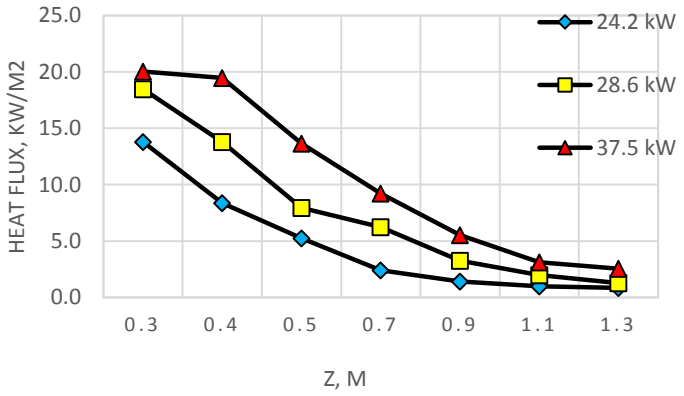

(a) 15 cm (H) x 15 cm (W)

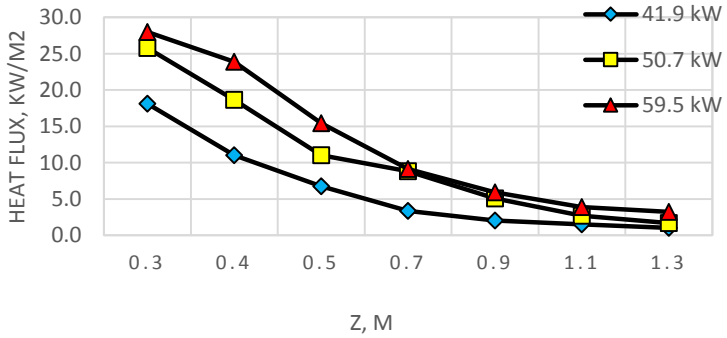

(b) 20 cm (H) x 20 cm (W)

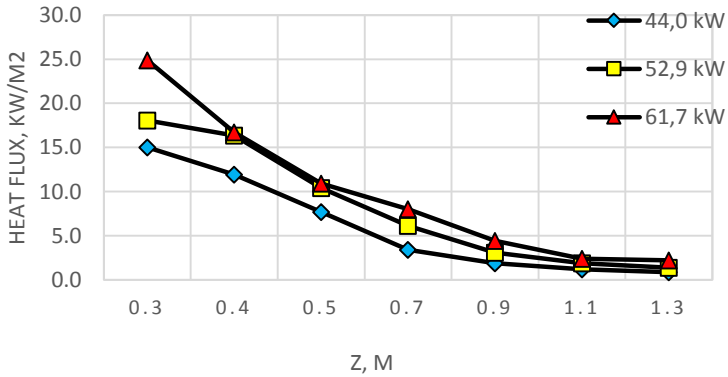

(c) 25 cm (H) x 15 cm (W)

Appendix 2. Materials after the Cone calorimeter test

Expanded polystyrene (EPS)

Polyisocyanurate (PIR)

35 kW/m2

50 kW/m2

Polyisocyanurate with covering (PIR-COV)

25 kW/m2

36.2 kW/m2

Appendix 3. FDS code for ISO 13785-2 simulation

```
&HEAD CHID='IsoTest'/

Grid cell size: dx = dy = dz = 0.1 m

Combustion chamber 4.3m x 3.0m x 1,7m
Facade test specimen 5.7m high, 3.0m wide (main wall)
Facade test specimen 5.7m high, 1.2m wide (side wall)
Opening 1.2m high, 2.0m wide

Fire mesh(es).
&MESH ID = 'm1', IJK=30,43,17, XB= 0.0,3.0, 0.0,4.3, 0.0,1.7 / Room
&MESH ID = 'm3', IJK=35,30,60, XB= 0.0,3.5, -3.0,0.0, 0.0,6.0 /Front wall + side wall

&MISC TMPA=20.0/

&TIME T_END=1800.0  /

&RADI NUMBER_RADIATION_ANGLES = 100.0 , RADIATIVE_FRACTION = 0.20 /

&DUMP SMOKE3D = .TRUE.,

            NFRAMES             = 1800,

            DT_PART= 1.0,

            DT_HRR  = 1.0,

            DT_SLCF = 0.25,

            DT_BNDF             = 1.0,

            DT_PL3D = 60.0,

            DT_ISOF  = 1000000.0

            DT_RESTART=50./

---------------------------------FIRE SOURCE-----------------------------------

&REAC FUEL = 'PROPANE', SOOT_YIELD=0.015/

ISO max 5.6 MW
&SURF ID='BURNER', HRRPUA=1261.261, RAMP_Q='fireramp', MATL_ID = 'CALSIUM_SILICATE_BOARD', COL-
OR='RASPBERRY', THICKNESS = 0.025, TMP_FRONT = 300.0 /

&RAMP ID='fireramp', T=0.0, F=0.0 /
&RAMP ID='fireramp', T=300.0, F=0.63 /
&RAMP ID='fireramp', T=1500.0, F=0.63 /
&RAMP ID='fireramp', T=1800.0, F=0.0 /

&OBST XB= 0.3,0.4, 0.3,4.0, 0.0,0.1, SURF_ID='PIPE' /
&OBST XB= 1.0,1.1, 0.3,4.0, 0.0,0.1, SURF_ID='PIPE' /
&OBST XB= 1.8,1.9, 0.3,4.0, 0.0,0.1, SURF_ID='PIPE' /
&OBST XB= 2.6,2.7, 0.3,4.0, 0.0,0.1, SURF_ID='PIPE' /
&VENT XB= 0.3,0.4, 0.3,4.0, 0.1,0.1, SURF_ID='BURNER' /
&VENT XB= 1.0,1.1, 0.3,4.0, 0.1,0.1, SURF_ID='BURNER' /
&VENT XB= 1.8,1.9, 0.3,4.0, 0.1,0.1, SURF_ID='BURNER' /
&VENT XB= 2.6,2.7, 0.3,4.0, 0.1,0.1, SURF_ID='BURNER' /
&VENT XB= 0.3,0.3, 0.3,4.0, 0.0,0.1, SURF_ID='BURNER' /
&VENT XB= 1.0,1.0, 0.3,4.0, 0.0,0.1, SURF_ID='BURNER' /
&VENT XB= 1.8,1.8, 0.3,4.0, 0.0,0.1, SURF_ID='BURNER' /
&VENT XB= 2.6,2.6, 0.3,4.0, 0.0,0.1, SURF_ID='BURNER' /
&VENT XB= 0.4,0.4, 0.3,4.0, 0.0,0.1, SURF_ID='BURNER' /
&VENT XB= 1.1,1.1, 0.3,4.0, 0.0,0.1, SURF_ID='BURNER' /
&VENT XB= 1.9,1.9, 0.3,4.0, 0.0,0.1, SURF_ID='BURNER' /
&VENT XB= 2.7,2.7, 0.3,4.0, 0.0,0.1, SURF_ID='BURNER' /

-------------------------------MATERIALS---------------------------------

&MATL ID = 'WOOL',
    EMISSIVITY    = 0.9,
    DENSITY= 94,
```

```
            CONDUCTIVITY_RAMP= 'c-wool',
            SPECIFIC_HEAT_RAMP= 's-wool'/

&RAMP ID = 'c-wool', T = 10., F = 0.034/
&RAMP ID = 'c-wool', T = 20., F = 0.035/
&RAMP ID = 'c-wool', T = 30., F = 0.036/
&RAMP ID = 'c-wool', T = 40., F = 0.037/
&RAMP ID = 'c-wool', T = 50., F = 0.038/
&RAMP ID = 'c-wool', T = 100., F = 0.045/

&RAMP ID = 'c-wool', T = 150., F = 0.05/
&RAMP ID = 'c-wool', T = 200., F = 0.055/
&RAMP ID = 'c-wool', T = 250., F = 0.06/
&RAMP ID = 'c-wool', T = 300., F = 0.065/
&RAMP ID = 'c-wool', T = 350., F = 0.07/
&RAMP ID = 'c-wool', T = 450., F = 0.085/

&RAMP ID = 's-wool', T = 0., F = 0.84/
&RAMP ID = 's-wool', T = 400., F = 0.84/

-------------------------------------------------------------------------

EUROCODE 1993-1-2:1995  &3.4.1.3 carbon steel
&MATL ID = 'STEEL',
     EMISSIVITY = 0.9,
     DENSITY = 7850.,
     CONDUCTIVITY_RAMP = 'c-steel',
     SPECIFIC_HEAT_RAMP= 's-steel'/

&RAMP ID = 'c-steel', T = 0., F = 53.3/
&RAMP ID = 'c-steel', T = 800., F = 27.3/
&RAMP ID = 'c-steel', T = 1200., F = 27.3/

&RAMP ID = 's-steel', T = 0., F = 0.439/
&RAMP ID = 's-steel', T = 600., F = 0.759/
&RAMP ID = 's-steel', T = 640., F = 0.798/
&RAMP ID = 's-steel', T = 680., F = 0.890/
&RAMP ID = 's-steel', T = 720., F = 1.388/
&RAMP ID = 's-steel', T = 735., F = 5.0/
&RAMP ID = 's-steel', T = 740., F = 2.525/
&RAMP ID = 's-steel', T = 760., F = 1.159/
&RAMP ID = 's-steel', T = 780., F = 0.909/
&RAMP ID = 's-steel', T = 800., F = 0.803/
&RAMP ID = 's-steel', T = 820., F = 0.745/
&RAMP ID = 's-steel', T = 840., F = 0.708/
&RAMP ID = 's-steel', T = 860., F = 0.683/
&RAMP ID = 's-steel', T = 880., F = 0.664/
&RAMP ID = 's-steel', T = 900., F = 0.65/
&RAMP ID = 's-steel', T = 1200., F = 0.65/

ISOWOOL 1260
&MATL ID = 'CERAMIC_FIBRE_BLANKET',
     EMISSIVITY = 0.9,
      DENSITY = 100. ,
     CONDUCTIVITY_RAMP = 'c-ceramic',
     SPECIFIC_HEAT= 1.0/

&RAMP ID = 'c-ceramic', T = 0., F = 0.1/
&RAMP ID = 'c-ceramic', T = 600., F = 0.15/
&RAMP ID = 'c-ceramic', T = 800., F = 0.22/

ISOWOOL BOARD
&MATL ID = 'CERAMIC_FIBRE_BOARD',
    EMISSIVITY = 0.9,
     DENSITY = 250. ,
    CONDUCTIVITY_RAMP = 'c-board',
    SPECIFIC_HEAT= 1.0/

&RAMP ID = 'c-board', T = 0., F = 0.07/
&RAMP ID = 'c-board', T = 400., F = 0.07/
&RAMP ID = 'c-board', T = 600., F = 0.12/
&RAMP ID = 'c-board', T = 800., F = 0.16/
&RAMP ID = 'c-board', T = 1000., F = 0.23/

According to EN 1094-4:1995
```

```
&MATL ID = 'CALSIUM_SILICATE_BOARD'

    EMISSIVITY = 0.9

    DENSITY = 225.

    CONDUCTIVITY= 0.21

    SPECIFIC_HEAT= 0.84/
ASTM C-182
&RAMP ID = 'c-calsium', T = 0., F = 0.08/
&RAMP ID = 'c-calsium', T = 200., F = 0.08/
&RAMP ID = 'c-calsium', T = 400., F = 0.1/
&RAMP ID = 'c-calsium', T = 600., F = 0.12/
&RAMP ID = 'c-calsium', T = 800., F = 0.14/

-----------------------------------------SURFACE PROPERTIES-----------------------------------

&SURF ID='PIPE', COLOR = 'RED', MATL_ID = 'STEEL', STRETCH_FACTOR = 2, THICKNESS = 0.006/
&SURF ID='CEILING', COLOR = 'SILVER', MATL_ID = 'CERAMIC_FIBRE_BOARD','STEEL', STRETCH_FACTOR = 2,2, THICK-
NESS = 0.05,0.006, BACKING = 'VOID'/
&SURF ID='FLOOR', COLOR = 'GRAY', MATL_ID = 'CERAMIC_FIBRE_BLANKET','CERAMIC_FIBRE_BOARD','STEEL',
STRETCH_FACTOR = 2,2,2, THICKNESS = 0.025,0.05,0.006, BACKING = 'VOID' /
&SURF ID='WALL', COLOR = 'SILVER', MATL_ID = 'CERAMIC_FIBRE_BOARD','STEEL', STRETCH_FACTOR = 2,2, THICK-
NESS = 0.05,0.006, BACKING = 'VOID', DEFAULT=.TRUE./
&SURF ID='FRONTWALL', COLOR = 'SILVER', MATL_ID = 'CERAMIC_FIBRE_BOARD','STEEL', STRETCH_FACTOR = 2,2,
THICKNESS = 0.05,0.006/

-----------------------------------------SPECIMEN---------------------------------------------

&SURF ID='FACADE',COLOR = 'SILVER',MATL_ID = 'WOOL','CALSIUM_SILICATE_BOARD', STRETCH_FACTOR = 1,2,
THICKNESS = 0.1,0.1/

-----------------------------------------GEOMETRY---------------------------------------------

&VENT   MB = 'ZMIN',                                          SURF_ID = 'FLOOR' /        Floor
&VENT   MB = 'ZMAX', MESH_ID='m1',                            SURF_ID = 'CEILING'        /        Ceiling
&VENT   MB = 'XMIN', MESH_ID='m1',                            SURF_ID = 'WALL'  /        Wall 1(side left)
&VENT   MB = 'XMAX', MESH_ID='m1',                            SURF_ID = 'WALL'  /        Wall 2(side right)
&OBST   XB = -0.1,3.1, 4.3,4.4, -0.1,1.8,          SURF_ID = 'WALL'  /        Wall 2(back)

&OBST   XB = -0.1,4.3, -0.2,0.0, -0.1,1.8,         SURF_ID6 = 'FRONTWALL','FACADE'    /        Facade SPECIMEN
&OBST   XB = 0.0,4.3, -0.2,-0.1, 1.8,6.0,          SURF_ID = 'FACADE'                 /        Facade SPECIMEN

&HOLE   XB = 1.0,3.0, -0.2,0.1, 0.5,1.7                                               /        Window opening on facade
&OBST   XB = 3.05,3.15, -1.4,-0.2, 0.0,6.0,SURF_ID = 'FACADE'                         /        Side wall(wing)

&VENT   MB='YMIN', MESH_ID ='m3',                  SURF_ID = 'OPEN'   / front
&VENT   MB='XMIN', MESH_ID ='m3',                  SURF_ID = 'OPEN'   / left
&VENT   MB='XMAX', MESH_ID ='m3',                  SURF_ID = 'OPEN'   / right
&VENT   MB='ZMAX', MESH_ID ='m3',                  SURF_ID = 'OPEN'   / above

-----------------------------------------MEASURING--------------------------------------------

&PROP ID                = 'TC',
    QUANTITY            = 'THERMOCOUPLE',
    BEAD_DIAMETER       = 0.0032/
---------------
Thermocouples
---------------
&DEVC   XYZ=1.1,-0.2,1.75,                         PROP_ID ='TC'      , ID='Tg1' , IOR = -2 /
&DEVC   XYZ=2.0,-0.2,1.75,                         PROP_ID ='TC'      , ID='Tg2' , IOR = -2 /
&DEVC   XYZ=2.9,-0.2,1.75,                         PROP_ID ='TC'      , ID='Tg3' , IOR = -2 /
&DEVC   XYZ=1.1,-0.2,5.7,                          PROP_ID ='TC'      , ID='Tg4' , IOR = -2 /
&DEVC   XYZ=2.0,-0.2,5.7,                          PROP_ID ='TC'      , ID='Tg5' , IOR = -2 /
&DEVC   XYZ=2.9,-0.2,5.7,                          PROP_ID ='TC'      , ID='Tg6' , IOR = -2 /
&DEVC   XYZ=3.05,-0.3,5.7,                         PROP_ID ='TC'      , ID='Tg7' , IOR = -1 / on the wing

-------------------
Gauge Heat flux components According to ISO 13785-2
-------------------
&DEVC XYZ=2.0,-0.2,2.3, QUANTITY = 'GAUGE HEAT FLUX', ID='HF_1', IOR = -2 /
&DEVC XYZ=2.0,-0.2,3.3, QUANTITY = 'GAUGE HEAT FLUX', ID='HF_2', IOR = -2 /
&DEVC XYZ=1.1,-0.2,5.3, QUANTITY = 'GAUGE HEAT FLUX', ID='HF_3', IOR = -2 /
&DEVC XYZ=2.0,-0.2,5.3, QUANTITY = 'GAUGE HEAT FLUX', ID='HF_4', IOR = -2 /
&DEVC XYZ=2.9,-0.2,5.3, QUANTITY = 'GAUGE HEAT FLUX', ID='HF_5', IOR = -2 /
```

```
&DEVC XYZ=3.05,-0.3,5.3,QUANTITY = 'GAUGE HEAT FLUX', ID='HF_6', IOR = -1 / on the wing
&DEVC XYZ=1.1,-0.2,2.3, QUANTITY = 'GAUGE HEAT FLUX', ID='HF_7', IOR = -2 /
&DEVC XYZ=2.9,-0.2,2.3, QUANTITY = 'GAUGE HEAT FLUX', ID='HF_8', IOR = -2 /

&BNDF QUANTITY = 'GAUGE HEAT FLUX'/
&BNDF QUANTITY = 'WALL TEMPERATURE'/
&SLCF QUANTITY = 'TEMPERATURE', PBX = 2.0 /
&SLCF QUANTITY = 'TEMPERATURE', PBY = 2.0 /

&TAIL/
```

Appendix 4. TGA test experimental results

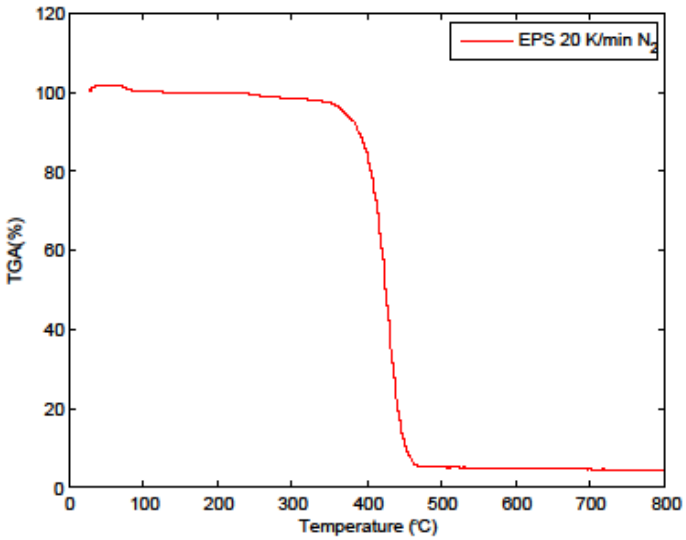

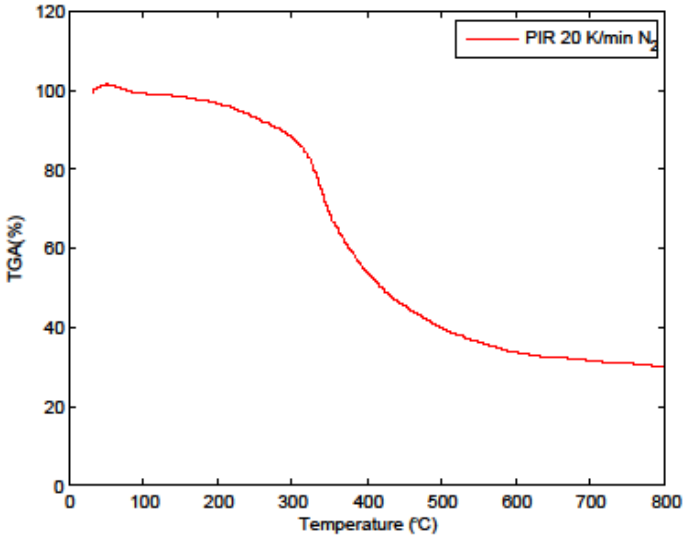

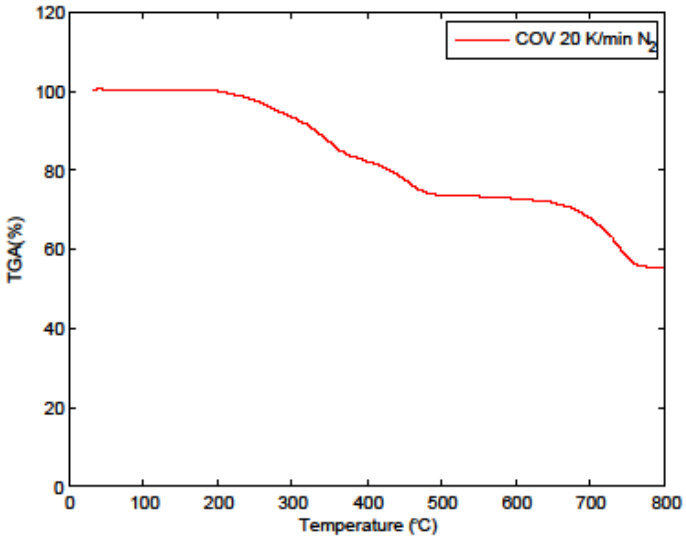

Appendix 5. Cone calorimeter test results. Mass loss.

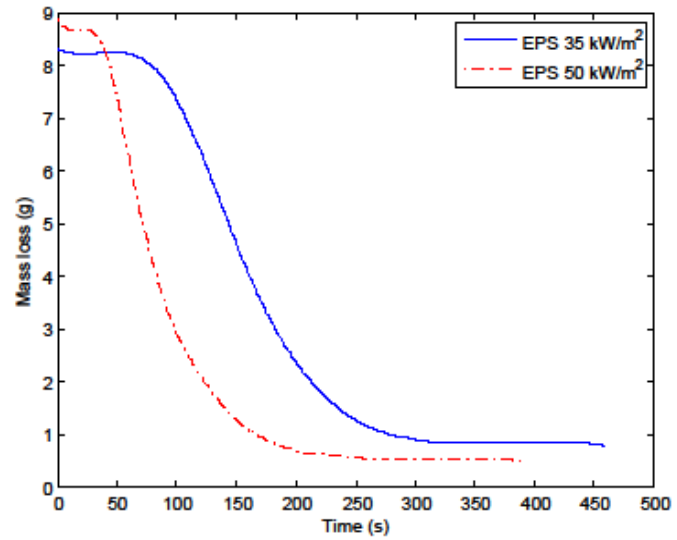

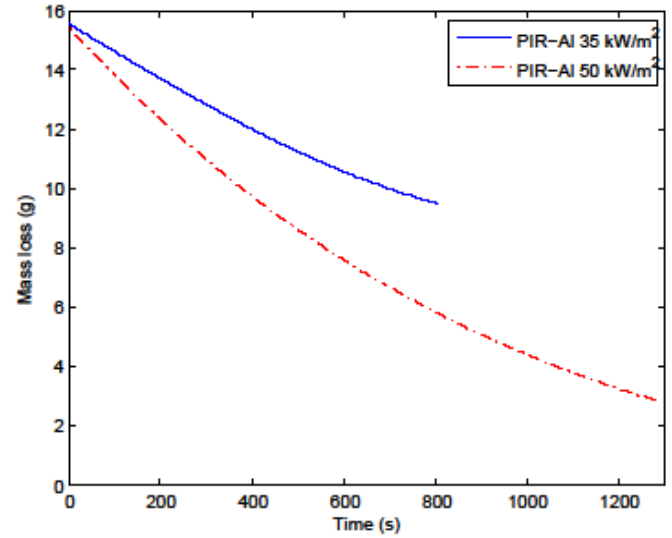

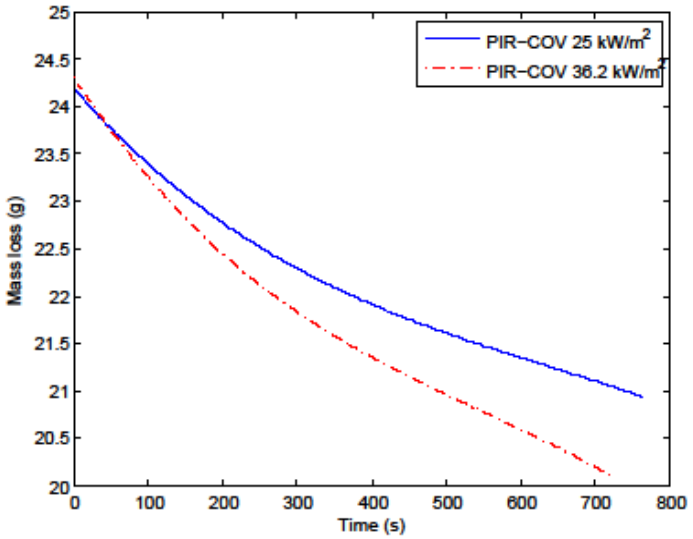

Appendix 6. Cone calorimeter test results. HRR.

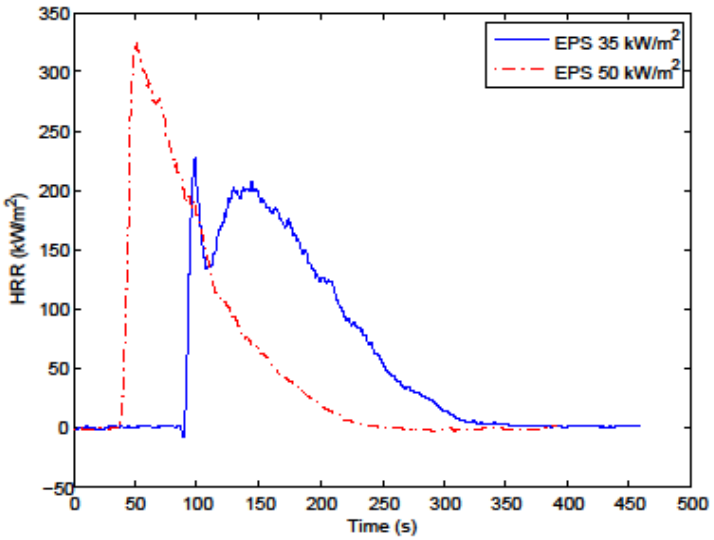

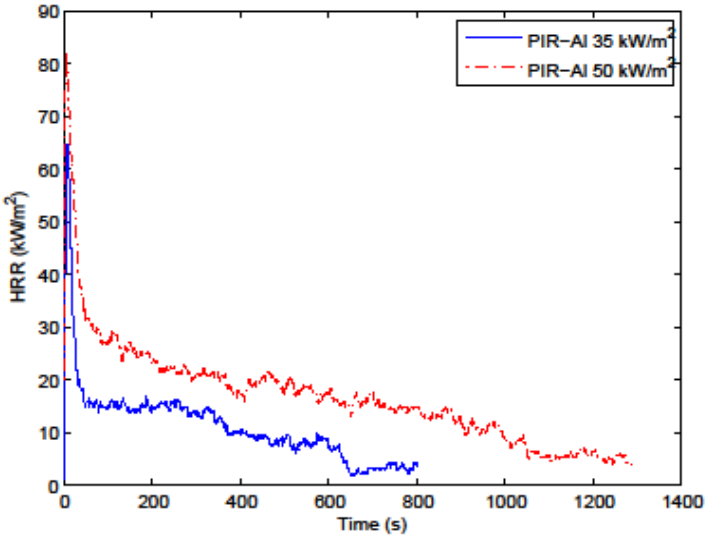

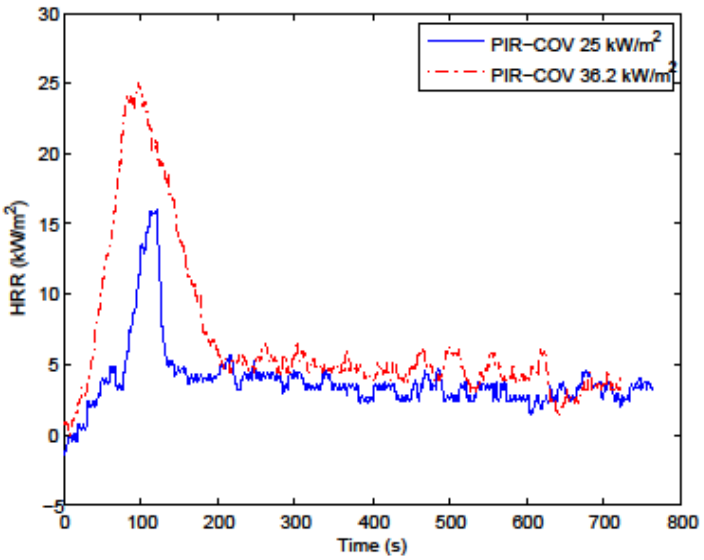

Appendix 7. Cone calorimeter test results. EHC.

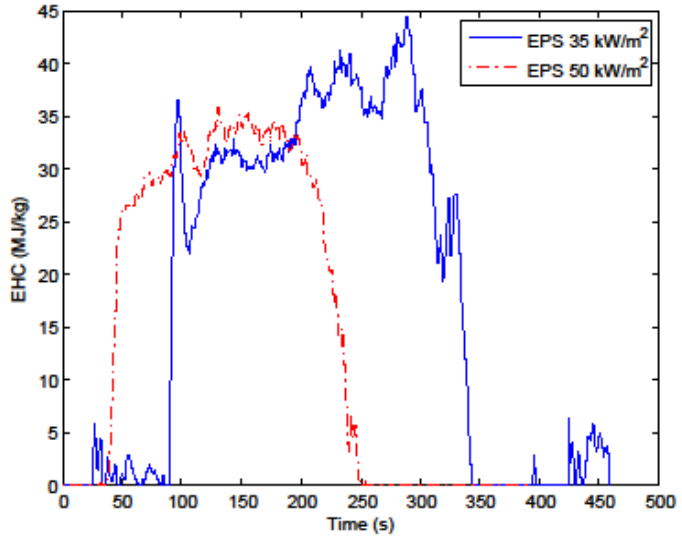

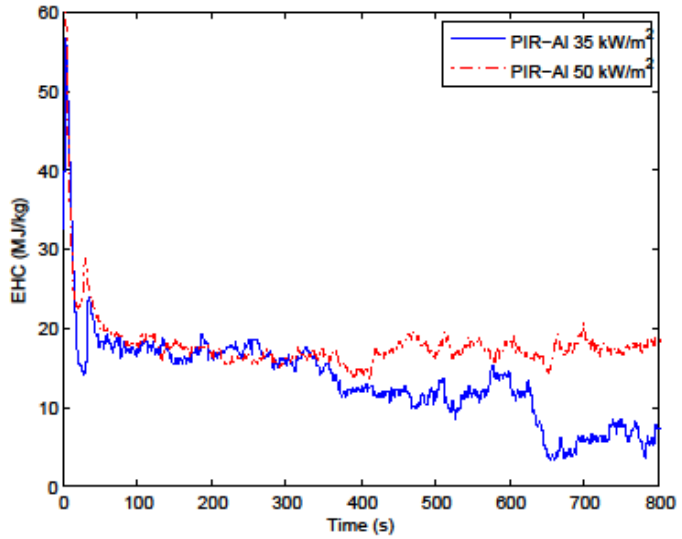

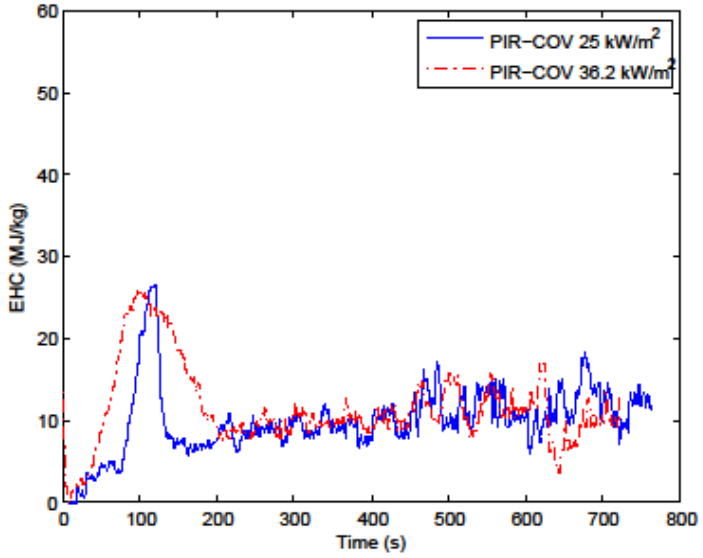

Appendix 8. Cone calorimeter test results. MLR.

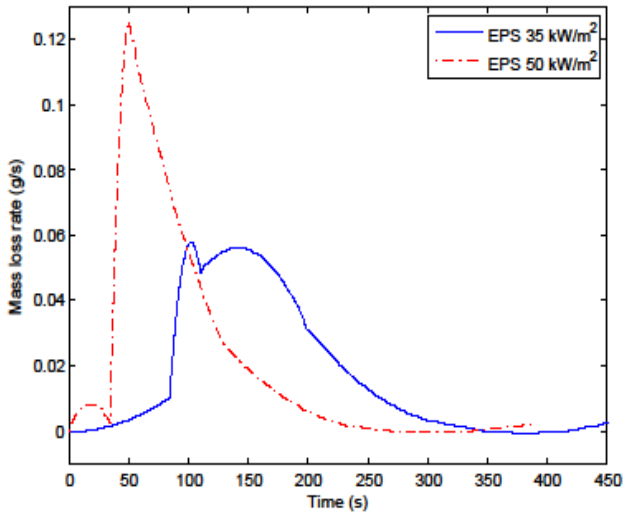

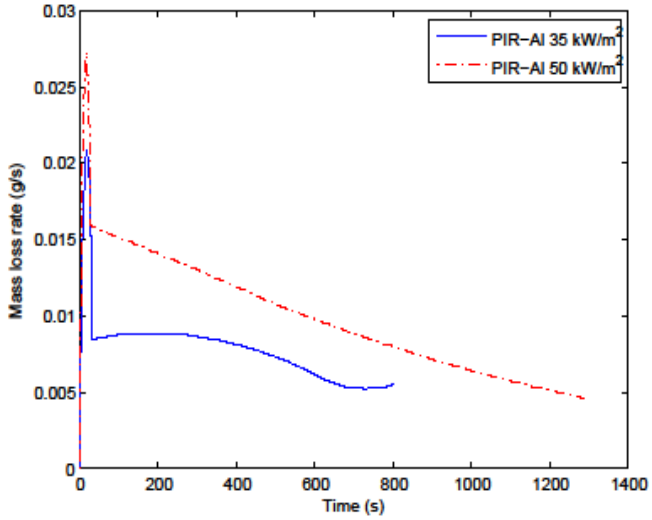

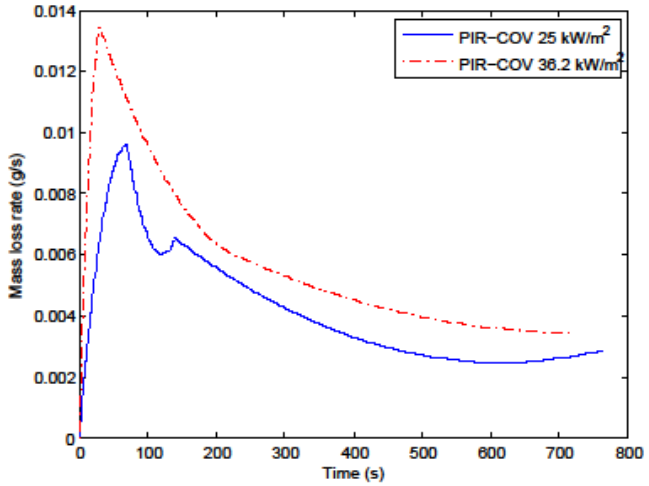

Appendix 9. Temperatures inside wall. Cone test.

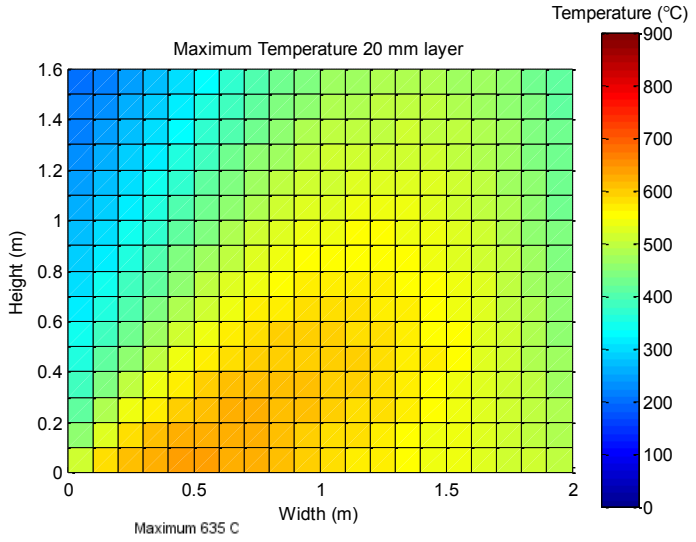

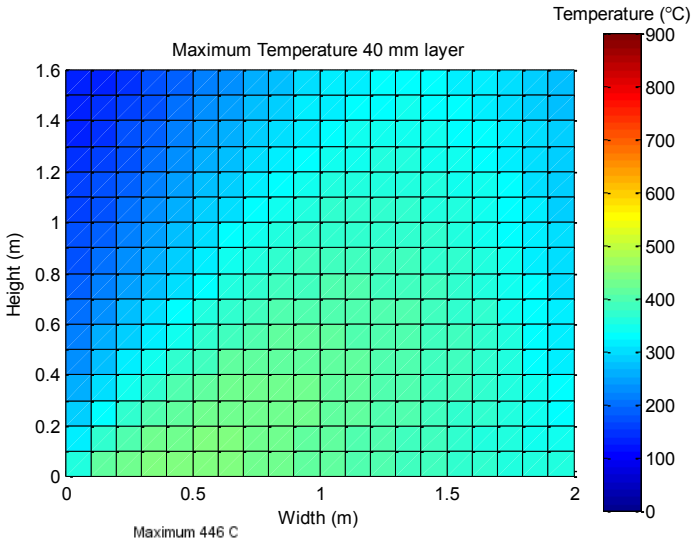

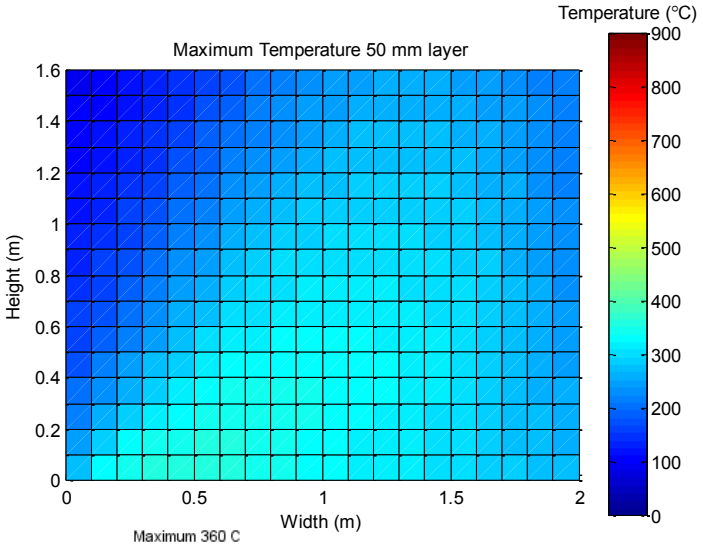

Appendix 9. Temperatures inside wall. Cone test. (2)

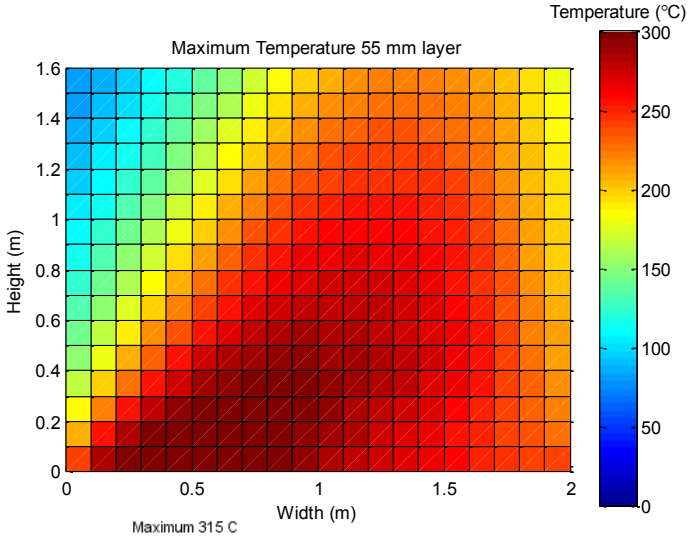

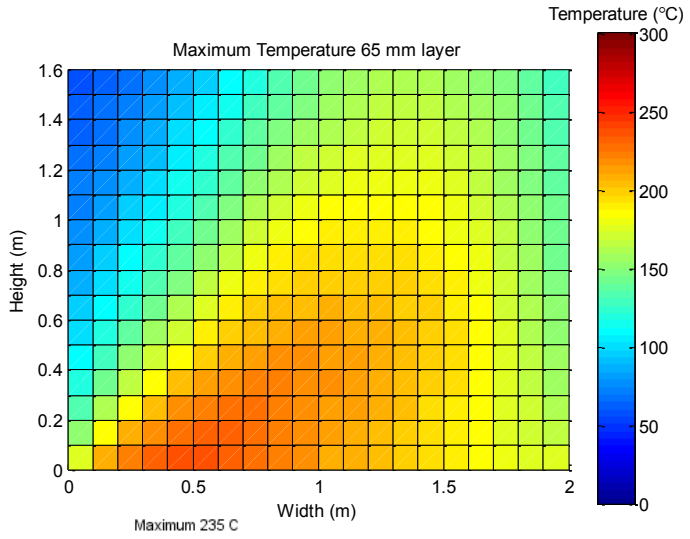

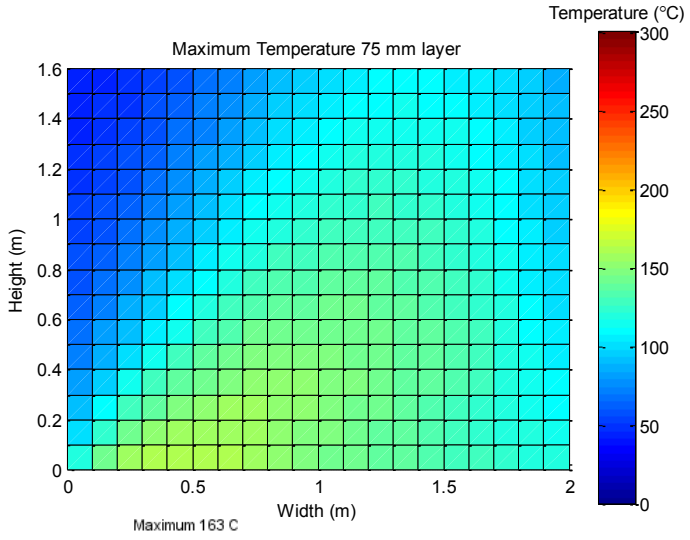

Appendix 10. Heat flux on façade according to ISO13785-2

Average heat flux at testing time (constant fuel flow rate) for case with chamber shifted to the left side

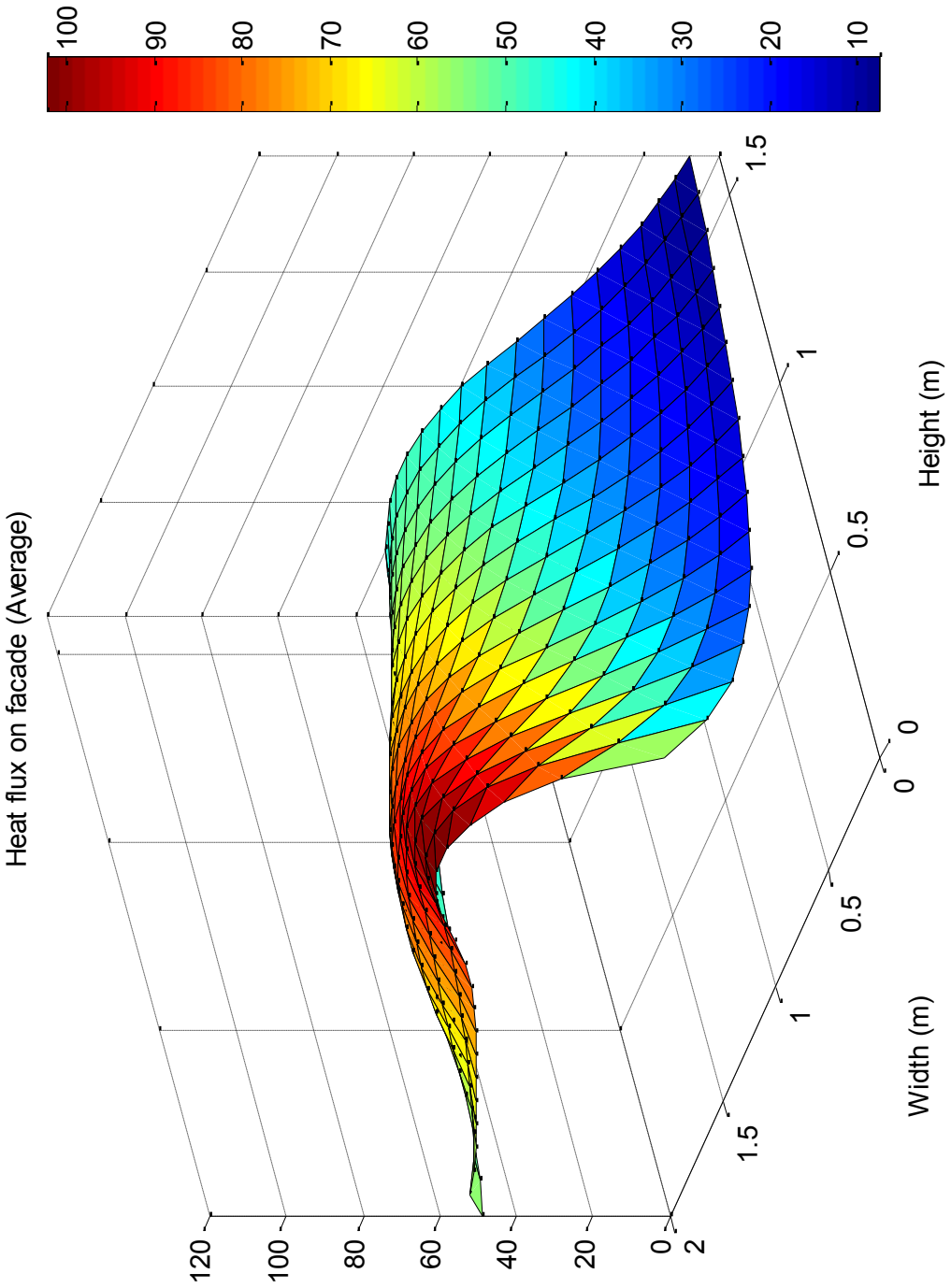

Appendix 11. FDS code of TGA test for EPS

```
&HEAD CHID='EPS_TGA', TITLE='TGA test of thermal degradation EPS' /

&MESH IJK=3,1,4, XB=-2,2,-0.5,0.5,0,1 /

&MISC SOLID_PHASE_ONLY =.TRUE./

&TIME T_END=1000. /

&REAC FUEL='PROPANE', SOOT_YIELD=0.015, HEAT_OF_COMBUSTION = 45000.0/

&VENT XB=-1,1,-0.5,0.5,0.0,0.0, SURF_ID='SAMPLE' /

&SURF ID            = 'SAMPLE'
    TGA_ANALYSIS   = .TRUE.
            TGA_HEATING_RATE = 20.0
            TGA_FINAL_TEMPERATURE = 800.0
    COLOR          = 'RED'
    THICKNESS      = 0.1
    MATL_ID(1,1) = 'component 1'
    MATL_MASS_FRACTION(1,1) = 1.0/

&MATL ID                = 'component 1'
    EMISSIVITY          = 1.0
    DENSITY                 = 20.
    CONDUCTIVITY        = 0.20
    SPECIFIC_HEAT       = 1.0
    N_REACTIONS         = 1
            REFERENCE_TEMPERATURE = 430.0
            PYROLYSIS_RANGE                 = 95.0
            HEATING_RATE                    = 20.0
    NU_SPEC                 = 0.95
    SPEC_ID             = 'PROPANE'
    NU_MATL             = 0.05
    MATL_ID             = 'residue'/

&MATL ID                = 'residue'
    DENSITY             = 5.
    CONDUCTIVITY        = 0.20
    SPECIFIC_HEAT       = 1.0 /

&TAIL /
```

Appendix 12. FDS code of TGA test for PIR

```
&HEAD CHID='PIR_TGA',TITLE='TGA test of thermal degradation PIR' /

&MESH IJK=3,1,4, XB=-2,2,-0.5,0.5,0,1 /

&MISC SOLID_PHASE_ONLY =.TRUE./

&TIME T_END=1000. /

&REAC FUEL='PROPANE', SOOT_YIELD=0.015, HEAT_OF_COMBUSTION = 38900.0/ This value should be larger than 25 MJ/kg because, assumed that degradation of PIR is three sequential chemical reactions process.

&VENT XB=-1,1,-0.5,0.5,0.0,0.0, SURF_ID='SAMPLE' /

&SURF ID = 'SAMPLE'
      TGA_ANALYSIS = .TRUE.
      TGA_HEATING_RATE = 20.0
      TGA_FINAL_TEMPERATURE = 800.0
      THICKNESS = 0.1
      MATL_ID(1,1) = 'MAT1'
      MATL_MASS_FRACTION(1,1) = 1.0/

&MATL ID = 'MAT1'
      EMISSIVITY                = 1.0
      DENSITY                   = 35.
      CONDUCTIVITY              = 0.045
      SPECIFIC_HEAT             = 1.5
      N_REACTIONS         = 1
      REFERENCE_TEMPERATURE = 327.0
      PYROLYSIS_RANGE = 240.0
      HEATING_RATE = 20.0
      NU_SPEC                   = 0.25
      SPEC_ID                   = 'PROPANE'
      NU_MATL                         = 0.75
      MATL_ID                   = 'MAT2'/

&MATL ID = 'MAT2'
      EMISSIVITY                = 1.0
      DENSITY                   = 35.
      CONDUCTIVITY              = 0.045
      SPECIFIC_HEAT             = 1.5
      N_REACTIONS         = 1
      REFERENCE_TEMPERATURE = 340.0
      PYROLYSIS_RANGE = 70.0
      HEATING_RATE = 20.0
      NU_SPEC                   = 0.55
      SPEC_ID                   = 'PROPANE'
      NU_MATL                         = 0.45
      MATL_ID                   = 'MAT3'/

&MATL ID = 'MAT3'
      EMISSIVITY                = 1.0
      DENSITY                   = 35.
      CONDUCTIVITY              = 0.045
      SPECIFIC_HEAT             = 1.5
      N_REACTIONS         = 1
      REFERENCE_TEMPERATURE = 526.0
      PYROLYSIS_RANGE = 500.0
      HEATING_RATE = 20.0
      NU_SPEC                   = 0.18
      SPEC_ID                   = 'PROPANE'
      NU_MATL                         = 0.82
      MATL_ID                   = 'CHAR'/

&MATL ID = 'CHAR'
      DENSITY = 5.0
      EMISSIVITY = 1.0
      CONDUCTIVITY = 1.0
      SPECIFIC_HEAT = 1.0 /

&TAIL /
```

Appendix 13. FDS code of TGA test for COV

```
&HEAD CHID='PIR_TGA',TITLE='TGA test of thermal degradation of PIR' /

&MESH IJK=3,1,4, XB=-2,2,-0.5,0.5,0,1 /

&MISC SOLID_PHASE_ONLY =.TRUE./

&TIME T_END=1000. /

&REAC FUEL='PROPANE', SOOT_YIELD=0.015/

&VENT XB=-1,1,-0.5,0.5,0.0,0.0, SURF_ID='SAMPLE' /

&SURF ID = 'SAMPLE'
      TGA_ANALYSIS = .TRUE.
      TGA_HEATING_RATE = 20.0
      TGA_FINAL_TEMPERATURE = 800.0
      THICKNESS = 0.1
      MATL_ID(1,1) = 'MAT1'/

&MATL ID = 'MAT1'
      EMISSIVITY                = 1.0
      DENSITY                   = 35.
      CONDUCTIVITY              = 0.045
      SPECIFIC_HEAT             = 1.5
      N_REACTIONS         = 1
      REFERENCE_TEMPERATURE = 325.0
      PYROLYSIS_RANGE = 50.0
      HEATING_RATE    = 20.0
      NU_SPEC                   = 0.165
      SPEC_ID                   = 'PROPANE'
      NU_MATL                         = 0.825
      MATL_ID                   = 'MAT2'/

&MATL ID = 'MAT2'
      EMISSIVITY                = 1.0
      DENSITY                   = 35.
      CONDUCTIVITY              = 0.045
      SPECIFIC_HEAT             = 1.5
      N_REACTIONS         = 1
      REFERENCE_TEMPERATURE = 450.0
      HEATING_RATE    = 20.0
      PYROLYSIS_RANGE = 16.5
      NU_SPEC                   = 0.105
      SPEC_ID                   = 'PROPANE'
      NU_MATL                         = 0.895
      MATL_ID                   = 'MAT3'/

&MATL ID = 'MAT3'
      EMISSIVITY                = 1.0
      DENSITY                   = 35.
      CONDUCTIVITY              = 0.045
      SPECIFIC_HEAT             = 1.5
      N_REACTIONS         = 1
      REFERENCE_TEMPERATURE = 730.0
      HEATING_RATE    = 20.0
      PYROLYSIS_RANGE = 37.0
      NU_SPEC                   = 0.248
      SPEC_ID                   = 'PROPANE'
      NU_MATL                         = 0.752
      MATL_ID                   = 'CHAR'/

&MATL ID = 'CHAR'
      DENSITY = 35.0
      EMISSIVITY = 1.0
      CONDUCTIVITY = 0.045
      SPECIFIC_HEAT = 1.5 /

&TAIL /
```

Appendix 14. Example calculation based on Lee model

Heat flux calculation for maximum fuel rate (120 g/s):

Amount of incoming air is:

$$\dot{m}_{air} = 0.5A\sqrt{H} = 1.315 \qquad kg/s$$

Fuel flow rate is:

$$\dot{m}_{fuel} = 0.120 \qquad kg/s$$

Total heat:

$$\dot{Q} = \dot{m}_{fuel}\Delta H_c = 5600 \qquad kW$$

Burned inside compartment:

$$\dot{Q}_{indide} = 1500A\sqrt{H} = 1500 \cdot 2 \cdot 1.2 * \sqrt{1.2} = 3943.6 \qquad kW$$

Burned outside compartment:

$$\dot{Q}_{ex} = \dot{Q} - \dot{Q}_{inside} = 1656.4 \qquad kW$$

Dimensionless HRR

$$l_1 = (A\sqrt{H})^{0.4} = 1.472$$

$$\dot{Q}^*_{ex} = \frac{\dot{Q}_{ex}}{\rho_\infty C_p T_\infty l_1^{5/2} g^{1/2}} = \frac{1656.4}{1.3 \cdot 1.0 \cdot 293 \cdot 1.472^{5/2} \cdot 9.81^{1/2}} = 0.528$$

Flame height

$$Z_f = 3.2 \cdot l_1 \dot{Q}^*_{ex} = 2.49 \qquad m$$

Heat flux on external façade

$$\dot{q}''_t = fcn(\frac{Z}{Z_f}) \cdot \frac{\dot{Q}_{ex}}{Z_f \cdot e^{0.6(\frac{H}{l_1})} \cdot l_1} = fcn(\frac{Z}{2.49}) \frac{1656.4}{2.49 \cdot e^{0.6(\frac{1.2}{1.472})} \cdot 1.472} = 277.35 \cdot fcn(\frac{Z}{2.49})$$

Heat flux meters 0.6m above the window, located in flame zone with $Z/Z_f \leq 0.8$ for case with fuel mass flow 120g/s. The value 0.35 can be used for *fcn(Z/Zf)* at continuous flame region.

$$\dot{q}''_t\left(Z/Z_f \leq 0.8\right) \approx 97 \qquad kW/m^2$$

Heat flux above the window opening at 600 mm height is about 97 kW/m^2 according to calculation results. Numerical simulation results for the same case are presented in Chapter 6.3.1.

Appendix 15. Samples before testing (Cone Calorimeter)

Grey EPS

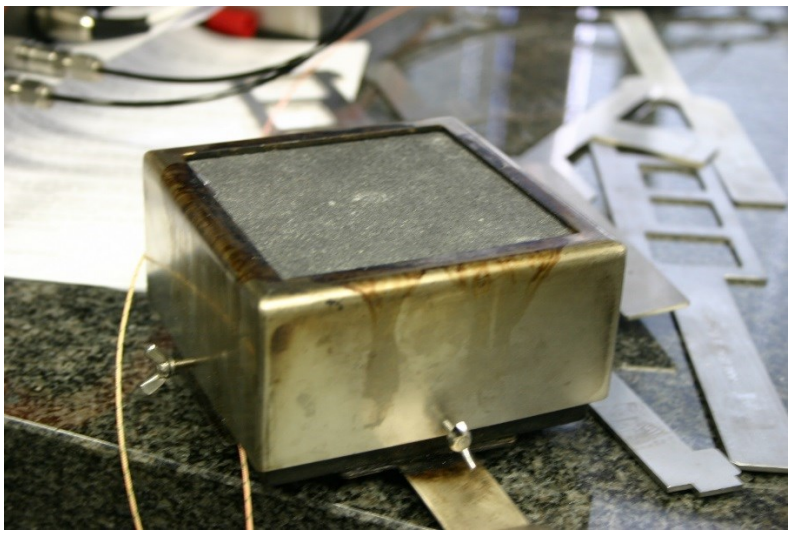

PIR

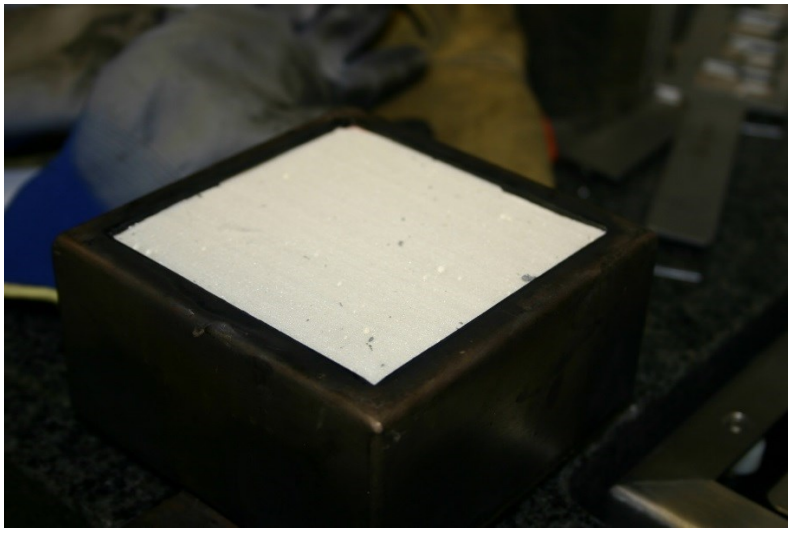

PIR-COV

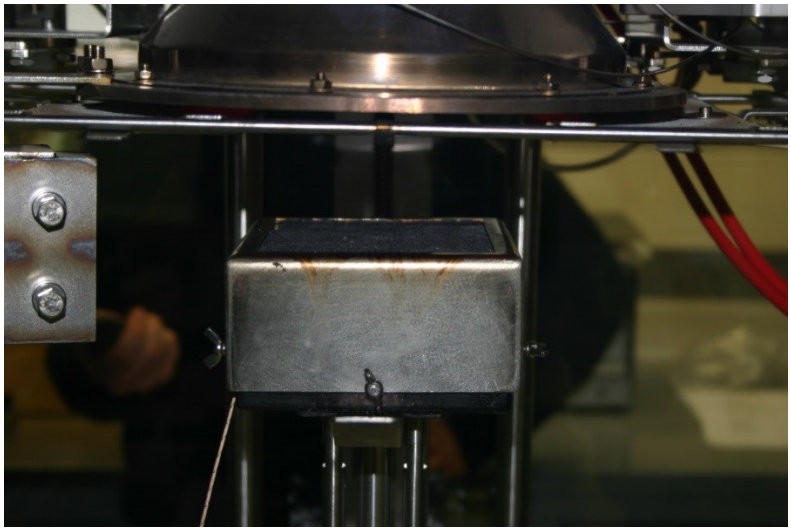

Appendix 16. Positions of thermocouples and heat flux meters used in validation

Heat flux meters (façade)

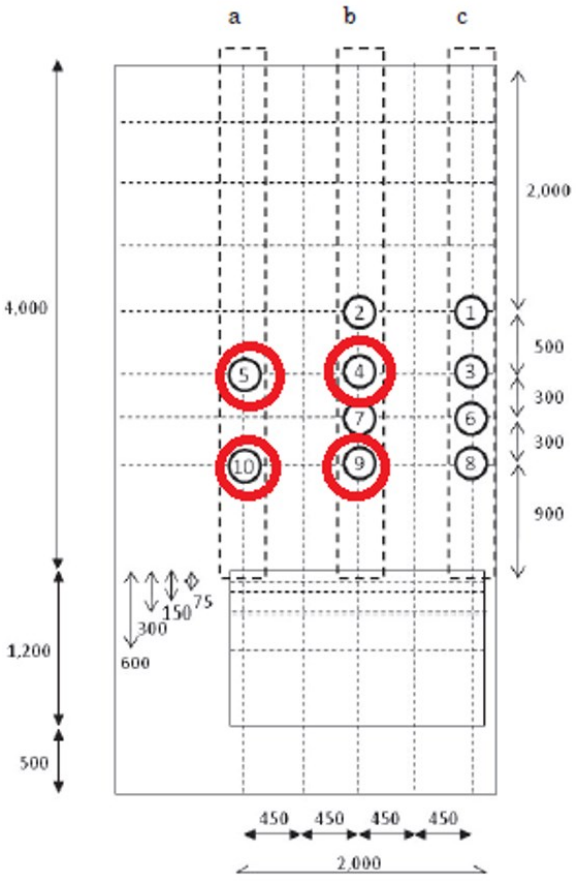

Thermocouples(façade)

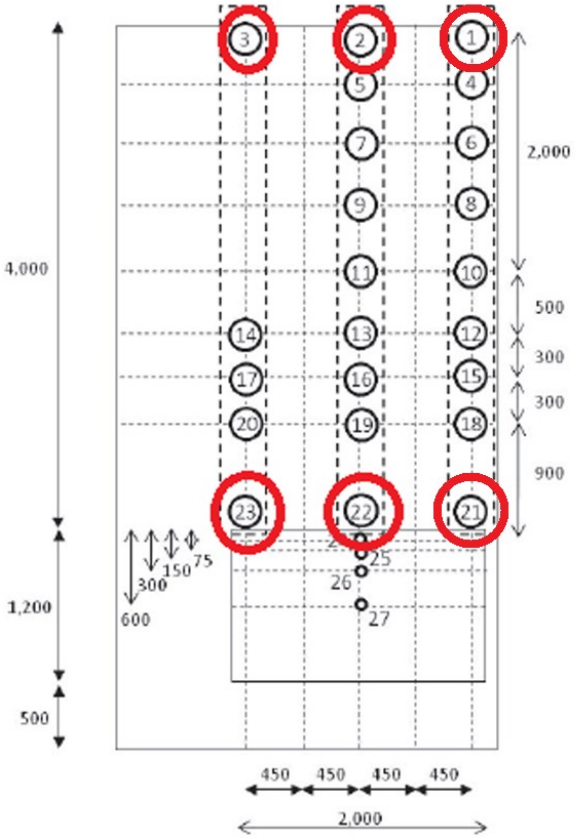

Thermocouples inside the combustion chamber